

The UNIVERSITY of WISCONSIN

Geophysical & Polar Research Center

DEPARTMENT OF GEOLOGY

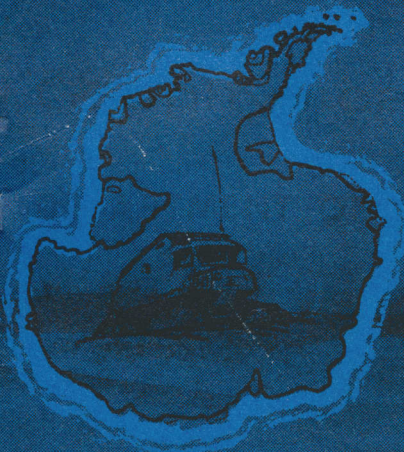
Research
Report
Series

A GRAVITY AND MAGNETIC SURVEY OF THE
ROSS ICE SHELF AREA, ANTARCTICA

by
Hugh F. Bennett

Research Report Series 64-3 - April, 1964

6021 South Highland Road
The Highlands
Madison, Wisconsin 53705



Research Report Series
Number 64-3
April 1964

A GRAVITY AND MAGNETIC SURVEY OF THE
ROSS ICE SHELF AREA, ANTARCTICA

by

Hugh F. Bennett

The University of Wisconsin
Geophysical and Polar Research Center
6021 South Highland Road
Madison, Wisconsin 53705

Abstract

The three layered velocity section measured at Little America Station (LAS) by Crary (1961) is considered to be representative of the Ross Ice Shelf area. This assumption is supported by the fact that the Bouguer anomaly at LAS and the mean Bouguer anomaly over the ice shelf are similar. The section consists of top, middle, and bottom layers with velocities of 2.4 km/sec, 4.24 km/sec, and 6.38 km/sec and probable densities of 2.0 gm/cm³, 2.7 gm/cm³, and 3.0 gm/cm³ respectively. The upper layer consists, in part, of glacial till and may be mostly morainal. The bottom layer is tentatively associated with gabbro.

Thick sections of the low density layer are indicated in the central portion of the ice shelf by the lower Bouguer anomalies there. This layer appears to thin in the southwest through northwest sector of the ice shelf and may therefore suggest that the source of this material lies to the southeast (Marie Byrd Land) and that the material was transported into the area by the ice shelf. The variation in Bouguer anomalies over most of the area is probably due to the variation in thickness of the low density layer. Since the ocean is thought to have a leveling influence on the low density layer, variations in thickness probably result from the underlying surface topography beneath this layer.

An increase in thickness and elevation of the middle layer is suggested in the northwest portion of the ice shelf by gravity and magnetic anomalies. Farther to the west, a rise of the bottom layer or presence of diabase sills may also be indicated. The gravity and magnetic anomalies in the northern Roosevelt Island area are probably caused by relatively low density low susceptibility intrusives which replace the country rock in that area.

The upper "magnetic horizon" appears to be associated with the bottom or 6.38 km/sec layer which lies at a depth of 2.6 km at LAS. A deep "magnetic basement" also found in the Ross Sea area to the north by Adams and Christoffel (1962) may suggest geologic similarity between the two areas. The maximum depth to the broad magnetic features, apparently confined to the peripheral areas of the ice shelf, is estimated to be between 8 km and 13 km.

The negative mean free air anomaly over the Ross Ice Shelf area is interpreted to be the result of former ice loading. Comparison of the degree of isostatic equilibrium between Fennoscandia and the Ross Ice Shelf area suggests that Würm or Wisconsin glaciation was contemporaneous in both hemispheres.



CONTENTS

	Page
Abstract	i
Part I Data Reduction	
Introduction	3
Altimeter Survey	3
Gravity Survey	4
Magnetic Survey	8
Discussion of Errors	17
Part II Interpretation	
Character of the Ocean Bottom Beneath the Ross Ice Shelf	41
Magnetic Interpretation and Its Contribution to the Knowledge of Ocean Bottom Materials	42
Determination of Rock Densities from a $\Delta g/\Delta h$ Plot	45
Amount of Overlying Low Density Material in Areas #1, 2, and 3 . . .	54
Source of the Gravity Anomalies in Areas where Densities were Determined	56
Source of the Gravity Anomalies over the Majority of the Ross Ice Shelf Area	57
Source of the Gravity Anomalies in the Roosevelt Island Area	58
Isostatic Status of the Ross Ice Shelf Area - Mean Free Air Anomaly.	59
Comparison of the Ross Ice Shelf Area with Fennoscandia - Two Former Ice Loaded Areas?	62
Summary	76
Acknowledgements	80
References	81
Appendix	85

Illustrations

Figure 1	Traverse Routes on Ross Ice Shelf.	2
Figure 2	Tidal Fluctuations in Southern Shelf Area as Indicated by Observed Gravity.	5
Figure 3	Free Air Anomaly Depths Compared with Seismic Depths (RIST). .	9
Figure 4	Free Air Anomaly Depths Compared to Seismic Depths (VLT 58-59, LAS-BT, DDT)	10
Figure 5	Traverse Z Intercomparisons.	14
Figure 6	Little America Station to Byrd Station Traverse (LAS-BS) . .	23
Figure 7	Ross Ice Shelf Traverse (RIST) Leg 1	24
Figure 8	Ross Ice Shelf Traverse (RIST) Leg 2	25
Figure 9	Ross Ice Shelf Traverse (RIST) Leg 3	26
Figure 10	Ross Ice Shelf Traverse (RIST) Leg 4	27
Figure 11	Little America Station to Mi 160 Byrd Trail (LAS-BT)	28
Figure 12	Victoria Land Traverse 1958-1959 (VLT 58-59) Leg 1	29
Figure 13	Victoria Land Traverse 1958-1959 (VLT 58-59) Leg 2	30
Figure 14	Discovery Deep Traverse (DDT).	31
Figure 15	Free Air Anomaly Map	32
Figure 16	Bouguer Anomaly Map.	33
Figure 17	Airborne Magnetic Flight High Jump 1947 (Total Magnetic Anomaly).	34
Figure 18	Magnetic Vertical Anomaly Map with Interpreted Regional. . .	35
Figure 19	Magnetic Horizontal Anomaly Map with Interpreted Regional. .	36
Figure 20	Magnetic Declinations on the Ross Ice Shelf.	37
Figure 21	Ocean Depth Map.	38
Figure 22	Calculated Magnetic Anomalies Produced by Two Dissimilar Bodies Lying at Different Depths.	46

Figure 23	$\Delta g/\Delta h$ Graph.	47
Figure 24	Slab Configurations Used in Computing Density Errors	50
Figure 25	Crustal Rise Diagram	64
Figure 26	Crustal Rise Diagram Assuming Sedimentation Contemporary with Adjustment	70
Figure 27	Schematic Section LAS to Skelton Glacier	79

Tables

	Page
Table 1. Listing of Data Sources	3
Table 2. Calibration of Arvela No. 149	11
Table 3. Mean Monthly Z Values at LAS Compared for Years 1957 and 1958	15
Table 4. Gravity Meter Drift Control (RIST) Frost C-3-65	18
Table 5. Traverse Absolute Gravity Ties	19
Table 6. Estimated Gravity Errors	20
Table 7. Horizontal Magnetometer Compared with the Absolute Base at LAS	22
Table 8. Velocity Section for the Little America Area, Antarctica	41
Table 9. Estimated Errors in Δh and Δg	48
Table 10. Maximum Errors in Calculated Densities Due to Errors in Gravity and Bottom Elevation Determinations	49
Table 11. Effect of Slope on Density Calculations	51
Table 12. Densities Computed from Free Air Anomaly Differences .	55
Table 13. Mean Free Air Anomalies and Depths in the Ross Ice Shelf Area	61
Table 14. Comparison of Uplift in Fennoscandia with the Assumed Uplift in the Ross Ice Shelf Area	67
Table 15. Computed Time (t) Since Load Removal Corresponding to Variations in the Estimated Mean Total Ice Thickness (T)	68
Table 16. Calculated Values of Sedimentary Deposition (R _t) since Ice Load Removal	72

PART I

DATA REDUCTION

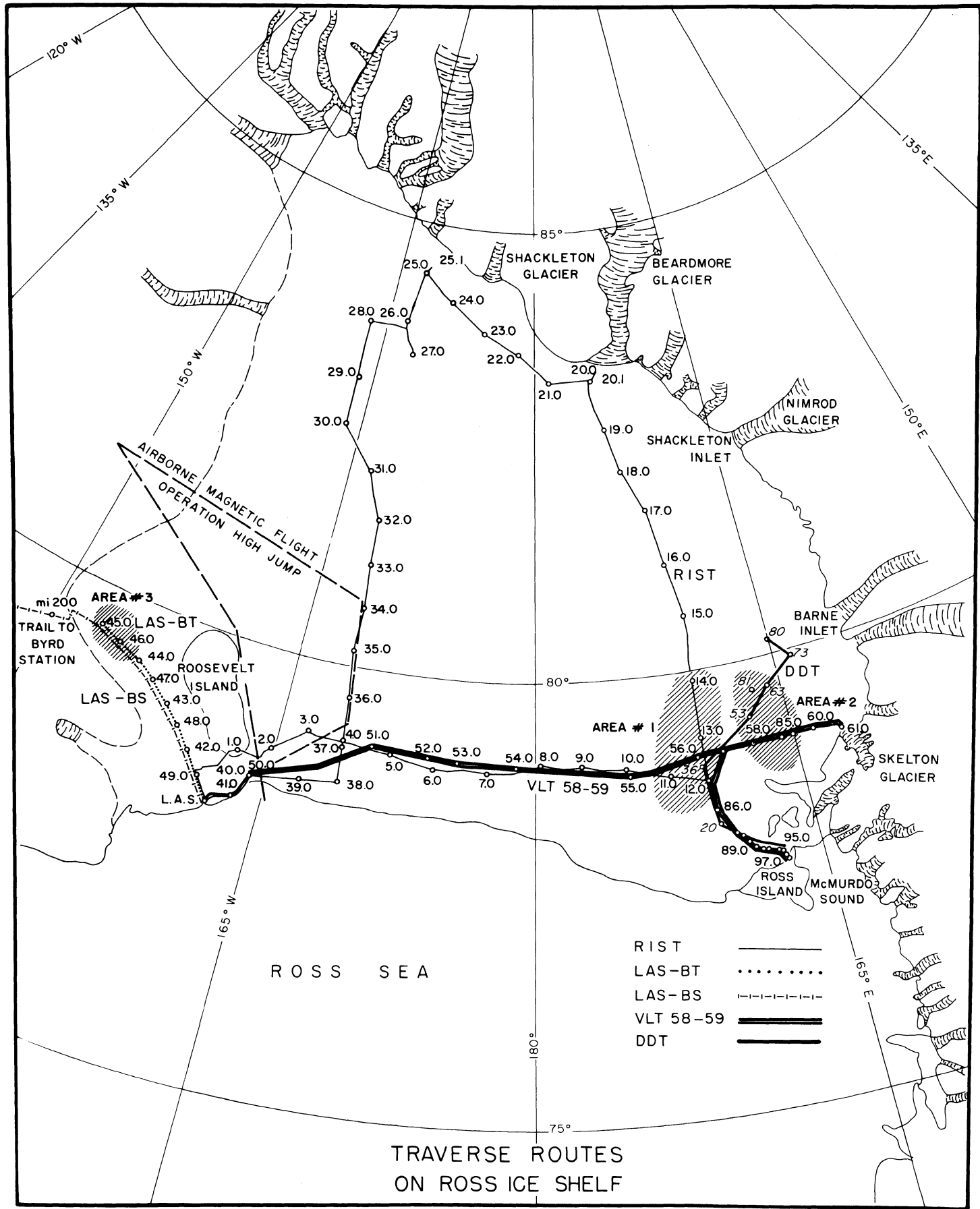


Figure 1

INTRODUCTION

The following report contains a compilation and interpretation of all the gravity and magnetic data collected on the Ross Ice Shelf by recent ground traverses. An airborne magnetic profile, flown during operation High Jump (1947), is also included. A map, showing individual traverse routes on the ice shelf, is presented in Figure 1 and data sources are listed in Table 1. The data are given in the Appendix.

Table 1

Listing of Data Sources

Traverse	Data Obtained on the Ross Ice Shelf
1. Airborne Magnetic Survey (Flux Gate) Little America, High Jump 1947	F
2. LAS-BS (Little America Station to Byrd Station Traverse, Jan.-Feb., 1957)	A,G
3. RIST (Ross Ice Shelf Traverse, Oct. 1957- Feb. 1958)	A,B,C,D,E,G
4. LAS-BT (Little America Station Byrd Trail Traverse, Mar.-Apr. 1958)	A,B,C,D
5. VLT-58-59 (Victoria Land Traverse, Oct. 1958- Jan. 1959)	A,B,C,D,E,G
6. DDT (Discovery Deep Traverse Feb.-Mar. 1960)	A,B,C,E,G

Key

- A - Observed gravity
- B - Seismic depths to ocean bottom
- C - Vertical magnetic intensity (Z)
- D - Horizontal magnetic intensity (H)
- E - Magnetic declination (D)
- F - Total magnetic intensity (F)
- G - Altimeter Elevations

ALTIMETRY SURVEY

The altimeters used by all ground parties on the Ross Ice Shelf were Wallace and Tiernan type FA-176 with a range of -150 to 500 m and a reading accuracy of about .2 meter. The temperature effect on this model, as listed by the manufacturer, is 1 part in 5000 for a 5°C change; the sensitivity is approximately .2 m.

On the Ross Ice Shelf Traverse (RIST) a "leap frog" type altimetry survey was used, whereby one of the three altimeters was always stationary. On the remaining traverses an "interval" method was used in which pairs of altimeters were read simultaneously, the trailing altimeter read in the position previously occupied by the leading one. The former method is thought to give greater accuracy.

The survey was controlled by measurements to sea level at three locations: Little America Station (LAS), station 41.0 (RIST), and station 97.0 (VLT 58-59). The closures on loops from McMurdo Sound (97.0) to near LAS (41.0) and from station 4.0 counterclockwise to 37.0 (RIST) were 11 m and 22 m respectively.

For a detailed discussion of the altimetry data reduction see Crary et al., 1962.

GRAVITY SURVEY

1. Instruments

With the exception of the LAS-BT party, which used a Worden geodetic gravity meter (No. 291) with a calibration constant of 0.10514 mgal/scale division, traverses used Frost thermostatically heat controlled meters of low drift rate. The LAS-BS party used Frost No. 47 which was operated at a temperature of 29°C and is known to have a low drift rate (unmeasurable for $1\frac{1}{2}$ years according to C. R. Bentley, personal communication). Its calibration constant is 2.667 mgal/scale division. The remaining traverses used Frost No. C-3-65, maintained at a temperature of 42°C. The calibration constant for this meter was 0.08598 mgal/scale division and its range without reset was about 150 mgal.

2. Method

Two types of vertical motion of the ice shelf influenced the manner in which gravity measurements were obtained. The first type is a long period (24 hr.) oscillation, due to ocean tides, and was measured with the gravity meter at LAS during June 1957 (Thiel et al., 1960). To compensate for this effect, several gravity measurements, separated by intervals of a few hours, were made at each seismic station.

On the RIST traverse these readings varied in a cyclic pattern over a range of 0.5 mgal. At stations 13.0 and 26.0, occupied during full moon periods, and at stations 18.0 occupied 4 days before the new moon, and 20.0 the fluctuation in readings indicates tidal causes. At station 34.0 which was occupied for 3 days, an attempt was made to observe tidal changes with the gravity meter. These readings did not show a 24 hour tidal component as might be expected from the tidal studies at LAS. However, this station was occupied during the first quarter phase of the moon; tides were therefore at their minimum amplitude and could easily have gone undetected (tides at LAS were about $\frac{1}{4}$ their maximum during the first and last quarter in June 1957).

TIDAL FLUCTUATIONS IN SOUTHERN SHELF AREA
AS INDICATED BY OBSERVED GRAVITY

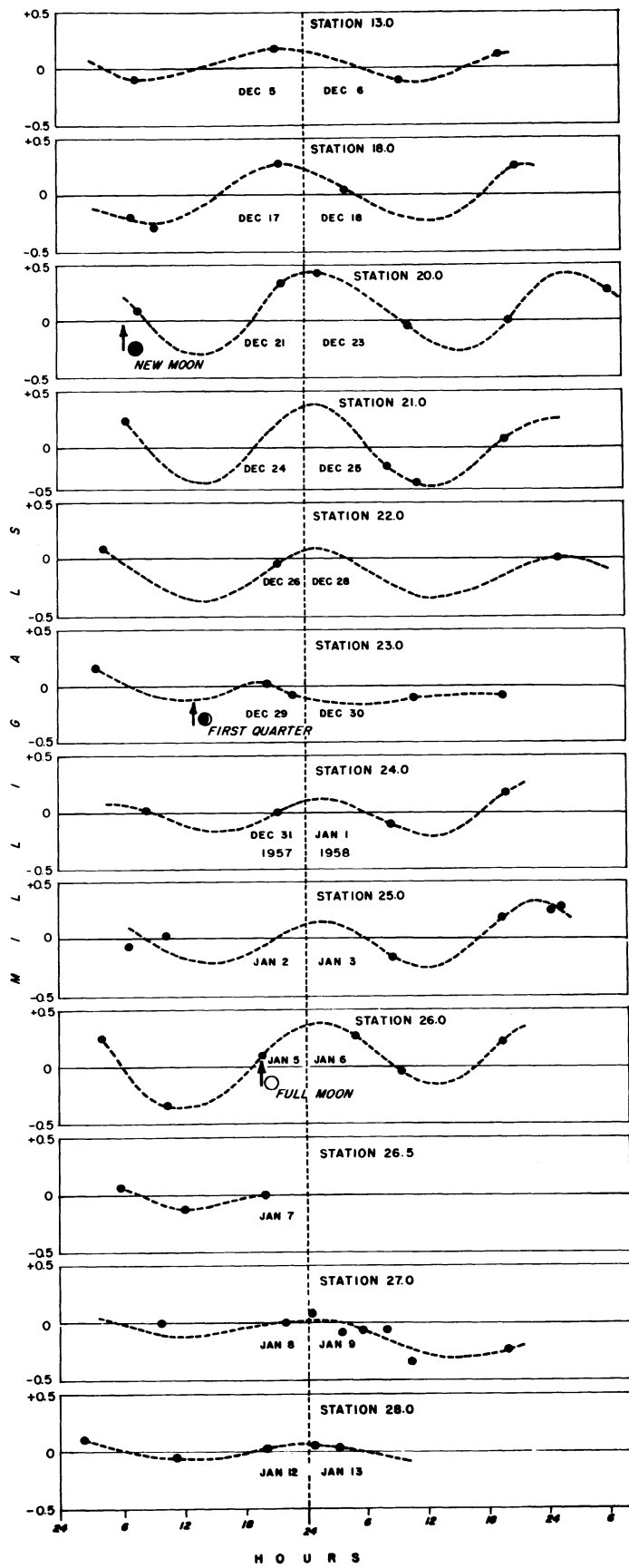


Figure 2

Due to a lack of tidal information in the Ross Sea area for the period of the RIST, it is impossible to show conclusively that the fluctuations in gravity readings were due only to tides. However, when the observed gravity fluctuations are compared with the phases of the moon for stations 13.0, 18.0, and 20.0 to 28.0 (Fig. 2), it appears that the tidal component is the major cause. Figure 2 also shows that tides are detectable in the far southern reaches of the Ross Ice Shelf. The 0.5 mgal variation in gravity corresponds to a 1.9 m vertical motion of the ice shelf (neglecting earth tides).

The second type of vertical motion was of a much shorter period (20-50 sec) and smaller amplitude. This type of motion was recorded by the oscillations of the gravity meter cross hair. To compensate for this type of oscillation, measurements were obtained by averaging 5 second readings of the cross hair position over a 5 minute interval and applying the correction obtained to the dial reading.

The short period motions diminished with an increase in sea ice cover adjacent to the ice shelf.

i. At LAS in January 1957, the gravity meter cross hair oscillation was so large that no reading could be obtained. In March, when sea ice had begun to form in Kainan Bay, the oscillations were small enough that the meter could be read.

ii. Short period oscillations increased in amplitude during the first leg of the RIST traverse (which paralleled the ice front), probably reflecting a decrease in sea ice cover to the north. Near station 4.0 (RIST) on the return leg to LAS, the short period amplitudes were greater than on the outgoing leg.

iii. This same phenomena of increase in amplitude with onset of austral summer has been observed by other traverses on the Ross Ice Shelf (S. L. DenHartog and J. G. Weihaupt, personal communication).

The short period motions also decreased with distance from the ice shelf edge.

i. Along the front of the ice shelf it was necessary to average cross hair readings as indicated above; it was not necessary at stations farther "inland" because the cross hair no longer oscillated.

ii. A short traverse to mile 40 on the Byrd Trail in April 1957 showed the oscillations to be considerably damped at mile 7 and absent at sites farther "inland" (also see Thiel et al., 1960).

The amplitude of the short period oscillations at LAS was about 0.4 mgal in April 1957; for a sinusoidal period of 20 to 50 sec, the computed vertical motion is between 0.08 and 0.5 mm. These motions are probably due to ocean waves.

3. Control

Reoccupation of stations and airborne gravity ties afforded good control for the gravity data collected on the Ross Ice Shelf.

i. Some of the stations of the LAS-BS traverse were reoccupied a year later by the LAS-BT traverse, making it possible to compare two sets of observed values.

ii. Several flights to RIST stations provided a means of determining the drift rate of their Frost No. C-3-65 meter. The Worden meter No. W283 was used to make ties between Scott Base and stations 14.0, 15.0, and 16.0; the LaCoste Romberg meter No. 1 tied stations 15.0, 20.0 (Beardmore Camp), and 23.5A to the McMurdo Sound pendulum station. The return to LAS provided a gravity closure for the RIST. Changes in gravity at LAS over the 3½ month period were probably negligible, since the ocean bottom is relatively flat beneath LAS and the horizontal ice movement there is estimated at only 270 m/yr. (Crary et al., 1962).

iii. The LAS-BT party overlapped its outgoing leg on the return trip so that, in spite of having a meter with a greater drift rate, the re-occupation of stations permitted adequate drift control.

iv. The VLT 58-59 party overlapped a portion of its route, and the DDT party returned to McMurdo Sound over its outgoing route.

4. Reduction

Because of the uncertainty in attempting to correct for ocean tides, all gravity values at each station were averaged and entered into a computer, with station latitude, longitude and elevation, to obtain free air anomalies based on the international gravity formula. Terrain correction was not necessary because of the flatness of the ice shelf and the fact that stations were far enough from any mountains to make their effect negligible. The ocean bottom under the ice shelf is flat (most slopes under 1°, Crary et al., 1962).

Changes in ocean bottom elevation, based on differences in free air anomalies between gravity stations, were computed using the formula for the gravitational attraction of an infinite slab:

$$\Delta g = 2\pi \gamma \Delta \rho \Delta h = .041393 \Delta \rho \Delta h \quad (1)$$

where Δg = difference in gravitational attraction between stations (mgal)

γ = the gravitational constant $6.673 \times 10^{-8} \text{ cm}^3 \text{ gm}^{-1} \text{ sec}^{-2}$
(Heyl and Chrzanowski, 1942; see Heiskanen and Vening Meinesz, 1958)

$\Delta \rho$ = density contrast between ocean and bottom materials (gm/cm^3)

Δh = change in ocean bottom elevation between stations (meters)

To determine how well free air anomalies reflected the change in ocean bottom, unadjusted ocean depths calculated from free air anomalies were compared with the bottom profile determined from seismic soundings. For this comparison, densities of 2.67 gm/cm^3 , 2.2 gm/cm^3 , and 2.0 gm/cm^3 were assumed for the bottom materials (14.5, 20.4, and 24.6 m/mgal respectively). The density of sea water was assumed to be 1.03 gm/cm^3 . The results showed that, in general, there is poor correlation between free air anomalies and ocean depths (see Figs. 3 and 4).

The "free air depths" computed for all stations were adjusted to the seismic stations by linearly distributing the error, determined between consecutive seismic stations, over the intervening distance. The densities assumed for these calculations were 2.67 gm/cm^3 for the ocean bottom materials and 1.03 gm/cm^3 for the ocean. These adjusted "free air depths" are plotted on all the traverse profiles (Fig. 6 through 14).

Bouguer anomalies were computed by assuming the ocean to be filled with material of density 2.67 gm/cm^3 . Since the intermediate station depths were computed on the basis of gravity, not an independent study, the Bouguer anomalies computed using these depths should yield no new information. In areas where free air anomalies reflect ocean topography well, the difference in Bouguer anomalies would be uniformly distributed between seismic stations; in areas of poor correlation, the Bouguer anomalies would merely be a manifestation of this poor correlation. For this reason the Bouguer anomalies were computed at seismic stations only. The free air and Bouguer anomaly maps are shown in Figs. 15 and 16. Free air and Bouguer anomalies are plotted on traverse profiles in Figs. 6 through 14.

MAGNETIC SURVEY

1. Instruments

The instrument used on the RIST, LAS-BT, and the VLT 58-59 traverses for measuring the vertical magnetic component of the earth's field (Z) was the Arvela No. 149, Model T-7 null type magnetometer. This instrument consists of a bar magnet suspended on a metal fiber with a nulling magnet attached to the reading scale. The instrument is equipped with an adjustable temperature compensating magnet which permitted reduction of the temperature coefficient to $1.5\gamma/\text{°C}$ before the start of the RIST. Over the period of its use in traverse work, the magnetometer was calibrated several times; results are shown in Table 2. This instrument can measure differences in the vertical magnetic field (Z) of $\pm 10\gamma$.

FREE AIR ANOMALY DEPTHS COMPARED WITH SEISMIC DEPTHS (RIST)
(NOT TIED TO SEISMIC DEPTHS)

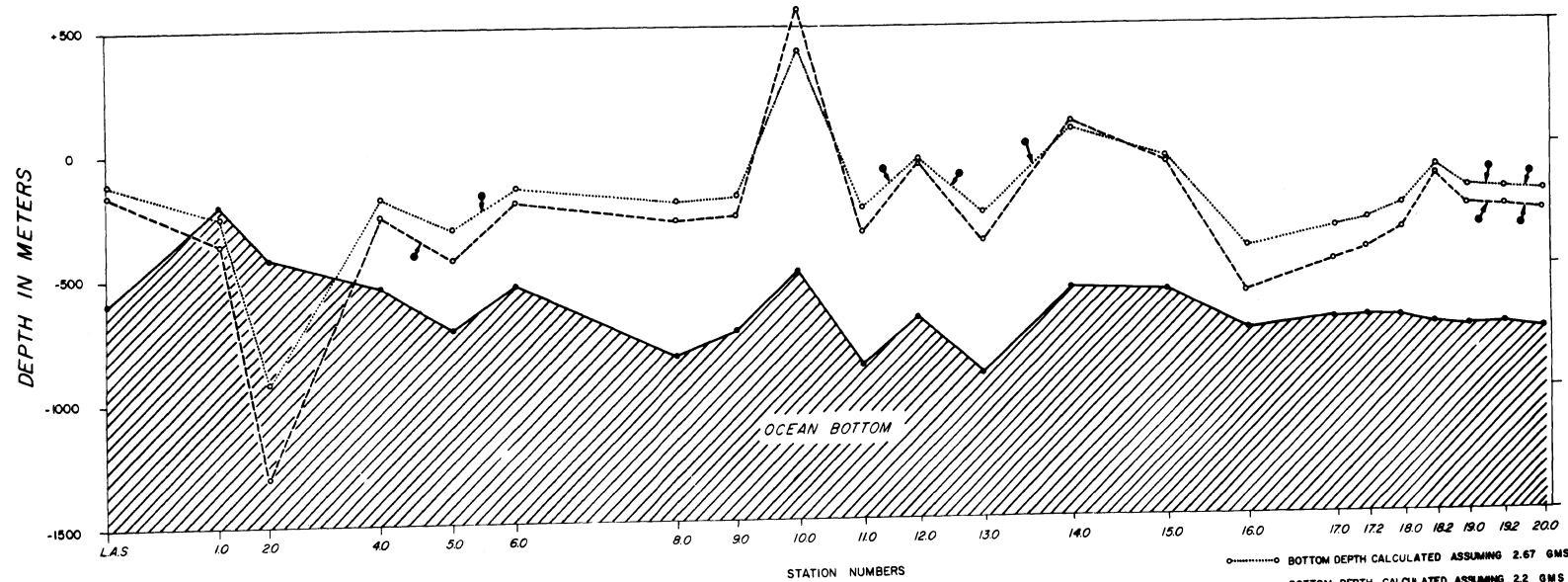
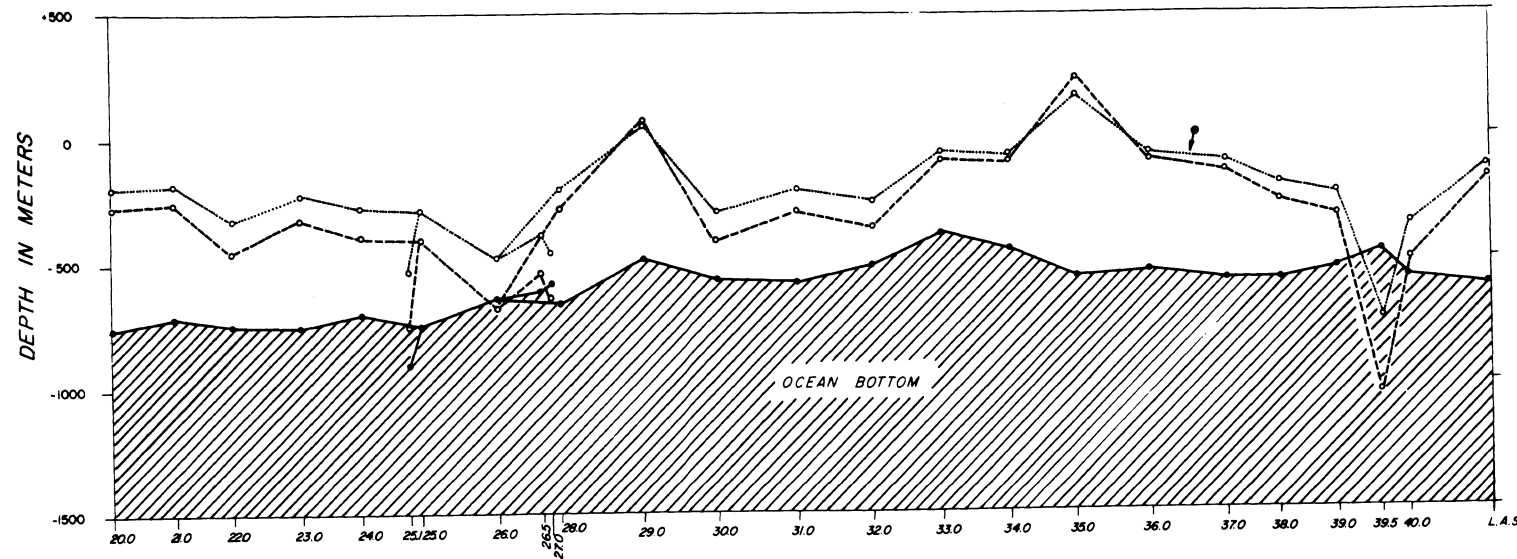


Figure 3

O-----O BOTTOM DEPTH CALCULATED ASSUMING 2.67 GMS/CM³
 O---●--- BOTTOM DEPTH CALCULATED ASSUMING 2.2 GMS / CM³
 ─●─ BOTTOM DEPTH FROM SEISMIC SHOTS
 ─●─ BOTTOM CORRELATES BEST WITH CURVE INDICATED

FREE AIR ANOMALY DEPTHS COMPARED TO SEISMIC DEPTHS (NOT TIED TO SEISMIC DEPTHS)

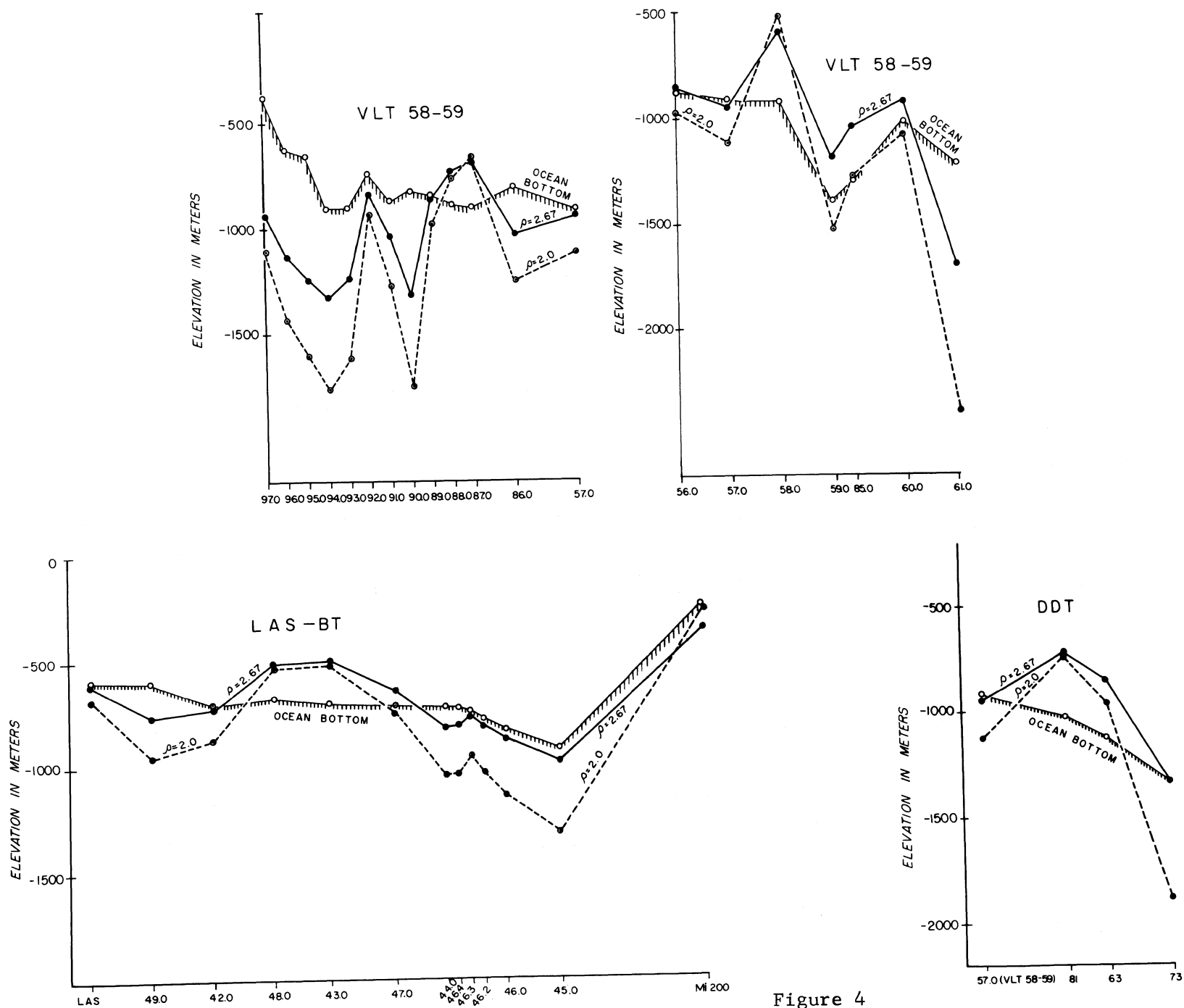


Figure 4

TABLE 2
Calibration of Arvela No. 149

<u>Location</u>	<u>Calibration</u>	<u>Method</u>	<u>Date</u>	<u>Temp. Coeff.</u>	<u>Vertical Magnetic Field (Z) at Cal- ibration Site</u>
LAS	-26.3γ/dial div.	instrument coil	8 Oct.57	+1.5γ/°C	~63,900γ
Station 11.0	-27.4γ/dial div.	instrument coil	2 Dec.57	---	~65,000γ
LAS-Scott Base	-27.5γ/dial div.	tie between LAS-Scott to Base 5,545γ range	10 Dec.57 to 8 Feb.58	---	~63,900γ to 69,450γ
LAS	-26.1γ/dial div.	instrument coil	8 Feb.58	+2.0γ/°C	~63,900γ
LAS	-26.1γ/dial div.*	instrument coil	1 Sept.58	---	"
Scott Base	-28.7γ/dial div.*	instrument coil	7 Oct.58	---	~69,450γ
Scott Base	-28.7γ/dial div.*	instrument coil	27 Jan.59	---	"

* L. D. McGinnis, personal communication.

It is apparent from Table 2 that the instrument calibration varies slightly with the vertical magnetic field. For this reason, a calibration of -27.5γ/dial division was used for magnetic latitudes between LAS and Scott Base and a calibration of -26.1γ/dial division for magnetic latitudes lower than LAS. All southern hemisphere magnetic values are treated as positive in this report.

The vertical instrument used on the DDT was the Askania torsion magnetometer No. 590623 with a calibration of 265.6γ/degree of twist. The calibration was determined in the Scott Base absolute magnetic hut using a Helmholtz coil. The temperature correction for this instrument was determined by Robinson (1962) to be about +17γ/°C for the temperatures encountered on the DDT. A smoothing of these data, discussed later, should reduce any large errors due to the measurable temperature influence on the instrument. This instrument has a measuring accuracy of better than ±10γ.

The horizontal magnetic component (H) was measured on the RIST, LAS-BT and VLT 58-59 traverses using the U. S. Coast and Geodetic Service transit magnetometer No. 38975. It was flown to the RIST near the Beardmore Glacier (station 18.2). The transit magnetometer measures the horizontal deflection produced on a compass needle by a standard calibrated magnet at a fixed distance and orientation. Unlike the vertical magnetometer, the transit magnetometer is an absolute instrument. The determination of H is made by solving the equation:

$$\log H = \log C - (t-20) \log(1+q) - \log \sin U \quad (2)$$

where C, q = constants dependent on the deflector magnet used

t= average temperature of the deflector magnet ($^{\circ}$ C)

U= deflection produced by the magnet

The measuring accuracy of this instrument is about $\pm 25\gamma$ on a day when there is little magnetic activity.

2. Method

One set of readings of the vertical magnetometer, comprising observations made every 5 to 10 minutes for a half hour period, was obtained at all stations on the VLT 58-59. On the RIST and LAS-BT traverses, one set was taken at intermediate stations and two or three sets at seismic stations; at seismic stations these sets were spread over a 36 to 48 hr. period. On the DDT two readings were usually taken at each station. The Arvela magnetometer, which is quite sensitive to horizontal orientation, was oriented to magnetic N at each station with a Brunton compass. The instrument is also affected by wind, due to openings in the sides of the case. Therefore, a windbreak of canvas and bamboo was used during observations.

With the transit magnetometer, two measurements of H (one hour apart) and one declination measurement (D) were generally made at seismic stations; one measurement of H was made at intermediate stations. A stake mounted Brunton compass was used exclusively to measure declinations on DDT and from LAS to station 18.2 on the RIST. Sun shots provided a reference azimuth for all declination measurements.

3. Control

During the period of traverse activities, two magnetic observatories were located in the Ross Ice Shelf area. One was at LAS where Z, H and D were recorded; the other, still in operation, is at Scott Base where the X, Y, and Z components were recorded. Magnetograms from both stations were used in the data reduction. These stations also provided absolute values to which the vertical instruments could be tied. At the beginning and end of the RIST and LAS-BT traverses, the vertical instrument was tied to LAS. On the RIST the instrument became unstable at station 11.0 and required adjustment. Later, while the party was at station 15.0, the Arvela was flown to Scott Base for a magnetic tie. The VLT 58-59 tied the Z instrument to LAS at the beginning of the traverse and to Scott Base at the end of the traverse. The DDT started and finished at Scott Base to which the vertical instrument was tied. Reoccupation of their own stations by the LAS-BT, VLT 58-59, and DDT parties also permitted better control of the vertical magnetic measurements.

Reoccupation of stations and closure were generally not undertaken for the horizontal instrument. It is an absolute instrument and more rugged than the two Z instruments used; therefore, it is probably less subject to drift. The horizontal instrument was compared with absolute H determinations at LAS following completion of the RIST and LAS-BT traverses (see errors section).

4. Data reduction

a). Vertical Component

Before the reduction of the RIST Z data, a comparison was made between the vertical magnetic activity at the field stations and at the magnetic observatories (LAS & Scott Base) for short ($\frac{1}{2}$ hr.) and long (over 36 hrs.) periods. Although no quantitative analysis was made, there appeared to be a general tendency for the magnetic activity at the field station to correlate with the closer base station. Therefore, corrections for vertical magnetic activity (both diurnal and other) were applied to the RIST data in proportion to the distance of the field station from each base station. From station 24.0 to LAS, however, the vertical magnetic observations were corrected exclusively to LAS. LAS-BT values were corrected to LAS (L. D. McGinnis, personal communication). A mean diurnal correction alone was applied to the magnetic values on the VLT 58-59 (L. D. McGinnis, personal communication); all Z values on the DDT were corrected to Scott Base (E. S. Robinson, personal communication). The diurnal corrections ranged between -80γ and $+130\gamma$ and the corrections taken directly from the magnetograms were generally under 150γ ; on five occasions, however, they approached or exceeded 400γ (stations 2.7, 9.1, 18.3, 24.1, and 37.1 RIST).

The traverses originated from different locations over a two year period. Since the secular magnetic change in the Ross Ice Shelf area is considerable, it is important to know the base value to which each traverse is tied and the time to which these base values correspond. The RIST and LAS-BT Z values were tied to an adopted base value of $63,894\gamma$ at LAS. This value corresponds to the mean Z value at LAS for March 1958. The VLT 58-59 data were originally tied to LAS using a preliminary base line value that was 240γ too low (as published by Crary et al. 1962). These data were subsequently corrected and tied to a base value at LAS of $63,805\gamma$, the mean Z value at LAS for November 1958. The DDT values were tied to an assumed value at Scott Base of $69,220\gamma$ for March 1960. This value is believed to be too low, based on the field comparison between the DDT values and those obtained on the McMurdo to South Pole Traverse (MSPT).

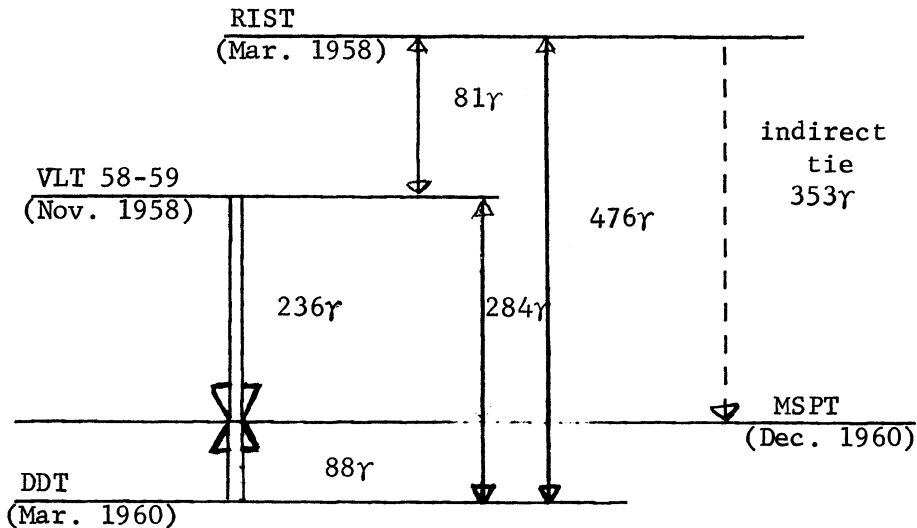
The MSPT overlapped several stations of the VLT 58-59 and DDT in the northwestern ice shelf area, providing a means of tying the Z values to an absolute measurement in the field. The MSPT made total magnetic intensity measurements (F) with a Varian M-49 precession magnetometer (Robinson, 1962) and dip measurements (I) with a CARL magnetometer (Meyer, 1961); therefore, the absolute value of Z can be calculated at the jointly occupied locations. From the comparison of values VLT 58-59 values are 236γ higher and DDT values are 88γ lower than MSPT values. Therefore to adjust the values of the VLT 58-59 and DDT to the absolute value of Z, determined from the MSPT measurements, -240γ and $+90\gamma$ respectively, were added to their observed Z values.

Other traverse intercomparisons were possible in the same general area, thus permitting an indirect adjustment of the RIST and LAS-BT values to the MSPT absolute Z value. The RIST Z values averaged 81γ higher than the VLT 58-59 values for stations in the same area. The RIST values also averaged higher ($+476\gamma$) than the DDT values for stations

which were jointly occupied. These two comparisons showed that the RIST Z values averaged about 353γ higher than the MSPT values. The RIST and the LAS-BT traverses were compared over that part of the Byrd Trail which they both traveled. Since the RIST values were only 30γ higher on the average, both traverses were considered to be in adjustment with each other. Therefore, to adjust the RIST and LAS-BT Z values to the MSPT values, -350γ was added to all Z observations of both traverses.

The accuracy of this method can be checked by determining the closure around three possible loops (see Figure 5). The direct comparison of VLT 58-59 values with DDT values in an overlap area showed VLT 58-59 values to be higher by 284γ . The indirect comparison between these two traverses (both compared with the MSPT) indicates VLT 58-59 values to be higher by 324γ , resulting in a 40γ discrepancy. Closure errors of 111γ and 71γ are found in the other two loops of Figure 5. All discrepancies can be explained, however, by assuming a $\pm 20\gamma$ error in each traverse value where intercomparisons were made. After adjusting all traverses to the absolute value of Z, determined by the MSPT, the values should be representative of December 1960.

Fig. 5
Traverse Z Intercomparisons



The secular change at LAS for the year 1957-1958 was determined by subtracting the mean hourly value at LAS for each month, July through December 1957, from the corresponding mean hourly value for the months July through December 1958. The average annual change at LAS was $-113\gamma \pm 11\gamma$ (Table 3). This value may be compared with a secular change of $-92\gamma/\text{yr}$ from 1929-1934 and of $-107\gamma/\text{yr}$ from 1934-1958 (Hatherton, 1961). Little error is introduced from ice movement since it is estimated at only 270 m/yr (Crary et al., 1962) and the gradient of Z at LAS is only about $9\gamma/\text{nautical mile}$. At Cape Evans, in the McMurdo Sound Area, the secular change was determined to be $-48\gamma/\text{yr}$ between 1911 and 1958 (Hatherton, 1961). Therefore, in the area where the traverse comparisons were made, the secular change should be somewhere between -113γ and $-48\gamma/\text{yr}$.

TABLE 3

Mean Monthly Z Values at LAS Compared for Years 1957 and 1958

	<u>1957</u> [*]	<u>1958</u> [*]	
July	63,994 gammas	63,911 gammas	- 83 gammas
August	63,999 "	63,889 "	-110 "
September	64,033 "	63,875 "	-158 "
October	63,957 "	63,843 "	-114 "
November	63,894 "	63,806 "	- 88 "
December	63,894 "	63,771 "	-123 "
		Mean	$-113\gamma/\text{yr} \pm 11\gamma$

* From Magnetograms and Hourly Values,
Little America, Antarctica, 1960.

From Figure 5 a secular change in the overlap area of $-113\gamma/\text{yr}$ is calculated using the direct tie of the VLT 58-59 to the MSPT value. A secular change of $122 \gamma/\text{yr}$ is determined from the tie between the RIST and VLT 58-59 values (a comparison using the same vertical instrument). These determinations suggest that the secular change in the overlap area is probably more than $100\gamma/\text{yr}$.

b). Total Field

On Operation High Jump in 1947 an airborne total intensity profile, using a flux gate magnetometer, was obtained in the vicinity of Roosevelt Island by J. R. Balsley of the U. S. Geological Survey and is published herein with his permission. The regional values were subtracted from the absolute values by Balsley, and the resulting anomaly profile is shown in Figure 17. The large $+770\gamma$ anomaly shown on the airborne profile was not recorded by ground parties in the same area; an error in flight navigation of ± 5 nautical miles could easily account for the discrepancy. Balsley estimates the flight navigation at ± 10 miles. At station 33.3 (RIST) an anomaly of $+225\gamma$, recorded by the ground party, agrees with the $+200\gamma$ to $+320\gamma$ anomaly recorded by the airborne party at the turning point between legs #2 and #3 (Z anomalies should be about 98% of total anomalies in this area). It is felt that the ground and airborne magnetic profiles over this area agree fairly well, within the limitations of the data and position errors.

c). Horizontal Component and Declination

The corrections for magnetic activity were made in the same manner for H measurements as for Z. Thus the horizontal values taken on the RIST were corrected to LAS and Scott Base on a proportional distance basis from stations LAS to 24.0; the remaining stations were corrected to LAS only. The LAS-BT traverse values were corrected to LAS. Corrections taken from the magnetograms averaged about -100γ and generally ranged between 0 and -200γ . At only three stations were the magnetogram corrections larger than -300γ ; two of these were near LAS (41.0 and 37.1); the third was station 30.5. The VLT 58-59 values were corrected for diurnal variation only, with corrections of -100γ to $+80\gamma$ (L. D. McGinnis, personal communication). All H observations were made within an 11 month period. The secular change at LAS (calculated as in section a) was found to be only $+45\gamma/\text{yr}$ $\pm 6\gamma$; therefore, no adjustment corrections were necessary. The declination measurements were averaged for each station with no correction made for magnetic activity.

d). Regional and Anomaly Maps of Z, H, and D.

Regional maps of Z, H, and D over the whole Ross Ice Shelf area were prepared by first drawing isomagnetic lines in areas which seemed to be relatively "smooth" and then using these lines as a guide in anomalous areas (Figs. 18, 19, and 20). These regional values were then used to obtain vertical (ΔZ) and horizontal (ΔH) anomalies. Because of the time base to which values were corrected, the regional map of Z is dated December 1960, and that of H, March 1958. For several reasons including closer station spacing, fewer readings per station, large temperature correction, and scatter of values when compared with MSPT measurements, the DDT Z anomaly values were smoothed before incorporating them with the other ΔZ values on the map (The anomalies on both sides of each station were averaged with the station anomaly). Regional and individual values of the total intensity (F), determined from the corresponding H and Z values corrected to March 1958, were used to obtain total intensity anomalies (see Appendix).

In determining the validity of a vertical intensity anomaly, several factors were considered. All anomalies less than 100γ to 150γ , depending on the distance from the recording base stations, were discounted. If the anomaly occurred regardless of whether data were corrected to LAS, to Scott Base, or left uncorrected, it was considered real. Further consideration was given to whether the anomaly occurred on a quiet or stormy magnetic day. Because of the high magnetic latitude, H anomalies were considered as confirmatory only.

In analyzing anomalies, the displacement (or disturbance) vector method (Heiland, 1940 and Jakosky, 1950) was employed. This method assumes that a vector of horizontal magnitude proportional to ΔH and vertical magnitude proportional to ΔZ parallels the magnetic field produced by the source of an anomaly. Considering the source a dipole, a rough estimate of the depth of the upper pole can be determined by noting where the displacement vector extensions intersect on a profile over the anomaly. The method, as used here, assumes that, (1) declinations are not anomalous, (2) linear anomalies are oriented perpendicular to the magnetic gradient, and (3) the profiles cross over the center of the anomaly. Corrections must be made for profiles not parallel to the magnetic field gradient by multiplying the depth obtained by $\cos \theta$, where θ is the angle between the profile direction and the magnetic gradient. Profiles of ΔZ , ΔH , ΔF , and the displacement vectors are found in Figures 7 through 14. In these figures the vertical scale is identical to the horizontal scale on the displacement vector profiles.

DISCUSSION OF ERRORS

1. Gravity Errors

a). Free air anomalies

Errors may be introduced into free air gravity anomalies in the process of applying corrections for latitude, elevation, instrument drift, and tides. Crary et al. (1962) state that the accuracy in position latitude is $\pm 0.5'$, equivalent to ± 0.25 mgal. Crary et al. have also made comparisons of ice thickness and elevation over the Ross Ice Shelf. All station elevations except one are within ± 13 m of the theoretical curve which takes into account the known surface densities and assumes the ice shelf to be floating in equilibrium (at station 28.0 RIST, the discrepancy is 18 m). The error in elevation is therefore estimated to be ± 13 m, corresponding to an error in the free air gravity anomaly of ± 4.0 mgal. Along the front of the ice shelf the error in closure from LAS to McMurdo Sound was only 11 m. In order that the estimated error in gravity anomalies be the same for all stations the elevation error along the front of the ice shelf is estimated at ± 9 m. In a later discussion of the average free air anomaly over the continental shelf, it is assumed that the errors in elevation, which make up the major part of errors in the free air anomaly, are random and therefore tend to cancel. This assumption is supported by the fact that the points in Crary's ice thickness vs. elevation plot tend to fall on both sides of the theoretical curve.

The airborne gravimetric ties were well spaced over the route of the RIST (Table 4), and the closure at LAS provided additional control for determining the drift rate of the meter. It is possible that a temperature jump, which occurred at station 5.0 (11°C), may have been responsible for the 4 mgal tare which showed up at station 14.0. An attempt to locate the tare by comparing ocean depths computed from free air anomalies with seismic depths proved unsuccessful, and the 4 mgal difference was finally distributed between LAS and station 14.0 on a time basis. The observed gravity on the RIST is therefore estimated to be within ± 2 mgal between LAS and station 14.0 and within ± 1 mgal at the remainder of stations.

TABLE 4
Gravity Meter Drift Control (RIST)
Frost C-3-65

<u>Station</u>	<u>Difference (traverse meter value minus airborne meter or reoccupation value)</u>	<u>Date</u>
LAS	0 mgal	23 Oct. 1957
14.0	+4.0 mgal	8 Dec. 1957
15.0	+5.0 mgal	9 Dec. 1957
16.0	+4.4 mgal	14 Dec. 1957
20.0	+4.3 mgal	22 Dec. 1957
23.5A	+4.2 mgal	31 Dec. 1957
LAS	+4.5 mgal	26 Feb. 1957

Many of LAS-BS gravity stations were reoccupied a year later by the LAS-BT party. Comparison of observed gravity was made at the 19 reoccupied stations; two differed by 2.4 mgal, two differed by 1.2 mgal and the rest were all within less than 1 mgal. On the basis of this comparison, the observed gravity of both traverses is probably within ± 1 mgal. Since the VLT 58-59 and the DDT parties both reoccupied several of their gravity stations and since both had relatively driftless meters, the observed gravity values on these traverses are also estimated to be within ± 1 mgal.

Gravity fluctuations on the Ross Ice Shelf due to tides were about ± 0.3 mgal (see Fig. 2). By averaging values measured at each station, the error due to this effect is reduced to an estimated ± 0.2 mgal. All traverses were indirectly tied to the pendulum station at McMurdo Sound where the scatter of observed values indicates an error of ± 0.5 mgal (Thiel, 1959). A tabulation of the traverses and their adopted base station gravity values is found in Table 5.

TABLE 5

Traverse Absolute Gravity Ties		
Traverse	Base Station with Adopted Gravity Value	Tied to the McMurdo Sound Pendulum Station with assumed Value of
(1) LAS-BS	(LAS) 982.9831 gal & (BS) 982.6009 gal	982.9928 gal
(2) RIST	(LAS) 982.9824 gal, (SB#1) 982.9926 gal, & McMurdo Pendulum Station	982.9923 gal
(3) LAS-BT	(LAS) 982.9831 gal	982.9928 gal
(4) VLT 58-59	(LAS) 982.9831 gal & (SB#1) 982.9920 gal	unknown
(5) DDT	McMurdo Pendulum Station	982.9928 gal

b). Bouguer anomalies

The error in Bouguer anomalies depends upon the accuracy with which the ocean bottom elevations are known. Errors in bottom elevation, determined by seismic soundings, arise from three general sources:

(1) errors in elevation, (2) errors in ice thickness determination, and (3) errors in the measurement of the water bottom reflection time. An error in elevation e_h will cause an error in the free air correction

$e_{fa} = 0.31 e_h$. However, since an error in elevation will create a corresponding error in ocean depth, the Bouguer anomaly error will be only $0.31 - 0.07 = 0.24$ times e_h ; for a ± 13 m elevation error this amounts to

± 3.1 mgal. An estimated error of ± 20 m in ice thickness leads to an error of ± 7 m in the water depth and thus to a ± 0.5 mgal gravity error. An estimated error in reflection time of ± 0.005 sec leads to a depth error of ± 3.5 m, thus an error of ± 0.24 mgal. The estimated error in the Bouguer anomalies, due to the combined errors in elevation and seismic measurements, is ± 3.8 mgal.

Because the ice shelf and ocean bottom are reasonably flat (most slopes under 1° , Crary et al., 1962) no terrain corrections were necessary on the Ross Ice Shelf and any errors introduced by terrain are considered negligible. The estimated absolute and relative errors in gravity are summarized in Table 6.

TABLE 6

ESTIMATED GRAVITY ERRORS

Source of Error	Estimated Error in Free Air Anomalies	
	Absolute Error	Relative Error (between consecutive stations of the same traverse)
(1) Elevation	± 2.8 mgal (± 9 m; LAS-14.0) ± 4.0 mgal (± 13 m; all other stations)	0.6 mgal (2 m)
(2) Latitude	± 0.3 mgal ($\pm .5'$)	0.5 mgal (1.0')
(3) Instr. Drift	± 2.0 mgal (LAS-14.0) ± 1.0 mgal (all other stations)	0.3 mgal (estimated) ---
(4) Earth & Ocean tides	± 0.2 mgal	0.2 mgal
(5) Pendulum Value	± 0.5 mgal	---
	~± 6.0 mgal	~1.5 mgal

Source of Error	Estimated Error in Bouguer Anomalies	
	Absolute Error	Relative Error
(1) Elev. & Seismic	± 2.9 mgal (LAS-14.0) ± 3.8 mgal (all other stations)	1.9 mgal (2 m elev. 23 m bottom error)
(2) Latitude	± 0.3 mgal ($\pm .5'$)	0.5 mgal (1.0')
(3) Instr. Drift	± 2.0 mgal (LAS-14.0) ± 1.0 mgal (all other stations)	0.3 mgal (estimated) ---
(4) Earth & Ocean tides	± 0.2 mgal	0.2 mgal
(5) Pendulum Value	± 0.5 mgal	---
	~± 6.0 mgal	~3.0 mgal

Note: At a later date, after the observed gravity, free air gravity, and Bouguer gravity values were computed, a value of 982.9919 gals was adopted for the pendulum station at McMurdo Sound (Behrendt et al., 1962b). The final values of observed gravity, free air anomalies and Bouguer anomalies should therefore lie between 0.4 and 0.9 mgal below the computed values indicated in this paper.

2. Magnetic Errors

a). Vertical component

The absolute error in Z has two general sources. The major source, due to the inability to correct for magnetic activity, is estimated to be $\pm 100\gamma$ at seismic stations and $\pm 150\gamma$ at intermediate stations. A second source of error is introduced by a combination of three factors: 1) variation in the instrument scale value over the range of Z encountered on the ice shelf, 2) error in the determination of the adjustment corrections, and 3) variation of secular change over the ice shelf (error results from the adjustment of Z values). The error due to the combination of these factors is estimated at $\pm 70\gamma$ for the Southern areas of the ice shelf.

The absolute vertical magnetic values, after adjustment to the absolute Z value measured by the MSPT, are probably correct to an estimated $\pm 170\gamma$ at seismic stations and $\pm 220\gamma$ at intermediate stations in the southern ice shelf area. Since, in the northern areas of the ice shelf, the secular change is better known and the field stations are closer to the magnetic observatories, the absolute Z values should be more accurate.

The relative error in Z between stations was determined from the standard deviation of the observed values at seismic stations (equation 3). For the observations taken on the RIST, the standard deviation was 88γ from the uncorrected values and 63γ from the corrected values (using magnetograms from LAS and Scott Base). The smaller standard deviation of the corrected values clearly indicates that the standard type of correction did reduce the errors slightly. With 95% confidence, it can be said that the relative error is $\pm 125\gamma$. Since the difference between the observed value and the mean at each station was independent of time (up to at least 60 hrs.) the relative error is probably applicable over distances as large as the anomalies determined on the Ross Ice Shelf. Note that the standard deviation of observed values gives some measure of the inability to correct for magnetic activity.

$$\sigma = \left[\frac{\sum_{i=1}^m \sum_{j=1}^{n_i} (Y_{ij} - \bar{Y}_i)^2}{N - m} \right]^{\frac{1}{2}} \quad (3)$$

where m = number of seismic stations used

n_i = number of measurements at station i

N = total number of measurements

\bar{Y}_i = mean of the measurements at station i

Y_{ij} = measurement j at station i

(Note: for Z measurements, $m = 40$, $N = 98$)
for H measurements, $m = 24$, $N = 48$)

b). Horizontal component

After the RIST and LAS-BT traverses, the transit magnetometer was compared with measurements made in the LAS absolute magnetic hut to determine the accuracy of the instrument. The results are given in Table 7.

TABLE 7

Horizontal Magnetometer Compared with the Absolute Base at LAS

<u>Set No.</u>	<u>Time</u>	<u>Instrument</u>	<u>LAS Absolute Hut</u>	<u>Difference (Instr.-LAS)</u>
1	2220 Feb. 8, 1958	11,267 γ	11,278 γ	-11γ (Moderate activity)
2	2240 Feb. 8, 1958	11,388 γ	11,362 γ	+26γ (Strong activity)
3	2205 Feb. 18, 1958	11,121 γ	11,176 γ	-55γ (Moderate activity)
4	0147 May 5, 1958	11,296 γ	11,286 γ	+10γ (Quiet)
5	0207 May 5, 1958	11,298 γ	11,286 γ	+12γ (Quiet)
6	0239 May 5, 1958	11,324 γ	11,301 γ	+23γ (Quiet)

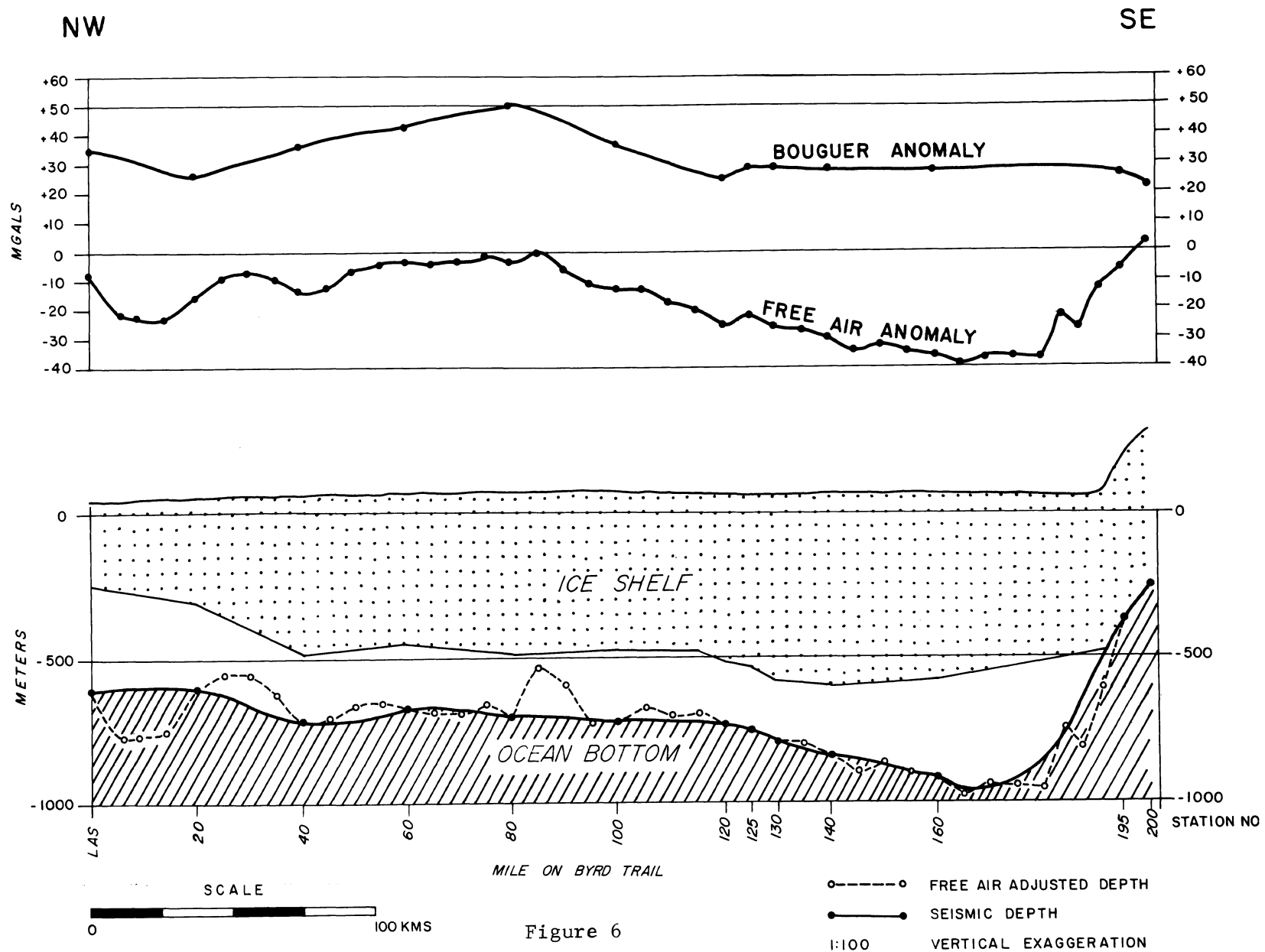
On the basis of Table 7 the absolute accuracy of the instrument is estimated to be $\pm 50\gamma$. The horizontal magnetic activity is slightly less than the vertical activity at these latitudes, therefore the estimated absolute error in H is $\pm 125\gamma$ at seismic stations and $\pm 150\gamma$ at intermediate stations.

The standard deviation of observed H at seismic stations on the RIST was determined to be $\pm 50\gamma$ for uncorrected values and $\pm 49\gamma$ for corrected values. Since all measurements at the seismic stations were made only one hour apart, it is reasonable to infer that the magnetogram corrections do not improve data that have been taken over a period of less than one or two hours. The relative error in H cannot be determined from the above standard deviations because of the short time interval between measurements. The relative error in H is probably near that for Z and is estimated at $\pm 100\gamma$.

c). Declination

The maximum variation in declination at LAS during the period of the magnetic survey was about 4° during a very active magnetic storm; most of the variations were less than 1° . It is probable, therefore, that the measured declinations are accurate to within $\pm 1^\circ$.

LITTLE AMERICA STATION TO BYRD STATION TRAVERSE
(LAS - BS)



ROSS ICE SHELF TRAVERSE (RIST)
LEG I

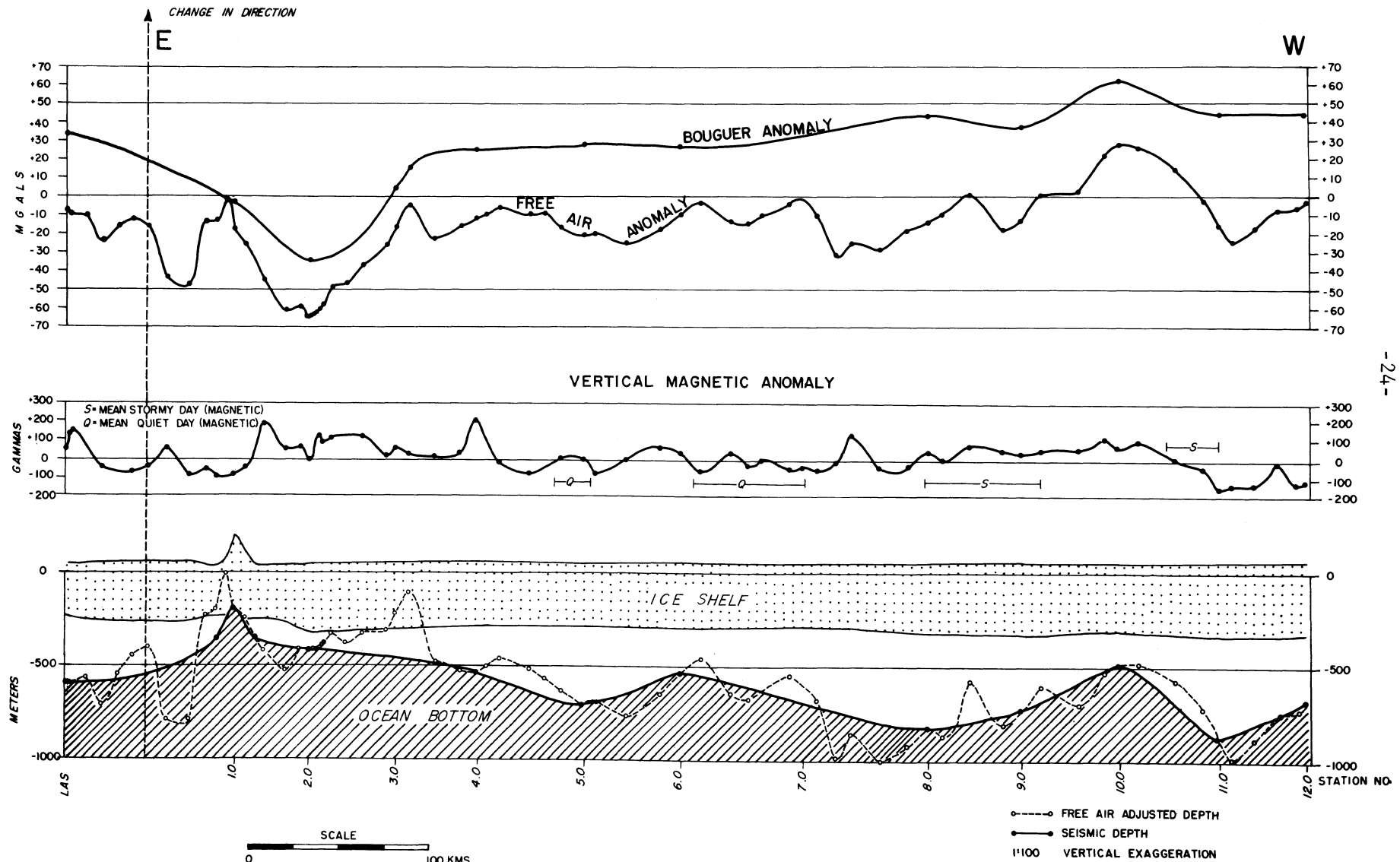


Figure 7

ROSS ICE SHELF TRAVERSE (RIST)
LEG 2

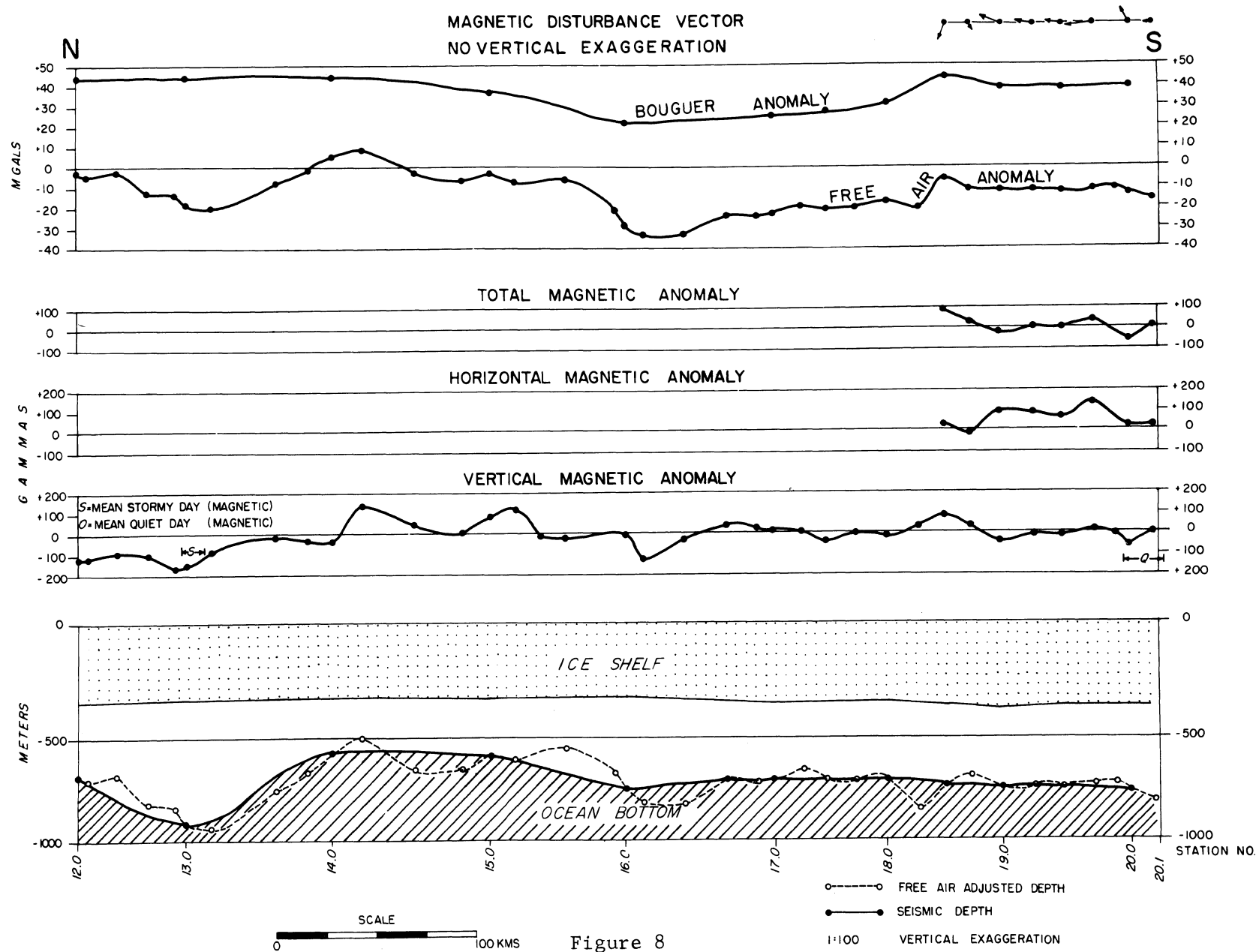


Figure 8

ROSS ICE SHELF TRAVERSE (RIST)

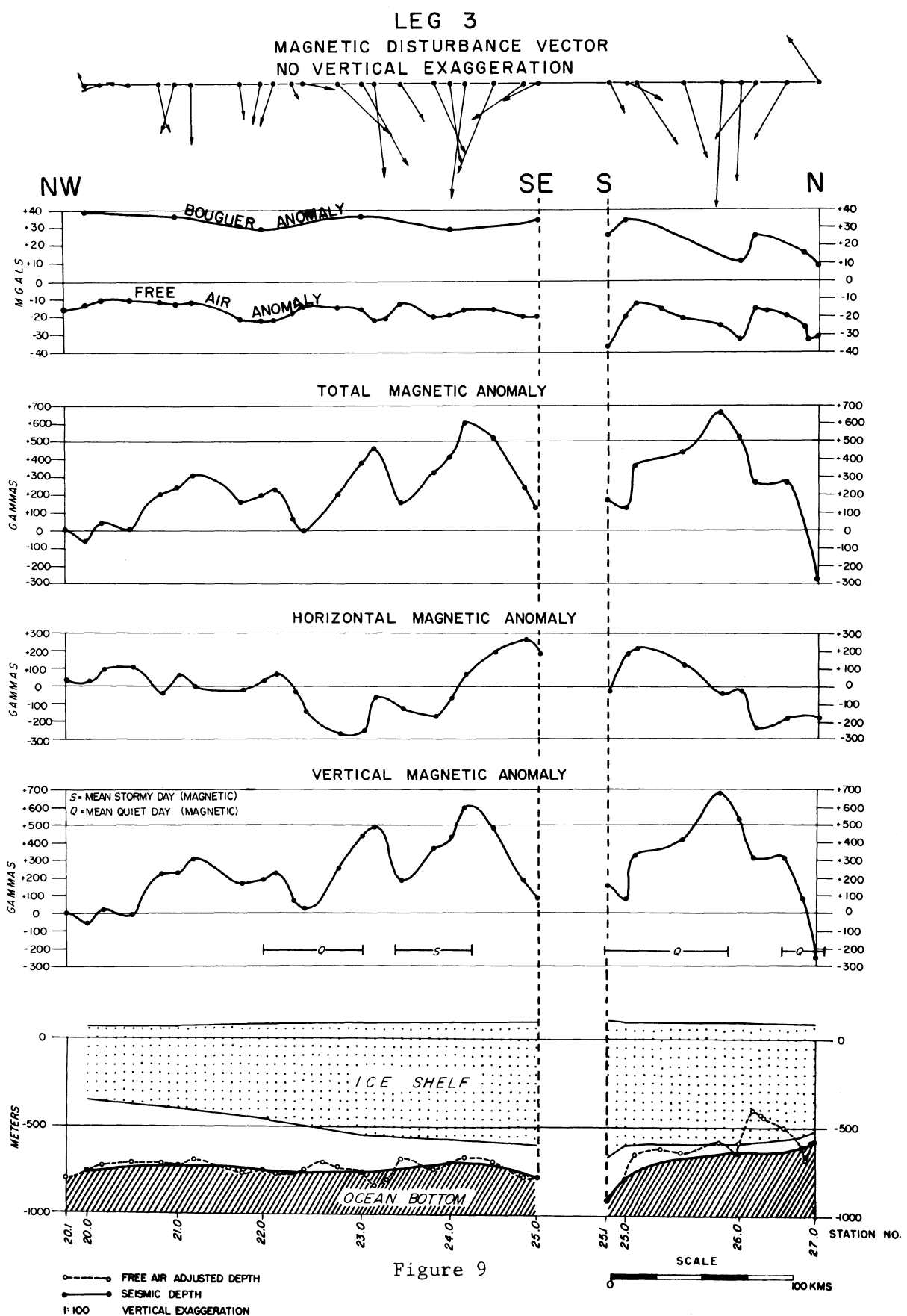


Figure 9

ROSS ICE SHELF TRAVERSE (RIST)

LEG 4

MAGNETIC DISTURBANCE VECTOR
NO VERTICAL EXAGGERATION

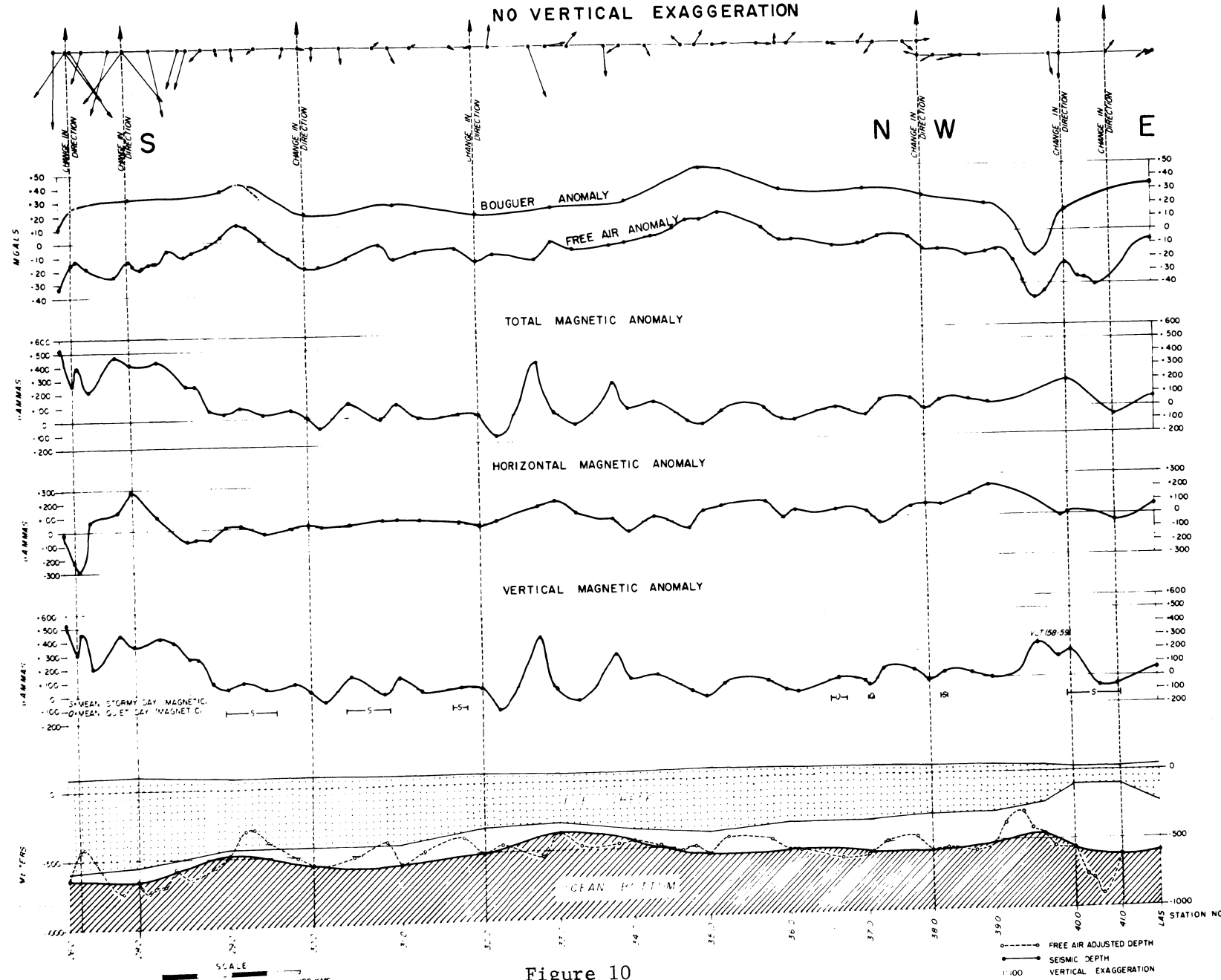


Figure 10

LITTLE AMERICA STATION TO MI 160

BYRD TRAIL (LAS-BT)
MAGNETIC DISTURBANCE VECTOR
NO VERTICAL EXAGGERATION

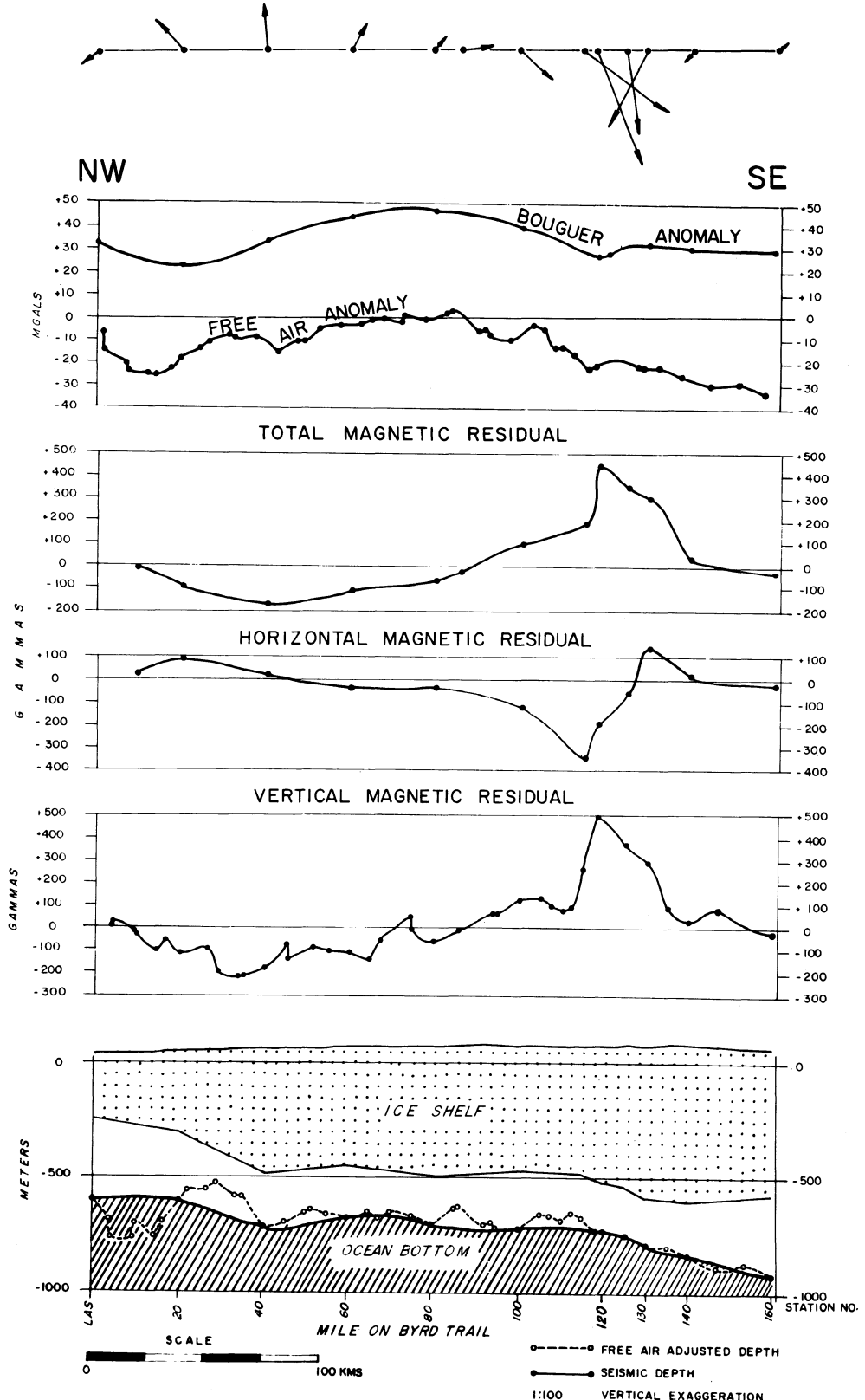


Figure 11

⁻²⁹⁻
VICTORIA LAND TRAVERSE 1958-1959 (VLT 58-59)

LEG I

MAGNETIC DISTURBANCE VECTOR
NO VERTICAL EXAGGERATION

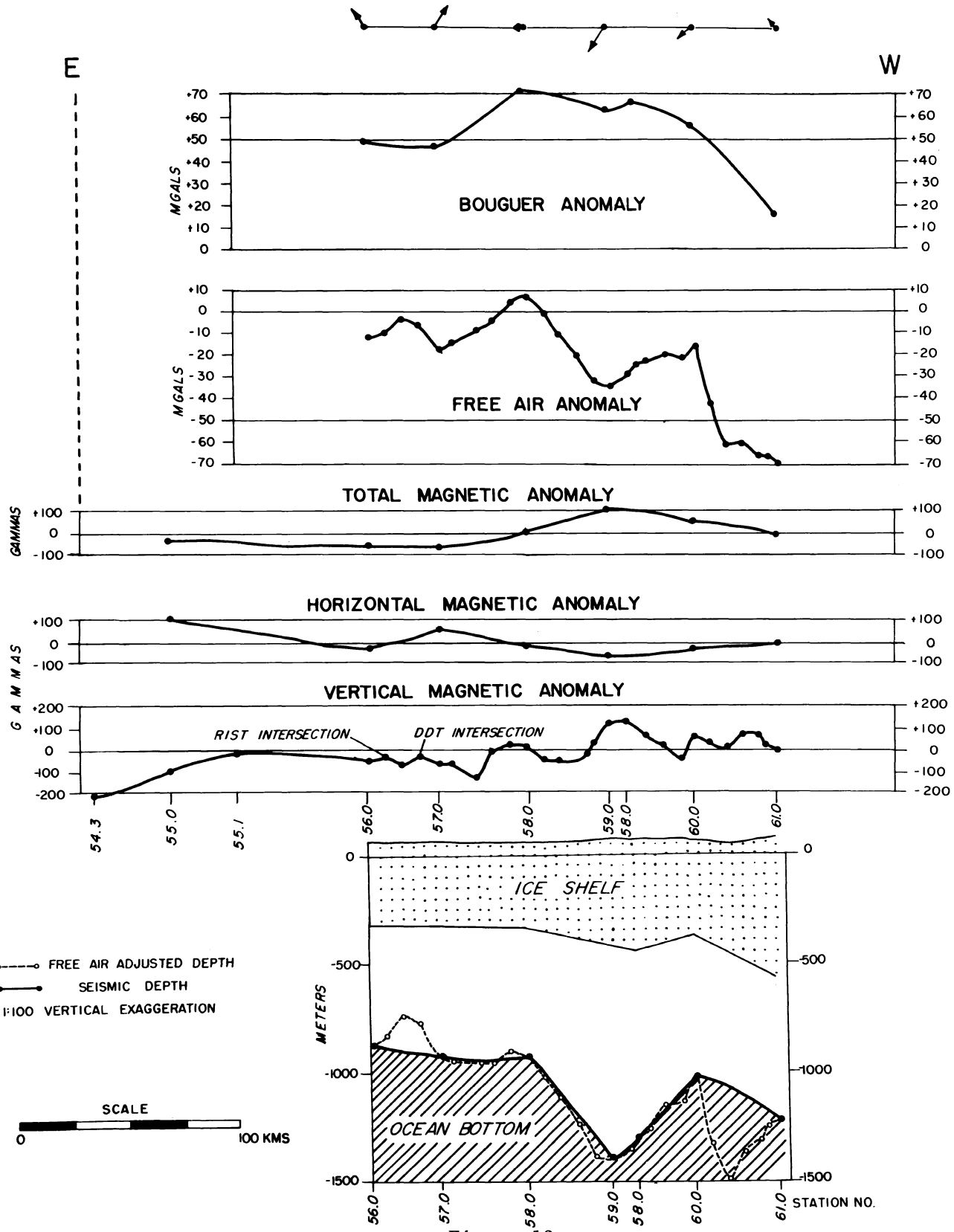


Figure 12

VICTORIA LAND TRAVERSE 1958-1959 (VLT 58-59)
LEG 2

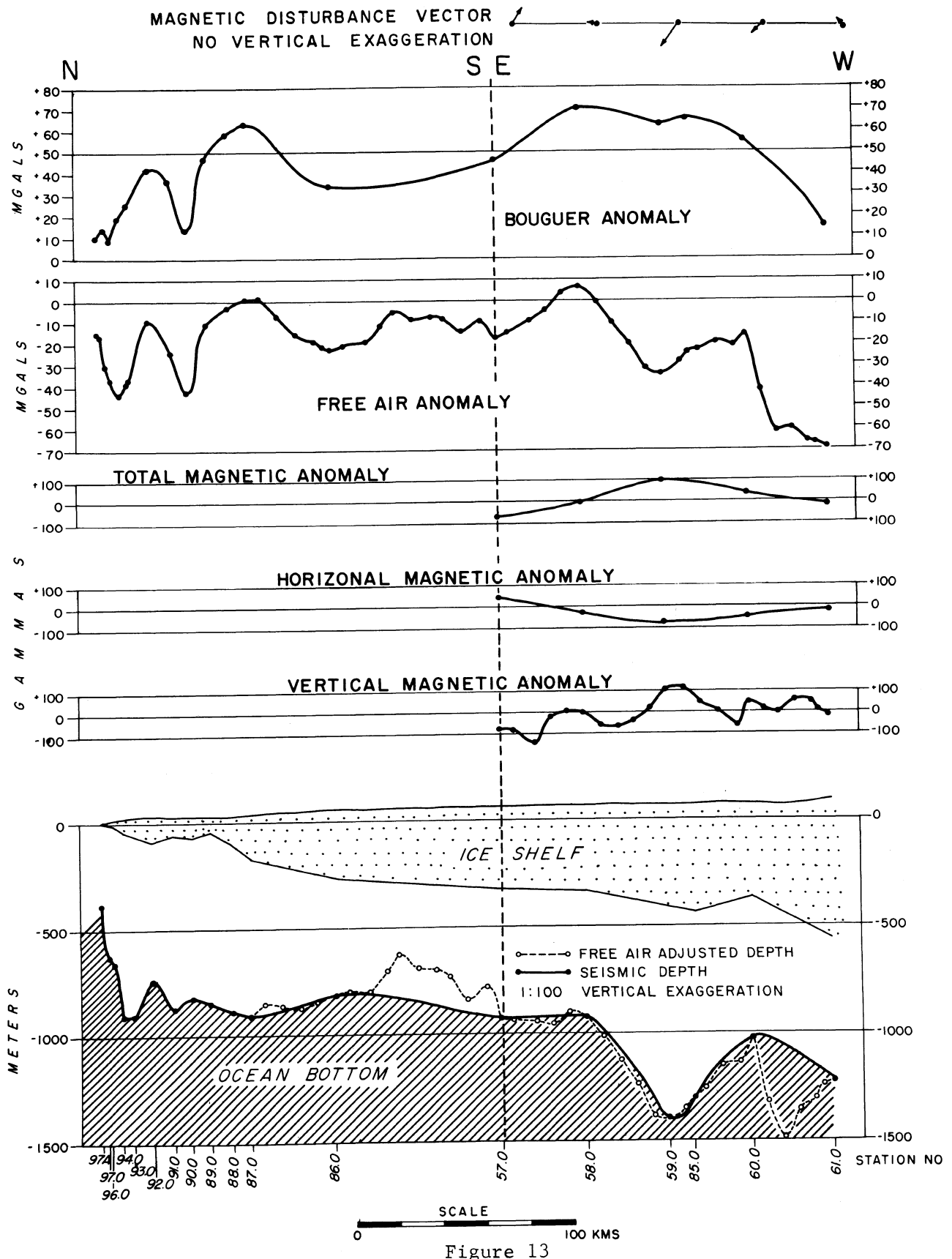


Figure 13

DISCOVERY DEEP TRAVERSE (DDT)

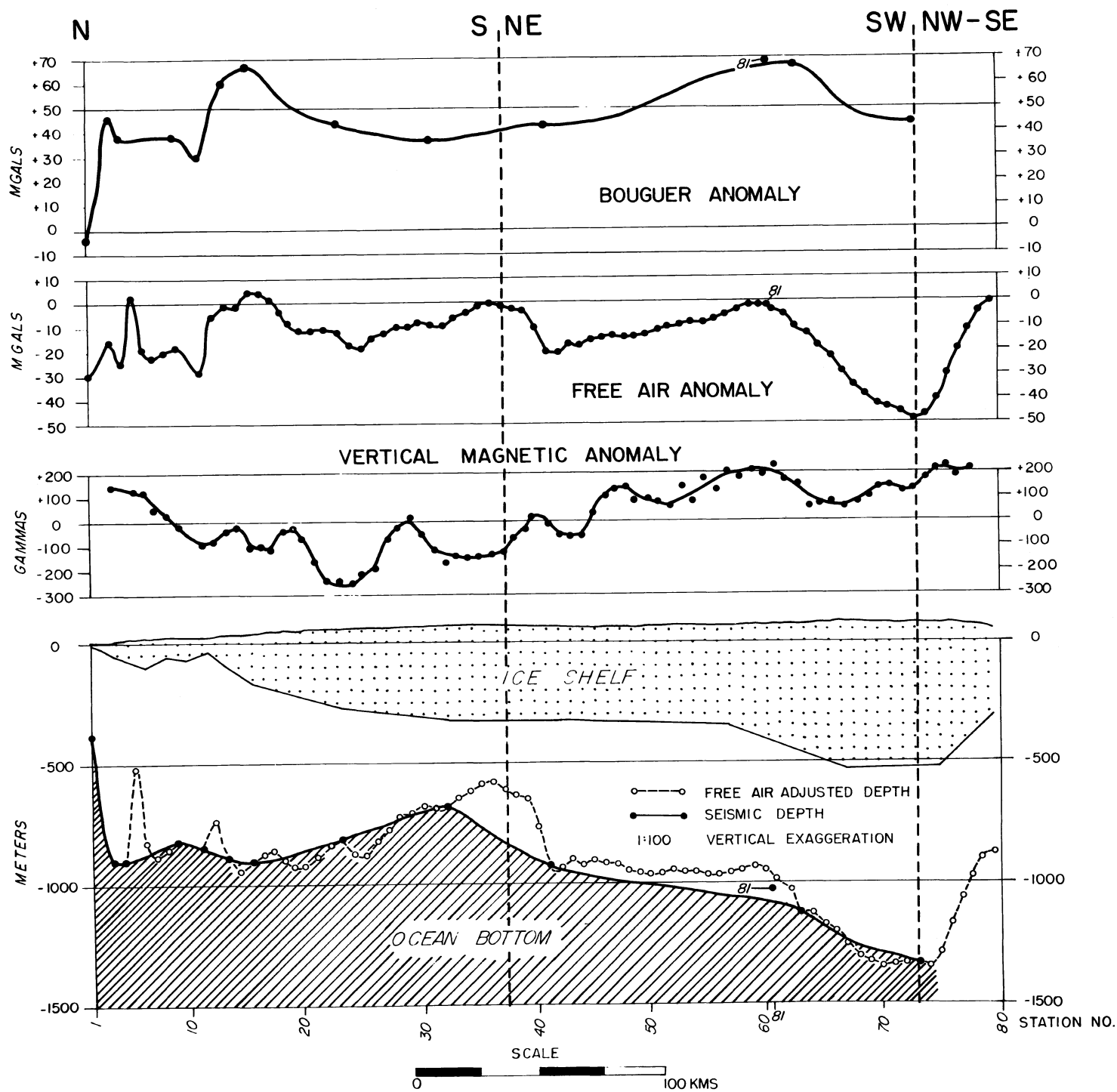


Figure 14

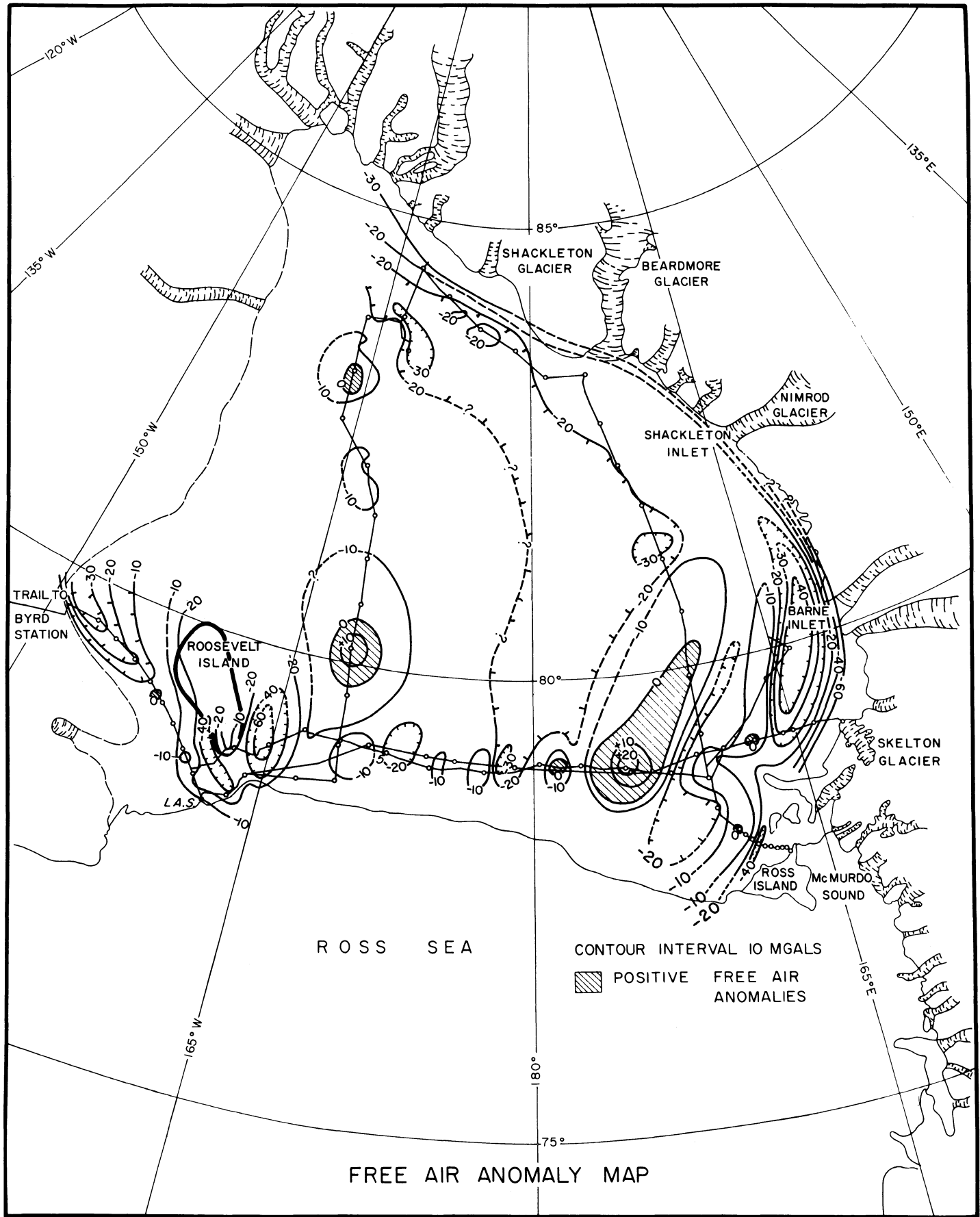


Figure 15

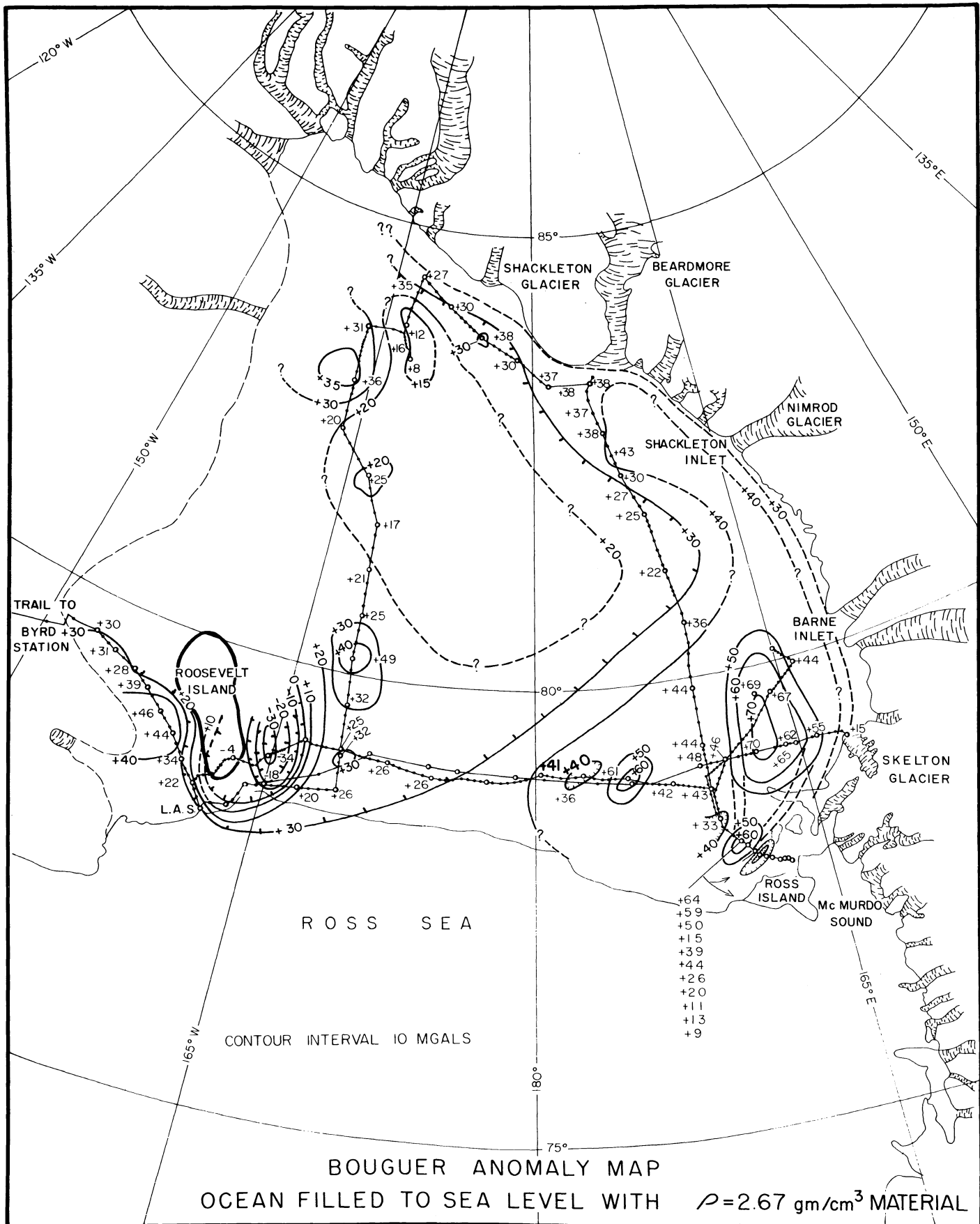
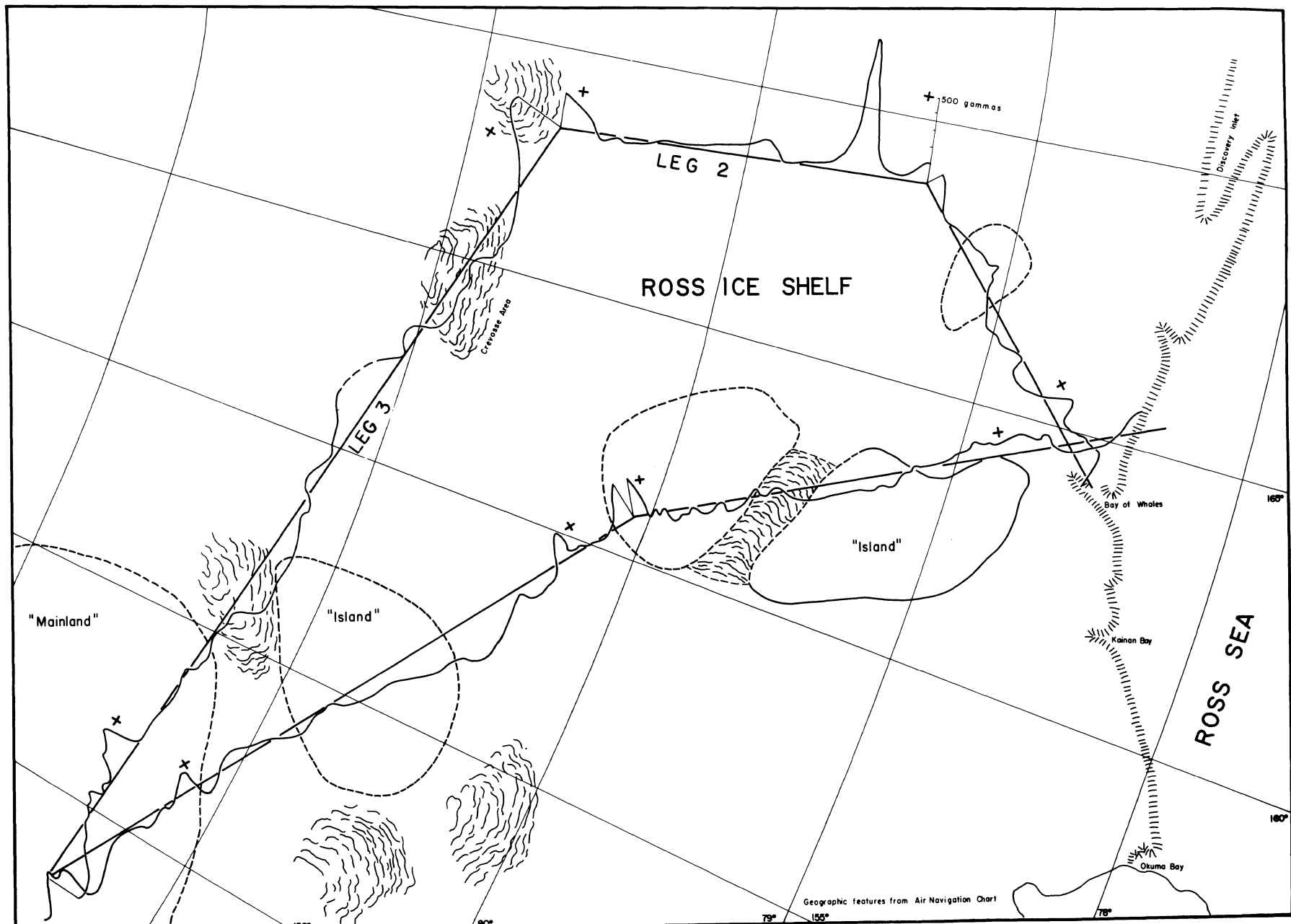


Figure 16



AIRBORNE MAGNETIC FLIGHT HIGH JUMP 1947
(TOTAL MAGNETIC ANOMALY)

Figure 17

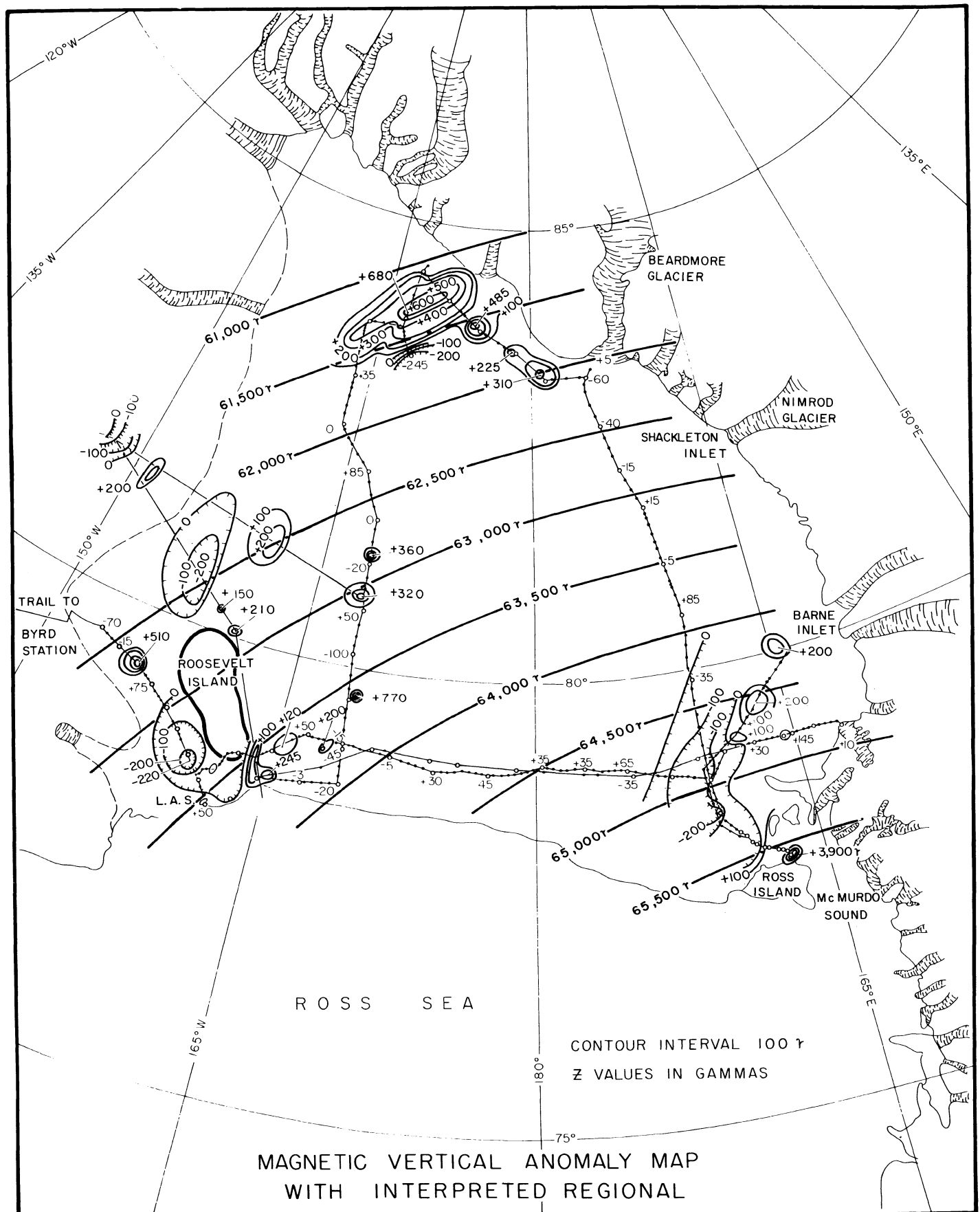


Figure 18

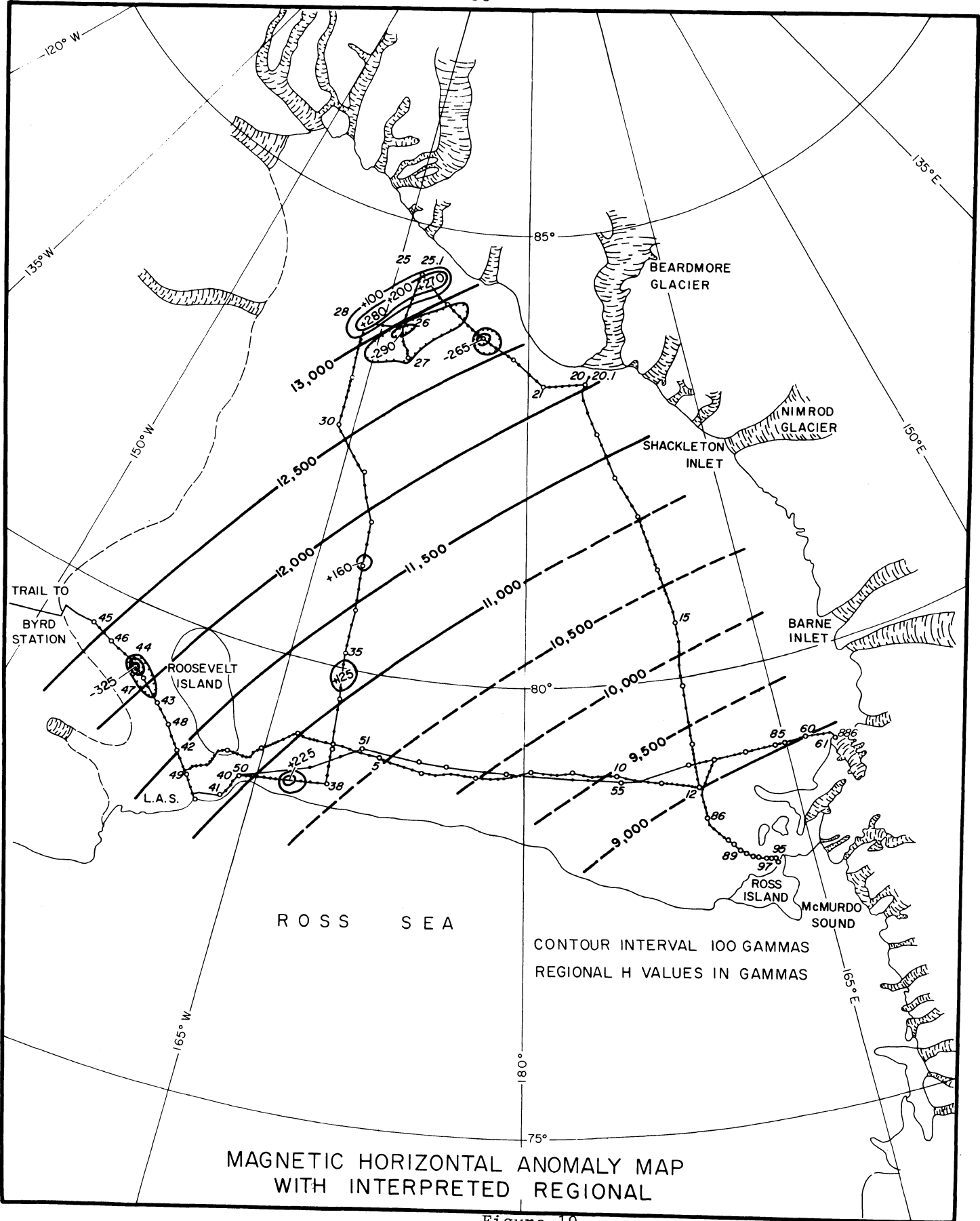


Figure 19

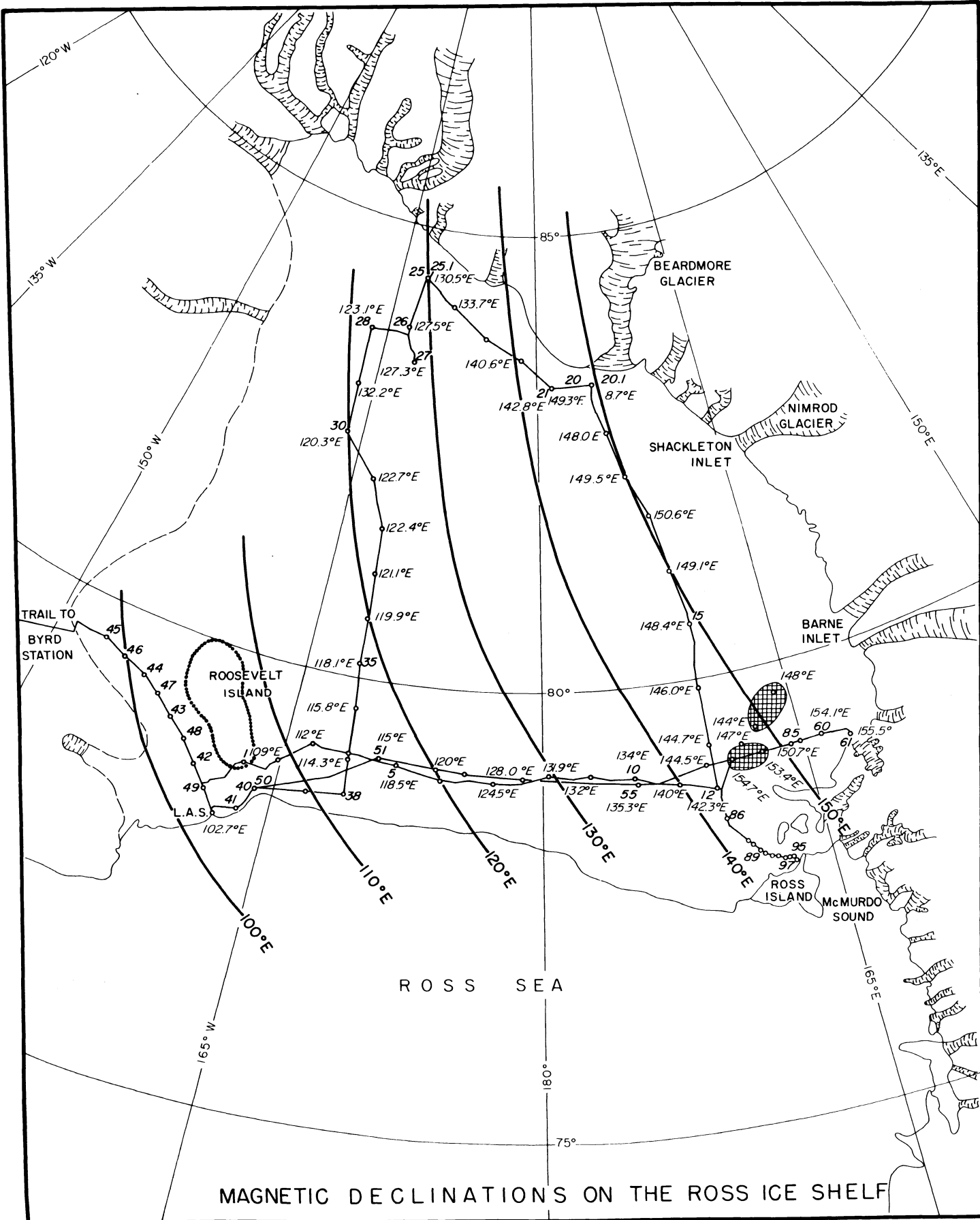
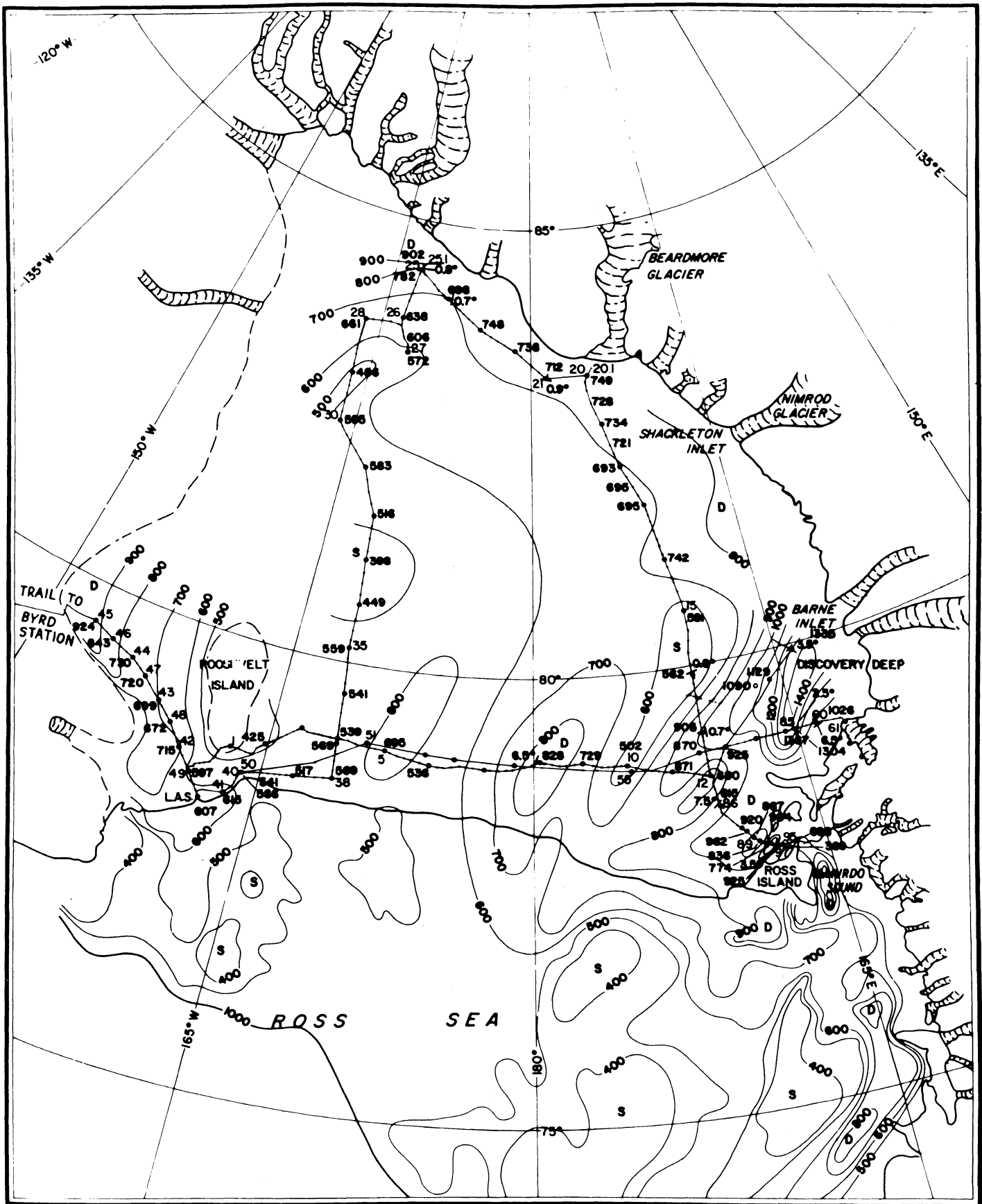


Figure 20



OCEAN DEPTH MAP (AFTER CRARY ET AL., 1962)

Figure 21

PART II

INTERPRETATION



GENERAL GRAVITY AND MAGNETIC INTERPRETATION
IN THE ROSS ICE SHELF AREA

A. Character of the Ocean Bottom Beneath the Ross Ice Shelf

The ocean bottom beneath the Ross Ice Shelf is relatively smooth and ranges in depth from 400 m near Roosevelt Island to 900 m east of Roosevelt Island and in the areas adjacent to the southern and western edges of the ice shelf (see Ocean depth map Fig. 21). One exception is Discovery Deep near Barne Inlet which has a depth of approximately 1400 m. All the average ocean bottom slopes between seismic stations are less than 1° and of the 46 local dip determinations only 7 are greater than 1°; all are located in the northwest sector of the ice shelf.

In the following discussion, it will be assumed that the generalized stratigraphic sequence beneath the Ross Ice Shelf is reflected in the measured velocity section at LAS (Crary, 1961b). This assumption is supported by the fact that the mean Bouguer anomaly over the entire Ross Ice Shelf area of +33 mgal is nearly the same as that of +34.0 mgal at LAS. The velocity section at LAS consists of 3 layers and is shown in Table 8.

TABLE 8
Velocity Section for the Little America Area, Antarctica
(after Crary 1961b)

<u>Station</u>	<u>Layer</u>	<u>Velocity</u>	<u>Thickness</u>
LAS	1 (top)	2.4 km/sec	1325 m
	2 (middle)	4.24 km/sec	645
	3 (bottom)	6.38 km/sec	-----
Mi 20 (Byrd Trail)	1 (top)	2.4 km/sec (assumed)	754 m
	2 (middle)	4.51 km/sec	-----

Cores taken from the upper meter of ocean bottom sediment are generally composed of coarse and fine glacial till (Crary, 1961b). Crary states that "Though there is no reason to believe that the total sediment column was deposited by ice, most of it may have been." Assuming the material composing Berkner Island in the Filchner Ice Shelf area was deposited in the same manner as the surface sediments beneath the Ross Ice Shelf, the density value of 2.0 gm/cm³ estimated by Behrendt (1962a) for the materials composing Berkner Island will be adopted for the 2.4 km/sec layer. This density was determined from the differences in gravity over the island and adjacent trough (elevation difference of 1190 m at a horizontal distance of 60 km).

A density of 2.6 gm/cm^3 and 2.9 gm/cm^3 is estimated for the 4.24 km/sec and 6.38 km/sec layer respectively. The densities predicted by the P wave velocity vs. density curves of Nafe and Drake (Talwani et al., 1959) and Woollard (1959) are, respectively, 2.45 gm/cm^3 and 2.64 gm/cm^3 for the 4.24 km/sec layer and 2.87 gm/cm^3 and 2.92 gm/cm^3 for the 6.38 km/sec layer. Crary (1961b) tentatively associates a 4.3 km/sec layer obtained at Plateau Depot (Skelton Glacier area) with the Beacon Sandstone which has an overall density greater than 2.67 gm/cm^3 according to W. Hamilton (personal communication). Since the 4.24 km/sec velocity is similar to 4.3 km/sec the higher density is probably more representative of the middle layer and 2.6 gm/cm^3 is adopted. Note that in the three layered section, the density contrast between layer 1 and 2 (0.6 gm/cm^3) is twice as great as that between layer 2 and 3 (0.3 gm/cm^3).

B. Magnetic Interpretation and Its Contribution to the Knowledge of Ocean Bottom Materials.

1. Shallow Magnetic Features

The vertical component magnetic anomalies over the shelf are small in magnitude, generally ranging from -250γ to $+680\gamma$ (the largest total magnetic anomaly is $+770\gamma$ just west of Roosevelt Island). Because stations were widely spaced over most of the area, anomalies from shallow sources are not delineated. However, the smooth magnetic profiles over the center of the ice shelf (see Figs. 7, 8, & 10) indicate an "absence of any disturbing igneous rock close to the surface," as was similarly concluded for the Ross Sea by Adams and Christoffel (1962). The two areas, both probably part of the continental shelf, are thus considered to be geologically similar. Conversion of Adams and Christoffel's total magnetic field map to the vertical intensity, using a dip of 82° , revealed a difference of 135γ from the present work in the McMurdo Sound area. This is within the estimated error of $\pm 170\gamma$ for Z.

There is a general lack of correlation between magnetic and gravity anomalies over the Ross Ice Shelf Area. Since nearly all gravity and magnetic stations coincide, this indicates that the major susceptibility contrasts and the major density contrasts lie at different depths. At stations 10.0, 29.0, and 35.0 (RIST) relatively high Bouguer anomalies of $+61$, $+36$, and $+49$ mgals respectively, are unaccompanied by magnetic anomalies (see Figs. 1, 16, & 18). Because the ocean bottom elevation is at least as high at these stations as at surrounding stations, it appears that ocean bottom sediments thin and the underlying 4.24 km/sec layer thickens with little change in the combined thickness. Since an anomaly should be associated with variations in thickness of a magnetic layer, the above factors indicate that both the top 2.4 km/sec and middle 4.24 km/sec layer have negligible susceptibility.

The shallow magnetic features thus appear to arise from sources beneath the middle layer - perhaps in the bottom 6.38 km/sec layer. It is reasonable that a greater susceptibility may be associated with material

of this high a velocity (e.g., Birch, 1942, gives a velocity of 6.22 km/sec for the Sudbury Norite and Jakosky, 1950, gives a range of 0.00044 to 0.0041, cgs, for gabbro). Furthermore, a Peters depth determination on the +770 γ airborne anomaly west of Roosevelt Island (near station 36.0 RIST; Figs. 1, 17, & 18) places the source about 2 to 3 km below the flight elevation of approximately 0.6 km (J. R. Balsley, personal communication). Since this is about the depth to the bottom layer at LAS (2580 m) and the Bouguer anomalies and depths at both locations are similar, the upper "magnetic horizon" shall be considered to lie somewhere within the 6.38 km/sec layer.

Using the broad negative magnetic anomalies at the north and southeast end of Roosevelt Island (see Fig. 18), and assuming that the 6.38 km/sec material is replaced by a low susceptibility material in these areas, susceptibility contrasts were computed using the method of Vacquier et al., (1951). The results give a value between 0.0008 and 0.0011 cgs (Models A-82 and A-75), which is a lower limit approximation to the susceptibility of the bottom layer.

2. Broad Magnetic Features

Let us first consider the broad magnetic features in the northeastern sector of the ice shelf. The two large negative magnetic anomalies north and southeast of Roosevelt Island (mentioned above) are fairly broad in extent and are tentatively considered the result of replacement by lower susceptibility materials. The high magnetic anomalies along the northwest end of the island may suggest a boundary between two different rock types. The large magnetic anomaly (+510 γ) due east of Roosevelt Island (Mile 118, Byrd Trail) shows up clearly on both the vertical and horizontal profiles (see Fig. 11), facilitating a depth calculation by use of the displacement vectors. The depth to the source indicated is about 13 km. It is tempting to correlate this anomaly with the anomalies at the south end of Roosevelt Island and those to the southwest of the island (see Fig. 18), all of which fall on a straight line. A short traverse in the northeast and southwest directions showed, however, that the anomaly at Mile 118 decreases in both directions (L. D. McGinnis, personal communication). Furthermore, the two anomalies at the south end of Roosevelt Island are of shallower origin and may result from a boundary between two different rock types in the same manner as was postulated at the northwest end of the island.

The broad negative anomaly area located southeast of Ross Island was detected on three different traverses (RIST, DDT, and VLT 58-59; see Figs. 7, 8, 12, and 14) and therefore, even though its overall amplitude of -100 γ to -150 γ is about the same as the relative error between stations, it is considered real. This broad magnetic "low" may result from a downwarping of the 6.38 km/sec layer and thereby suggest an increase in thickness of one or both of the two upper layers. By approximating the downwarp with a two dimensional slab (infinite in the NNE-SSW direction, 50 km wide, 1 km thick, vertically polarized, and with a 45° slope at the edges) the anomaly profile perpendicular to the strike was calculated by the methods of Heirtzler et al., (1962). From this model, the profile can be made roughly to fit the data by using a susceptibility of 0.0031 to 0.0046 (cgs)

for the 6.38 km/sec layer. An alternate explanation might be a susceptibility change within the 6.38 km/sec layer itself or within underlying layers. The gravity and magnetic data do not, however, favor a low density, low susceptibility replacement material in this area as they do over Roosevelt Island (see Roosevelt Island section)

The largest magnetic feature found on the shelf is located in the south and yields a depth of approximately 18 km, calculated by both the displacement vector method (corrected to the maximum gradient direction) and the method of Vacquier et al., (1951) (Model A-81 and A-82). The calculated susceptibility contrast lies between 0.0028 and 0.004 (cgs), probably indicating a basic pluton. Magnetization cannot take place below the Curie point geotherm, which Vacquier and Affleck (1941) have determined at about 24 km (maximum depth), therefore, the criterion for the depth determination of this large anomaly is probably not met (i.e., vertical extent of the magnetic body should be greater than the depth below the recording level). This being the case, either the susceptibility contrast is far greater than computed or the depth to the feature is less. Assuming a two dimensional slab 6 km thick, 50 km wide, at 18 km in depth and with vertical polarization, the susceptibility contrast required to produce the $+680\gamma$ anomaly is about 0.018 (cgs). This figure is unreasonably large, thus the depth calculation is probably too great. Considering all sources of error, the depth calculations are probably no better than $\pm 40\%$ which could place the maximum depth to this feature as shallow as 11 km.

Since depth calculations generally give maximum depths, it is possible that the source of a magnetic anomaly may be shallower than indicated (e.g., see Fig. 22). With this in mind, the anomaly at the south end of the shelf can be approximated by a body near the surface, of infinite extent in the ENE-WSW direction with a trapezoidal cross section (base of 70 km, height of 6 km, vertical polarization, and with an apex 10 km across and lying 3 km in depth). A high susceptibility contrast of 0.007 to 0.008 (cgs) is required to approximate the observed anomaly. Because a thinner model requires an even greater contrast and would produce a relative "low" in the center, it is improbable that this anomaly is caused by volcanic sheet flows. Furthermore, since a measurable density contrast would probably be associated with buried volcanic features, the Bouguer and magnetic anomalies might then be expected to parallel one another. The trends of the Bouguer and vertical magnetic anomalies in this area are at right angles (Figs. 16 and 18) suggesting that the magnetic source is located considerably deeper than the ocean floor.

An exception to the generally poor correlation between magnetic and gravity anomalies is found south of the Shackleton Glacier at station 23.0 (RIST). Here a $+485\gamma$ magnetic anomaly, yielding a half width depth of about 13 km (single pole approximation), is accompanied by a relative Bouguer anomaly high of 8 mgal. It is possible that both anomalies originate from the same source. For example, the 8 mgal anomaly can be produced by a vertical cylinder 5 km in radius and 10 km in length, whose top surface is lying at 8 km in depth (40% depth calculation error), and has a density contrast of 0.19 gm/cm^3 (see Dobrin, 1952). The magnetic

anomaly of 485γ could be produced by the same body having a susceptibility contrast of approximately 0.004 (cgs). However, in view of the poor correlation between gravity and magnetic anomalies southeast of this feature, it is more probable that the relative gravity "high" is produced by sedimentary thinning, the apparent cause of high Bouguer anomalies over most of the area.

In conclusion it may be stated from the analysis of magnetic data collected on the Ross Ice Shelf that (1) the 2.4 km/sec and 4.24 km/sec layers appear to have negligible susceptibility, (2) the upper "magnetic horizon" is probably associated with the 6.38 km/sec layer, (3) maximum depths to the large magnetic features, located in the peripheral areas of the ice shelf, range between 8 km and 13 km, and (4) geologic similarity between the Ross Sea and Ross Ice Shelf area is suggested by the similar magnetic character of both areas.

C. Determination of Rock Densities from a Δg vs. Δh Plot.

1. Method

To provide an estimate of rock density, differences in free air gravity anomalies (Δg) and bottom elevations (Δh) between pairs of seismic stations were plotted on a Δg vs. Δh graph (Fig. 23). The differences were determined over distances smaller than those for which bottom topography could be regionally compensated (160 km). Only positive correlations were graphed. Lines representing densities of 3.3, 3.0, 2.67, 2.0, and 1.6 gm/cm^3 were superimposed on the graph. These lines were determined by assuming that a change in bottom elevation (Δh) produces a free air gravity change (Δg) identical to that produced by an infinite plate of thickness Δh , with appropriate density, lying beneath water of density 1.03 gm/cm^3 . Since the gravity survey was carried out at elevations close to sea level, the maximum distance from gravity stations to ocean bottom averaged 700 m and was generally not greater than 900 m. Furthermore, as mentioned earlier, slopes over most of the area studied were 1° or less. This type of density determination is therefore more suited to an ice shelf area than to regions over the ice cap where depths to the ice-rock interface are greater and where, in some areas, there is more local relief.

2. Evaluation of Method on the Ross Ice Shelf.

Errors in this method can arise from two general sources: (1) errors in measurement of gravity, elevation, and depth and (2) errors introduced by using an infinite plate to approximate the changes in bottom elevation (Δh). The estimated errors from the first source are shown in Table 9.

CALCULATED MAGNETIC ANOMALIES PRODUCED BY TWO DISSIMILAR BODIES
LYING AT DIFFERENT DEPTHS

(BODIES ARE INFINITE IN THE THIRD DIRECTION, HAVE VERTICAL
POLARIZATION, AND NO REMANENT MAGNETIZATION)

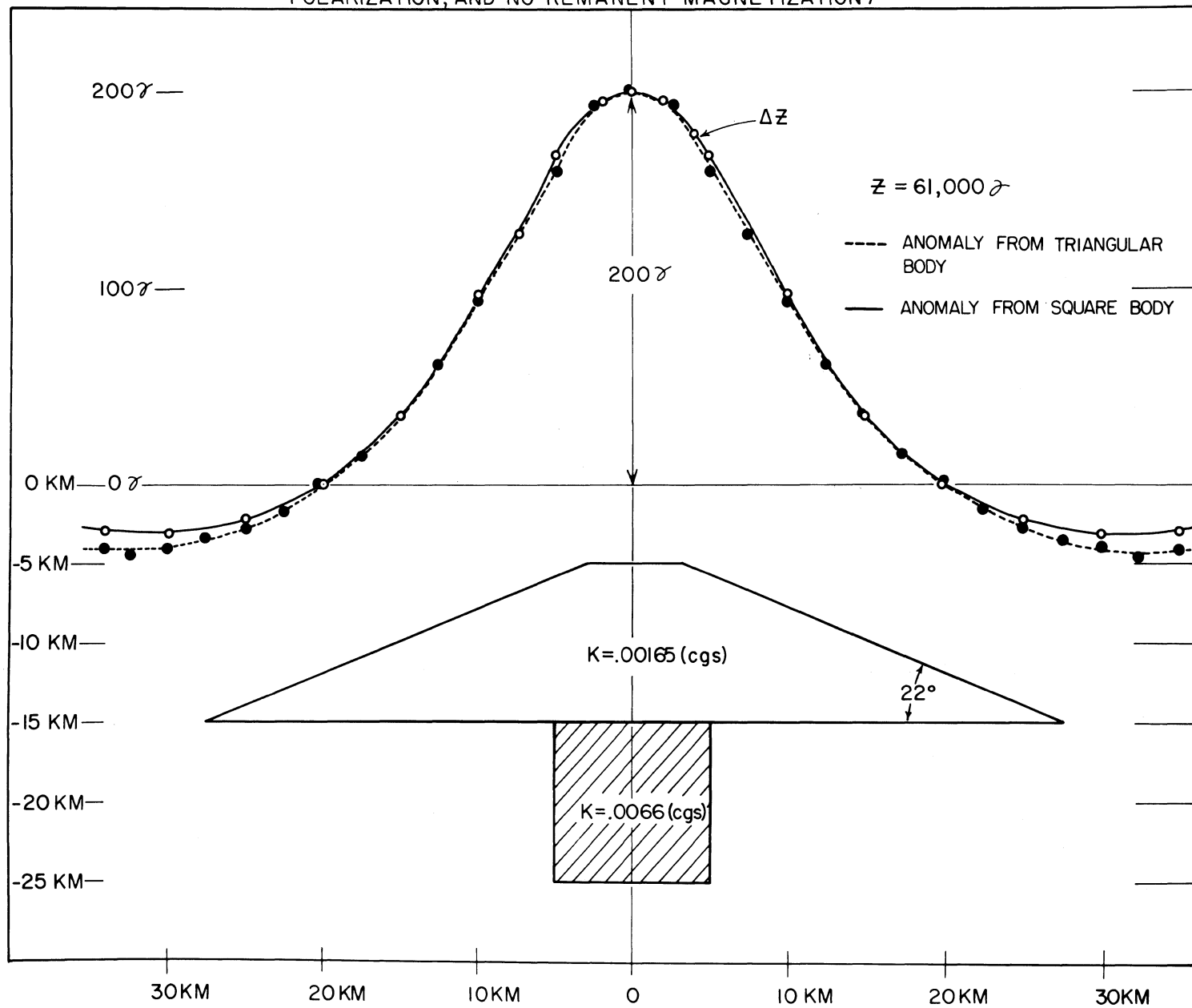


Figure 22

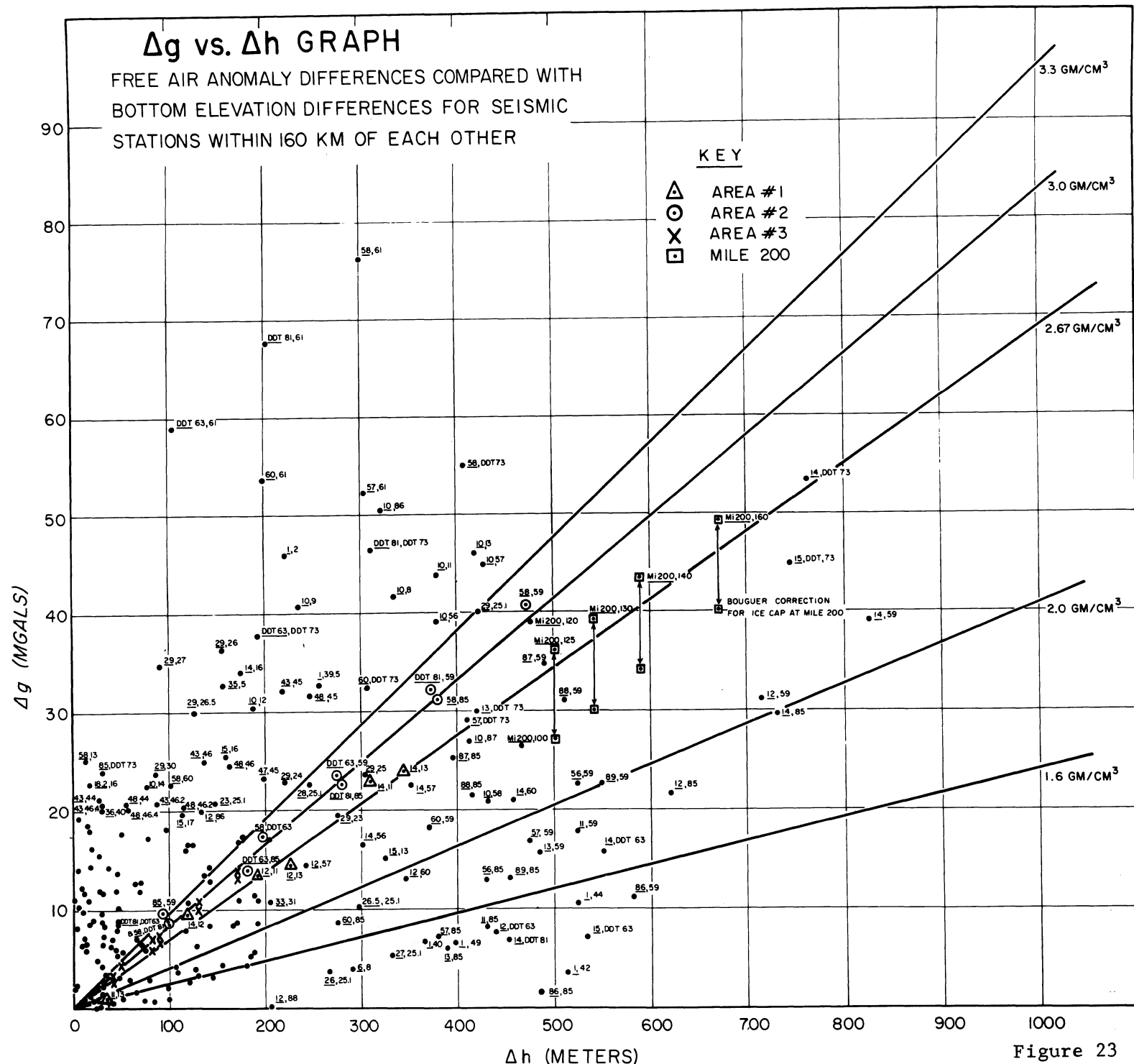


TABLE 9

Estimated Errors in Δh and Δg

<u>Errors in Δh due to Errors in Elevation and Seismic Depth Determinations</u>		<u>Errors in Δg</u>
Ice thickness (± 20 m)	± 7 m	Relative Elevation Error between Stations (4 m) 1.2 mgal
Bottom Reflection		Navigational Errors (± 0.5 mi. each station) ± 0.25 mgal
Picking Error ($\pm .005$ sec)	± 3.5 m	
Relative Elevation Error between stations	$\frac{4}{25}$ m	Drift of Meter 0.4 mgal
		Tides $\frac{0.3}{2.4}$ mgal
		2.4 mgal

The relative error in elevation which contributes to errors in both Δh and Δg does not contribute as greatly to the density error. This is so because a positive error in elevation between two stations will increase both the ocean elevation determination and also the free air gravity anomaly calculated for the same station. The converse is true for a negative error in elevation. The estimated errors in Δg and Δh have been used to find the highest and lowest calculated densities, assuming topography with a density of 2.7 gm/cm^3 and water with a density of 1.0 gm/cm^3 . Several values of Δh were assumed and the corresponding Δg for an infinite plate was computed. The errors in Δh and Δg were then combined to give maximum and minimum values for the computed densities. Equation 4 was used to compute the densities which are found in Table 10.

$$\rho_c = \left(\frac{\Delta g}{\Delta h} \cdot \frac{1}{2\pi\gamma} \right) + \rho_w \quad (4)$$

ρ_c = computed density (gm/cm^3)

Δg = difference in free air anomaly between stations (mgal)

Δh = difference in elevation between stations (meters)

$$\frac{1}{2\pi\gamma} = 23.85 \text{ gm m cm}^{-3} \text{ mgal}^{-1}$$

ρ_w = water density

TABLE 10
Maximum Errors in Calculated Densities
Due to Errors in Gravity and Bottom Elevation Determinations

<u>Δh</u>	<u>Lowest ρ_c</u>	<u>Highest ρ_c</u>	<u>Error</u>
100 m	2.36 gm/cm ³	3.26 gm/cm ³	- .34 to + .56 gm/cm ³
200 m	2.51 "	2.94 "	- .19 to + .24 "
300 m	2.57 "	2.86 "	- .13 to + .16 "
400 m	2.60 "	2.81 "	- .10 to + .11 "

Densities determined for stations whose bottom elevations differ by less than 200 m are probably not reliable for single determinations (see Table 10). However, for elevation differences greater than 200 m, and for some under 200 m where several points indicate nearly constant densities, the determinations can be used in interpreting the composition of the ocean bottom.

In order to estimate the errors in computed density due to the second source of error (infinite plate approximation), a two dimensional model has been used. It is assumed that two stations are situated over two different ocean depths and that the slope between the two depths is constant. On the opposite side of the slope at each station the bottom is assumed to be uniform in depth. In calculating the gravity effect of the wedge shaped material between the two stations, we start with the vertical component of attraction due to an infinitely long rod.

$$dg_z = 2\gamma\rho \frac{zdzdx}{x^2 + z^2} \quad (5)$$

Integrating this for a wedge shaped mass, we have:

$$g_z = 2\gamma\rho \int_{z_1}^{z_2} zdz \int_0^{x_o + z/m} \frac{dx}{x^2 + z^2} \quad (6)$$

where $\gamma = 6.67 \times 10^{-8} \text{ cm}^3 \text{gm}^{-1} \text{sec}^{-2}$ (the gravitational constant)

ρ = density of the wedge

z_1 = depth to top of wedge

z_2 = depth to bottom of wedge

x_o = the intercept of the slope with the line $Z = 0$

m = slope ($\tan \phi$) (see Fig. 24)

For a wedge which is flat on the undersurface and angled on the top surface, and for small angles ($m^2 + 1 \approx 1$; $m \approx \phi$), we have:

$$g_z = 13.34\rho \left[z_2 \tan^{-1} \left(\frac{z_2 - z_1}{mz_2^2} \right) - z_1 \tan^{-1} \left(\frac{z_2 - z_1}{mz_1} \right) + mz_1 - mz_1 \ln \left(\frac{z_2 - z_1}{mz_1} \right) \right] \quad (7)$$

and for a wedge which is flat on the top surface and angled on the undersurface, and for small angles:

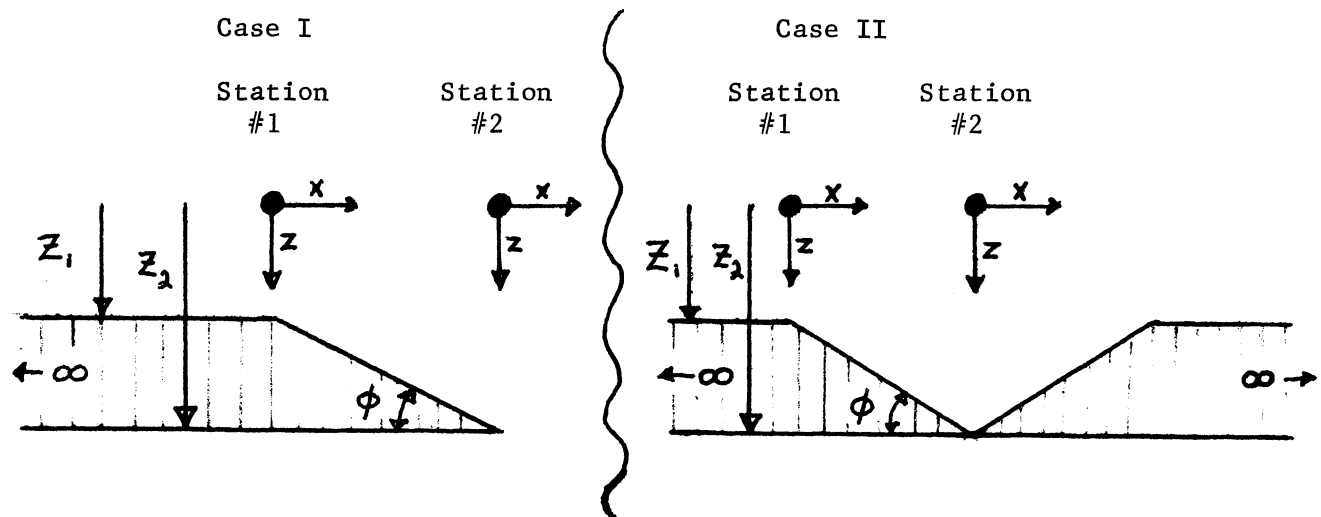
$$g_z = 13.34\rho \left[z_2 \tan^{-1} \left(\frac{z_2 - z_1}{mz_2} \right) - z_1 \tan^{-1} \left(\frac{z_2 - z_1}{mz_1} \right) + mz_2 + mz_2 \ln \left(\frac{mz_2}{z_2 - z_1} \right) \right] \quad (8)$$

In both formulas m , ϕ , z_2 and z_1 are positive and ϕ is the angle of inclination. Here m is given in radians, g_z in mgals, ρ in gm/cm³, and z_1 and z_2 in km.

The vertical attraction at stations 1 and 2 (Case I, Fig. 24) was calculated by computing the attraction of a semi-infinite slab and then adding or subtracting the attraction of the intervening wedge-shaped slab between the two stations (Equations 7 and 8 respectively). Using formula 4, the densities were then calculated on the basis of these computed differences in attraction. In Case II the attraction at station 2 is twice that in Case I, but the difference between the two cases for station 1 is less than $\frac{1}{2}$ mgal and was therefore neglected.

Fig. 24

Slab Configurations Used in Computing Density Errors



Of the 46 dip determinations mentioned earlier (Crary et al., 1962), 29 were less than $.3^\circ$, 38 were less than 1° , and the maximum was 7.5° . Calculations for Case I and Case II were therefore carried out for inclinations of 6° , 3° , 2° , 1° , and $\frac{1}{2}^\circ$. Table 11 summarizes the calculations, assuming $Z_1 = 600$ m, $Z_2 = 900$ m, and a density contrast of 1.7 gm/cm^3 , representative of one of the areas where densities appear to be uniform.

TABLE 11
Effect of Slope on Density Calculations

Bottom Slope Assumed	g_z attraction at Sta. 1 (mgal)	g_z attraction at Sta. 2(mgal) (Case I)	Case I		Case II	
			$\rho(\text{Calc})$ (gm/cm 3)	error (gm/cm 3)	$\rho(\text{Calc})$ (gm/cm 3)	error (gm/cm 3)
6°	17.18	3.77	1.07	.63	0.77	.93
3°	18.73	2.69	1.28	.42	1.06	.64
2°	19.40	2.09	1.38	.32	1.21	.49
1°	20.23	1.31	1.50	.20	1.40	.30
$\frac{1}{2}^\circ$	20.76	0.77	1.59	.11	1.53	.17

One may conclude from Table 11 that considerable error may occur in density computed from differences in free air anomalies for ocean bottom inclinations greater than $\frac{1}{2}^\circ$. There are two deviations from the model used here that do not effect this conclusion appreciably. First, if one or both stations were over the sloping surface, and not at the top and bottom of the slope, the errors in Table 11 would be reduced slightly because the density indicated would be higher. Second, considering a three dimensional model, the computed densities are as likely to be higher as they are to be lower than those in Table 11. This is because the addition of material near station 1 or removal of material near station 2 will lead to a slightly higher computed density and the reverse to a lower computed density. Since the probability of either happening is equal, this effect is considered to be of second order. From the evaluation of errors inherent in this method, it is concluded that bottom densities can be determined from changes in gravity and bottom elevation between stations in those areas where bottom slopes are $\frac{1}{2}^\circ$ or less and where elevation differences are 200 m or more.

3. Densities determined in Areas #1, #2, and #3.

In compilation of the Δg vs. Δh plot (Fig. 23) 390 combinations (station pairs) were used, from which 232 gave positive correlations and 158 gave negative correlations. Stations near McMurdo Sound (90 through 97 VLT 58-59) were not compared with those farther out on the ice shelf because of the lithologic difference near McMurdo Sound (Robinson, 1963). A separate determination was made for stations 86.0 through 97.0 (VLT 58-59), making a total of 66 combinations; 32 were positive and 34 were negative correlations.

In view of the large scatter of points on the Δg vs. Δh plot it would appear that little or no density information could be obtained; indeed this is the case over the major portion of the area studied. There are however small isolated areas of the shelf for which the comparison between stations indicates nearly constant density. In order to determine whether the assumption that changes in bottom elevation in these areas are due to the topography of a layer with indicated density and not to a combination of two or more layer variations, the following criterion was used to accept or reject an area. Within each area, defined by four or more stations, all combinations between stations were required to be within ± 2.4 mgal and ± 25 m of the mean density line determined by these combinations, regardless of the mean density indicated.

From the analysis of all station pairs, it was found that in only three areas was this criterion met. The three areas: Area #1 (stations 11.0, 12.0, 13.0, and 14.0 RIST) with a mean computed density of 2.74 gm/cm^3 , Area #2 (stations 58.0, 59.0, 85.0 VLT 58-59, and 61 and 81 DDT) with a mean computed density of 3.03 gm/cm^3 , and Area #3 (stations 45.0, 46.0, 46.2, and 46.3 LAS-BT and Mi 125, 130, 140, and 160 LAS-BS) with a mean computed density of 2.93 gm/cm^3 are marked on the Δg vs. Δh graph. Areas #1 and #2 are located in the northwest portion of the Ross Ice Shelf and Area #3 is located in the northeast portion (see Fig. 1). Areas #1 and #2 are suitable for analysis since (1) all average slopes in the area but one are near to or less than $\frac{1}{2}^\circ$ (the slope between stations 58.0 and 59.0 is $3/4^\circ$) and (2) several determinations in each area have bottom elevation differences (Δh) of more than 200 m. In Area #3 the average slope between stations is less than $\frac{1}{2}^\circ$. Unfortunately the elevation differences between these stations are all less than 200 m. However, since all combinations lie close to the average density of 2.93 gm/cm^3 , which is consistent with the density determined in Area #2, and that determined for the 6.38 km/sec layer, the determination may be a valid approximation.

In all three areas the average densities indicated were reasonable. If, in these areas, the changes in elevation and gravity are caused by a combination of two or more layer variations, then it is probable that unreasonable densities should also be indicated. Therefore, since (1) the indicated mean densities of 2.74 gm/cm^3 , 3.03 gm/cm^3 and 2.93 gm/cm^3 are similar to the densities of 2.6 gm/cm^3 and 2.9 gm/cm^3 , determined by independent means for the middle and bottom layers, and since (2) no unreasonable densities were indicated in this analysis, these data strongly favor the position taken at the beginning (i.e., changes in bottom elevation are due to the topography of a single layer in these areas). We therefore conclude that the gravity and elevation differences in Areas #1, #2 and perhaps in Area #3 are due to the topography of a 2.7 gm/cm^3 or 3.0 gm/cm^3 layer. From this point on we shall continue to use a density of 2.0 gm/cm^3 for the top layer but will assign a density of 2.7 gm/cm^3 to the middle layer and a density of 3.0 gm/cm^3 to the bottom layer.

4. Density determination at Mile 200

Since the bottom elevation at Mile 200 is 500 m to 670 m higher than the bottom elevation at Miles 125 to 160 of the Byrd Trail (Area #3) the large difference in elevation should offset errors in computed density, introduced by a rough bottom in the vicinity of Mile 200 (the average slope between Mile 160 and Mile 200 is $3/4^{\circ}$). Because there was only one seismic station in the vicinity of Mile 200, it was not possible to determine densities beneath more than one station as was done in Areas #1 and #2. However, the large elevation difference between Mile 200 and Area #3 probably justifies a density calculation. One must also deal with the problem of whether or not the ice cap is isostatically compensated beneath Mile 200. This fact must be taken into account when comparing gravity anomalies over ocean areas with those over grounded ice areas. Based on free air anomaly differences, the mean density indicated for material beneath the grounded ice at Mile 200 is 2.8 gm/cm^3 ; this value assumes isostatic compensation for the ice sheet. Using a Bouguer correction for the ice and ocean above the ice-rock and ocean-rock interface, thus assuming that the ice cap is not isostatically compensated, the computed mean density is 2.4 gm/cm^3 . Since the degree of compensation is not known beneath Mile 200, one can only conclude that the average density of the material responsible for the rise between Mile 160 and Mile 200 is somewhere between 2.4 gm/cm^3 and 2.8 gm/cm^3 .

Since the density of the top layer (probably morainal) is much lower than 2.4 gm/cm^3 , the topographic rise at Mile 200 cannot be attributed to an increase in this layer alone, nor can it be attributed solely to the bottom layer (density greater than 2.8 gm/cm^3). It could, however, result from an increased thickness of the middle layer or from an increased thickness of two or all three of the layers. Bentley and Osteno (1961) show the middle layer to be approximately 700 m thicker beneath Byrd Station than beneath LAS. It is therefore possible that the increase in topography at Mile 200 is primarily due to an increased thickness of the middle layer.

In Area #3, adjacent to Mile 200, one can only speculate on a possible interpretation since the changes in bottom elevation are less than 200 m and the indicated densities are thus subject to greater error. Perhaps the changes in gravity, instead of being controlled by the topography of the bottom layer (inferred from the higher indicated densities), are also controlled by the middle layer topography. An error of 0.2 gm/cm^3 , necessary to explain the discrepancy in indicated density, could easily result from a difference of $1\frac{1}{2}$ mgal error in Δg (Fig. 23). Furthermore if the ice cap were regionally compensated, creating a gravity gradient in Area #3, such a difference in Δg could occur. The Bouguer anomalies in Area #3 are similar to that at LAS, suggesting that the low density layer, comparable in thickness to LAS, is present. On the other hand the relatively high indicated density and deeper ocean depths in Area #3 suggest that the low density layer is thin or absent. A downward crustal thickening of $\sim 1.4 \text{ km}$ could account for the Bouguer anomalies in Area #3 assuming that the low density layer were missing. The explanation given here is speculative and the final interpretation should be based on more complete data than is presently available.

Table 12 lists all the computed densities for Areas #1, #2, and #3 and for Mile 200. In order to indicate the quality of each determination, the elevation differences and distances between stations are also shown. It was first assumed that topography was not isostatically compensated for distances up to 160 km. If topographic features were partially compensated, this fact would be observable in a systematic decrease in computed density beneath a given station as the distance to the other stations in the area is increased. A systematic density decrease is not observed in Areas #1 and #2 since both increases and decreases occur at greater distances. The changes in computed density in Area #3 are meaningless because of the small values of Δh and the changes in density (determined from free air anomalies) at Mile 200 are smaller than the experimental error. The changes in density, determined from Bouguer anomalies, at Mile 200 may, however, suggest regional compensation of the ice cap. Since Mile 200 is not located on the ice shelf it is therefore concluded that over the distances represented in this table (i.e., up to 125 km) the relative topography between stations on the ice shelf is not isostatically compensated. The assumptions made at the beginning of this section are thus valid.

D. Amount of Overlying Low Density Material in Areas #1 and #2.

In order to conclude that the topography of a 2.7 gm/cm^3 layer in Area #1 and a 3.0 gm/cm^3 layer in Area #2 controls the changes in gravity, the thick, overlying, low density layer (2.0 gm/cm^3) must either be nearly uniform in thickness or be absent. Two types of evidence indicate that the low density sediments thin over Areas #1 and #2. These are: (1) the ocean bottom has more local topography and is deeper in Areas #1 and #2 than over the rest of the ice shelf area, and (2) the Bouguer anomalies are higher in Areas #1 and #2 -- more than created by the increase in depth.

First, sedimentary displacement from higher to lower elevations probably takes place below sea level in the ice shelf area as a result of water movement (tide and other currents). Such displacement would cause sedimentary thinning over high areas, thickening over low areas, and would result in a leveling of the bottom and a variation in sedimentary thickness. The ocean depth map (Fig. 21) and seismic dip measurements (Crary et al., 1962) show that in the central area of the Ross Ice Shelf, the ocean bottom is smoother than in the northwest corner where Areas #1 and #2 are located. The smoother bottom in the central area probably results from the displacement process described above, and thus the sedimentary column is probably thinner in those areas with more local topography. The greater depths found at the northwest corner of the ice shelf also suggest sedimentary thinning there.

Finally, the Bouguer anomaly map (Fig. 16) tends to confirm this conclusion since the anomalies are somewhat higher in the northwestern ice shelf area than at LAS. If only the middle layer increases in thickness from LAS to Area #1, the average Bouguer anomaly difference of 10 mgal (assuming the ocean to be filled in with material of density 2.7 gm/cm^3) corresponds to a 340 m thinning of the low density layer. Taking

TABLE 12

Densities Computed From Free Air Anomaly Differences
Between Seismic Stations in the Ross Ice Shelf Area

	<u>Station Pair</u>	<u>Δh</u>	<u>ρ_c</u>	<u>Distance Between Stations</u>
Area #1	<u>14.0</u> , 13.0	343m	2.70 gm/cm ³	75 km
	<u>14.0</u> , 11.0	309	2.80	120
	<u>14.0</u> , 12.0	118	2.95	125
	<u>12.0</u> , 13.0	225	2.56	50
	<u>12.0</u> , 11.0	191	2.70	50
	<u>11.0</u> , 13.0	34	*1.73	60
			Mean Density 2.74 gm/cm ³	
Area #2	<u>58.0</u> , 59.0	471m	3.10 gm/cm ³	35 km
	<u>58.0</u> , 85.0	378	2.98	50
	<u>58.0</u> , 81	99	*3.10	70
	<u>58.0</u> , 63	197	3.13	75
	<u>81</u> , 63	98	*3.15	20
	<u>81</u> , 59.0	372	3.09	70
	<u>81</u> , 85.0	279	2.96	75
	<u>63</u> , 59.0	274	3.06	65
	<u>63</u> , 85.0	181	2.86	65
	<u>85.0</u> , 59.0	93	*3.49	10
			Mean Density 3.03 gm/cm ³	
Area #3	<u>46.3</u> , 46.2	40m	*2.70 gm/cm ³	5 km
	<u>46.3</u> , 46.0	89	*2.83	20
	<u>46.3</u> , 45.0	170	2.94	55
	<u>46.2</u> , 46.0	49	*2.93	15
	<u>46.2</u> , 45.0	130	3.01	45
	<u>46.0</u> , 45.0	81	*3.06	35
	mile <u>125</u> , 130	40	*2.88	5
	mile <u>125</u> , 140	89	*2.99	20
	mile <u>125</u> , 160	170	2.88	55
	mile <u>130</u> , 140	49	*3.08	15
	mile <u>130</u> , 160	130	2.88	45
	mile <u>140</u> , 160	81	*2.77	35
			Mean Density 2.93 gm/cm ³	
Mile 200	mile <u>200</u> , 160	671m	2.79 gm/cm ³	50 km
			2.46	B
	mile <u>200</u> , 140	590	2.79	80
			2.41	B
	mile <u>200</u> , 130	541	2.76	95
			2.35	B
	mile <u>200</u> , 125	501	2.75	105
			Mean Density 2.31 gm/cm ³	B
				2.77 gm/cm ³
				2.38 gm/cm ³ B

*Not used in determining the mean because of small Δh

B Bouguer Corrected

elevations into consideration, this thinning corresponds to a rise in elevation of the middle layer of from 50 m to 390 m in Area #1. Next, assuming an increase in only the bottom layer between LAS and Area #2, the average difference in Bouguer anomalies of 40 mgal (using 3.0 gm/cm^3 material to fill in the ocean) corresponds to a 950 m thinning of the low density layer and indicates a rise of 150 m to 650 m in the bottom layer (thickness of middle layer assumed constant).

Near absence of the low density material may be possible in Area #2, but is unlikely in Area #1. The assumption of a thicker crust (0.8 km) beneath Area #2 balances the effect of total thinning of the low density layer (additional thinning of 375 m) and thereby gives the same Bouguer anomaly (crustal-mantle contrast assumed to be 0.46 gm/cm^3). However, as Area #1 is farther from the mountain front than Area #2, greater crustal thicknesses are unlikely there. Therefore, in addition to a 0.8 km crustal increase, a downward thickening of the medium density layer into the high density layer (1.1 km) must be postulated to balance the effect of total thinning in Area #1 (additional thinning of $\sim 1 \text{ km}$). The broad negative magnetic anomaly area, which coincides approximately with Area #1 (Figs. 1 and 18), may suggest such a downwarp of the 6.38 km/sec layer. The total thickness of the middle layer then becomes about 3.1 km. This is somewhat greater than the 2.1 km accumulative thickness of the Beacon Group (without dolerite sills, Gunn and Warren, 1962) with which, in this area, it is possibly associated. Therefore, although the middle layer may displace part of the lower layer, it is probably no thicker than about 2 km and any appreciable downward thickening would be accompanied by overlying low density material.

From the above discussion it is concluded that the low density surface layer of 1325 m at LAS thins in Areas #1 and #2. Although it may be absent in Area #2, this layer is most likely present in Area #1, but is probably much thinner than 1 km as indicated by the difference in Bouguer anomalies (perhaps 0.3 to 0.5 km).

E. Source of the Gravity Anomalies in Areas #1 and #2.

As previously suggested, the topography of the middle layer in Area #1 and the bottom layer in Area #2 appear to cause gravity changes in those areas. In Area #2, however, other sources may be considered. In the first place, the indicated density of 3.0 gm/cm^3 could be produced by a thinning of low density (2.0 gm/cm^3) sediments over a higher density (2.7 gm/cm^3) dome. It is unlikely, however, that such is the case because the trends of the Bouguer anomaly high and topographic high do not parallel each other in this area (see Fig. 17 and 22). Furthermore this model would not explain the overall difference of 150 gammas between Areas #1 and #2 (see Fig. 19). Secondly, a vertically developed intrusive might account for the high Bouguer anomaly over Area #2. However, if such were the case, the excellent correlation between free air gravity anomalies and ocean bottom would probably be disturbed.

The most probable explanation is the postulation of horizontally intruded diabase sills, known to have widespread distribution throughout Victoria Land to the west of Area #2. Because the base of these sills is flat, the surface topography should correlate well with changes in gravity. The rise of 650 m in the elevation of the bottom layer between LAS and Area #2 corresponds to the thickness required for these sills (computed). Davies (1956) states that the aggregate thickness of the diabase sills in this region is probably over 4000' (1200 m). Gunn and Warren (1962) cite individual sill thicknesses of as much as 1000' (300 m). Furthermore the density of diabase, ranges between 2.9 gm/cm^3 and 3.1 gm/cm^3 (see Birch, 1942), values which include the density indicated in Area #2. Since the susceptibility of these sills, as measured by Bull, Irving and Willis (1962a) ranges from 0.000014 to about 0.0023 (cgs), the slightly higher magnetic values in Area #2, compared with Area #1, can be accounted for. Gravity and magnetic anomalies seem to favor a general thickening of the middle layer in Area #1. If this layer represents the Beacon Group there, it is quite natural to expect numerous diabase sills in Area #2 farther to the west. Thus the geophysical data can be considered to be compatible with the presence of Beacon Group sediments lying beneath the ice shelf in the NW sector.

F. Source of the Gravity Anomalies Over the Majority of the Ross Ice Shelf Area.

The large scatter of points on the Δg vs. Δh graph (Fig. 23) illustrates the poor correlation between free air anomalies and ocean bottom topography over the majority of the ice shelf area. This poor correlation indicates that changes in gravity are due not only to ocean bottom topography, but to variations in layer thickness or other horizontal changes in density beneath the ocean floor. Because the density contrast between the two upper layers is large (0.7 gm/cm^3) compared with density contrasts from other sources beneath the ocean, this contrast is considered the most important one. Therefore, the scatter of points on the graph is probably caused by variations in thickness of the low density layer. These variations may result from the burial of ancient topography by ice rafted sediments.

Using the above concept, explanation of many features found on the Bouguer Anomaly map (Fig. 16) is possible. Along the mountain front, where one would normally expect lower Bouguer anomalies as a result of the thicker crust beneath the mountains, the relatively high Bouguer anomalies indicate sedimentary thinning. Further support for this explanation is indicated by the increased depth along this zone. The general decrease in Bouguer anomalies toward the center of the ice shelf indicates thicker low density sediments; the thickest portions of this layer are probably found east of the +30 mgal contour. Those areas with high Bouguer anomalies (i.e. RIST stations 10.0, 29.0, 31.0, and 35.0) are probably former high areas over which the low density layer thins. The narrow low anomaly at the south end of the ice shelf (between stations 25.0 and 28.0, RIST) may be a sediment-filled former glacial valley associated with the glaciers to the southeast.

Northwest of Barne Inlet at station 73 (DDT) the Bouguer anomaly is 19 mgal lower than at station 59.0 (VLT 58-59), also located along the deepest part of Discovery Deep. Since both stations fall on a curved line projected from the Byrd Glacier at Barne Inlet, former glaciation may have eroded this channel. The deeper end near station 73 may contain more low density sediments (450 m of 2.0 gm/cm³ sediment could account for the gravity difference). A former glacial channel, empty or filled with sediment, may also account for the extremely steep gravity gradient (~4 mgal per nautical mile) to the west of station 60.0 (see Fig. 13) which cannot be explained by the terrain effect of the mountains nor by a thick crust beneath them. The general decrease in Bouguer anomalies as the mountain front is approached is, however, probably due to an increased crustal thickness beneath the mountains.

G. Source of the Gravity Anomalies in the Roosevelt Island Area

Salient features in the Roosevelt Island area (see Fig. 17) include a broad Bouguer anomaly low, about 40 nautical miles across with a minimum of -34 mgal, situated at the northwest end of the island. This low has a general SSE trend as indicated by limited data. In this same area vertical magnetic anomalies of +200γ to +250γ are found (see Fig. 19). Northeast of the island, a broad vertical magnetic low with a minimum of -200γ is centered at mile 40 on the Byrd Trail (42.0, LAS-BT). Southeast of mile 40, along the Byrd Trail, the Bouguer anomalies increase forming a high of +46 mgal at mile 80 (43.0, LAS-BT) east of the island. The single station on Roosevelt Island (1.0, RIST) yields a Bouguer anomaly of -4 mgal, 37 mgal lower than the mean Bouguer anomaly of +33 mgal over the Ross Ice Shelf area.

The gravity anomalies on and around Roosevelt Island cannot be explained solely by a variation in low density sediment thickness. Recent seismic investigations indicate that a thin low velocity layer (~2.4 km/sec), found in some parts of the island, is underlain by high velocity materials (4.5 to 5.35 km/sec) (M. Hochstein, personal communication). The high Bouguer anomaly area east of Roosevelt Island (centered at mile 80) can be explained by thinning of the low density layer. However, this explanation alone cannot account for the relatively low Bouguer anomaly (+22 mgal) northeast of Roosevelt Island at mile 20 (49.0, LAS-BT), where the 2.4 km/sec layer thickness is known to be less than at LAS. Furthermore this model does not fit the magnetic anomalies.

The most promising explanation of the gravity and magnetic anomalies on and around Roosevelt Island is the presence of a relatively low density intrusive exposed by erosion. Support for this explanation may be found in reviewing the geologic evidence in the adjacent areas. Wade (1945) states that "The greater part of the exposed portions of the Rockefeller Mountains is highly acidic, intrusive, igneous rock which appears to surround a remnant of the pre-existing metamorphosed sediments." Wade believes that the Edsel Ford Mountains are geologically similar to the Rockefeller Mountains. Since the Edsel Ford Mountains and Roosevelt Island are equidistant from the Rockefeller Mountains, it is possible that similar intrusives occur at Roosevelt Island.

Let us consider the three layer section measured at LAS. If an acidic body, probably granite with a density of 2.6 gm/cm^3 , were intruded into the high density layer, a Bouguer anomaly low outlining the general area of intrusion would result. The low Bouguer anomalies found along the northwest edge of Roosevelt Island could be explained by an intrusive, extending approximately 5 km into the high density bottom layer. The difference in Bouguer anomalies between station 1.0 on Roosevelt Island, and 2.0, 45 km to the west, could result from a 1.2 km thinning of low density sediments over Roosevelt Island, provided the vertical extent of intrusion were equal under both stations. The linear free air anomaly low of about -40 mgal located just east of the island's northern tip (Fig. 16), probably indicates the extension of a deep water channel found on the east side of the island by Hochstein (personal communication).

Magnetic anomalies in the area lend some support to the above explanations. The magnetic "lows" at the north and southeast ends of the island could represent replacement of the 6.38 km/sec layer by granitic material of lower susceptibility. Jakosky (1950) gives a susceptibility range for granite between 0.00003 and 0.0027 (cgs). Thus the susceptibility contrast of ~0.001 (cgs) calculated from these anomalies is reasonable for a granitic replacement of a higher susceptibility material such as gabbro (0.00044 to 0.0041 cgs). The narrow magnetic "highs" at the northwest and perhaps at the south end of the island may be caused by an edge effect produced at the boundary between the 6.38 km/sec layer and the intrusive.

The most graphic indication of lower susceptibility is illustrated by the displacement vectors plotted on a profile along the Byrd Trail (Fig. 11). These indicate a lower susceptibility material present beneath mile 20 (49.0, LAS-BT) and extending beyond mile 60 (48.0, LAS-BT). At mile 20 the low density layer is known to be thinner than at LAS but the Bouguer anomaly is lower. A relatively low density, low susceptibility material beneath mile 20 can explain this observation.

An active geophysical and glaciological program being carried out over Roosevelt Island will result in a more thorough understanding of this area in the future. The interpretation given here is simplified and revisions will probably have to be made. However, the basic idea of relatively low density intrusives replacing higher density "country rock" should explain the relatively lower Bouguer anomaly over the northern portion of Roosevelt Island.

H. Isostatic status of the Ross Ice Shelf Area - Mean Free Air Anomaly

In areas of low relief, the free air anomaly is a good approximation to the isostatic anomaly and is therefore assumed to indicate the degree of isostatic compensation over the Ross Ice Shelf. For this work the mean free air anomaly and mean depth for the Ross Ice Shelf area were determined by two different methods. In each case, the standard deviation and mean of the sets of observations were computed.

First, by weighing each value equally, all free air anomalies and seismic depths were treated as one sampling of the mean. To prevent bias from the overlap of traverses and from low free air anomalies around Roosevelt Island, and those associated with greater depths at the northwestern and southern ice shelf area, several groupings of data were used. The results are shown in the top portion of Table 13.

Second, the free air anomalies and seismic depths were averaged over areas having two different radii, 55 km (0.5°) and 155 km (1.4°). The mean free air anomaly and depth were then obtained by averaging the means from all areas. The variance in each area was computed, and the average of these values was considered to be the variance for the whole ice shelf area. The square root of this variance was used as the standard deviation of the observations (σ). The standard deviation of the mean ($\sigma_{\bar{A}}$) was computed by dividing the standard deviation of the observations by the square root of the number of observations. This second method gives equal weight to areas, compared with equal weight given observations according to the first method. The second method probably gives a more accurate mean value, due to the fact that station spacing varied widely over the ice shelf (seismic stations are much closer in the northwest corner of the ice shelf where deeper ocean is found).

In the case of the second method, three groupings of the same basic data were used. Group I included all the data. Group II excluded data around Roosevelt Island, McMurdo Sound, and along the mountain front from the Beardmore to the Liv Glacier. Group III consisted of Group II data excluding all data on the Byrd Trail. Groups II and III were used in order to exclude anomalous areas (near mountains, deep areas, and Roosevelt Island); little change in the mean free air anomaly resulted (see Table 13). From the average of the six mean free air anomalies and mean depths obtained from the 55 km and 155 km radius areas, values of -12.0 mgal and 650 m were adopted for the mean free air anomaly and mean depth over the Ross Ice Shelf. These values give a mean Bouguer anomaly of +33 mgal. Group III data gave an average free air anomaly of -10 mgal but this value was not used to represent the mean because of the limited number of observations. (Note: use of the triaxial formulas listed by Heiskanen and Uotila (1958) results in a more negative mean free air anomaly).

In the larger radii areas the standard deviations are observed to be slightly larger; indicating that, on the average, variation of observations within an area increases with the size of the area (for areas up to 155 km in radius). If there were a tendency for topography to be compensated over the larger distances, the standard deviations should be smaller. Therefore, these data tend to confirm the earlier conclusion that relative topography between stations (up to 125 km) is not compensated.

It is evident that the isostatic anomaly, approximated here by the mean free air anomaly, is significantly negative over the Ross Ice Shelf area. The free air anomaly map (Fig. 15), in which shading indicates the positive areas, illustrates this overall negative character. It is not surprising that this situation occurs in an area that has probably had an ice load in the not too distant past.

TABLE 13

Mean Free Air Anomalies and Depths in the Ross Ice Shelf Area

Single Area (4° radius)

Traverses	No. of gravity observations	Mean Free Air <u>Anomaly</u> (Δg)	No. of Depth Determinations	Mean Depth (D)	Standard Deviation (σ)	Standard Deviation of the mean ($\sigma_{\Delta g}$)
all traverses	430	-16.2 mgal	79	730 m	± 14.5 mgal	± 0.70 mgal
all values						
(LAS-BT)(RIST) (VLT 58-59)(DDT 41-81)	344	-17.3 mgal	79	730 m	± 15.8 mgal	± 0.85 mgal
(RIST) 4.0-37.0	155	-12.0 mgal	38	658	± 11.3 mgal	± 0.91 mgal
(RIST) 4.0-20.0 & 25.0-37.0	132	-11.0 mgal	33	642	± 11.8 mgal	± 1.03 mgal

55 km Radius Areas (0.5°)

Group	No. of Areas (M)	No. of Observations (N)	Mean Free Air <u>Anomaly</u> (Δg)	No. of Depth Determinations	Mean Depth (D)	Standard Deviation (σ)	Standard Deviation of the Mean ($\sigma_{\Delta g}$)
I	22	430	-15.0 mgal	79	714 m	± 10.6 mgal	± 0.51 mgal
II	15	257	-11.6 mgal	42	689 m	± 10.3 mgal	± 0.64 mgal
III	11	111	-9.5 mgal	25	602 m	± 10.0 mgal	± 0.95 mgal

155 km Radius Areas (1.4°)

Group	No. of Areas (M)	No. of Observations (N)	Mean Free Air <u>Anomaly</u> (Δg)	No. of Depth Determinations	Mean Depth (D)	Standard Deviation (σ)	Standard Deviation of the Mean ($\sigma_{\Delta g}$)
I	8	430	-14.4 mgal	79	683 m	± 13.4 mgal	± 0.65 mgal
II	5	172	-11.6 mgal	34	653 m	± 12.8 mgal	± 0.98 mgal
III	4	111	-10.4 mgal	25	622 m	± 13.0 mgal	± 1.24 mgal

Aver. -12.08 mgal
(55 & 155 km Areas) 660.5 m

There is evidence in the dry valley areas of McMurdo Sound that more extensive glaciation has occurred in the past (Péwé, 1962; Gunn and Warren, 1962). Ostenso (1958) has reported that in the Sentinel Mountains "glacial striations were found on the summit of one nunatak approximately 1000 feet (300 m) above the present snow surface." Priestly and David (1910) state that erratics were found at the lower end of the Beardmore Glacier on the summit of Mt. Hope presently 600 m or more above the present glacial surface. If the thicker ice sections indicated by this evidence previously existed over large areas and not just locally, there is reason to believe that the shelf area was formerly covered by grounded ice.

I. Comparison of the Ross Ice Shelf Area with Fennoscandia - Two Former Ice Loaded Areas?

Assuming that the negative isostatic anomaly of 12 mgal over the Ross Ice Shelf area is the result of former ice loading, we will analyze the data from the Ross Ice Shelf area according to the method used in Fennoscandia (Heiskanen and Vening Meinesz, 1958a). Vening Meinesz treats Fennoscandia as a region from which the ice load was removed over a short period of time compared to its isostatic relaxation time, and arrives at the following formulae for the rise of the center of the loaded area:

$$Z = Z_0 e^{-kt} \quad (9)$$

where

Z = depression of the surface below the equilibrium level,

Z_0 = maximum depression just after load removal (at $t = 0$)

t = time since load removal,

$$k = \frac{\rho_m g}{2\pi\eta} L \quad (10)$$

where

ρ_m = 3.27 gm/cm³ (mantle density),

g = 980 cm sec⁻² (acceleration of gravity),

η = 10²² poises (viscosity),

$$L = \left(\frac{XY}{X^2 + Y^2} \right)^{\frac{1}{2}} \text{ (in megameters)} \quad (11)$$

where

X = length of the loaded area in megameters, and

Y = width of the loaded area in megameters.

Since the area beneath the Ross Ice Shelf and its equilibrium level (depth for which complete rebound is realized and the mean free air anomaly becomes zero) are below sea level, a revision of the above formulae must be made. From equation 9:

$$\dot{Z} = -kZ \quad (12)$$

or $\left(\frac{2\pi\eta}{L}\right) \dot{Z} + \rho_m g Z = 0 \quad (13)$

The latter may be considered the equation of motion for the central loaded area of Fennoscandia. Over the Ross Ice Shelf area there is an additional load due to the water column of thickness Z (see Fig. 25) the equation of motion becomes:

$$\left(\frac{2\pi\eta}{L}\right) \dot{Z} + \rho_m g Z - \rho_w g Z = 0 \quad (14)$$

where

$$\rho_w = 1.03 \text{ gm/cm}^3 \text{ (the density of sea water)}$$

the solution is

$$Z = Z_0 e^{-k't} \quad (15)$$

where

$$k' = \left(\frac{\rho_m - \rho_w}{\rho_m} \right) k \quad (16)$$

Solving for t , equation 15 becomes:

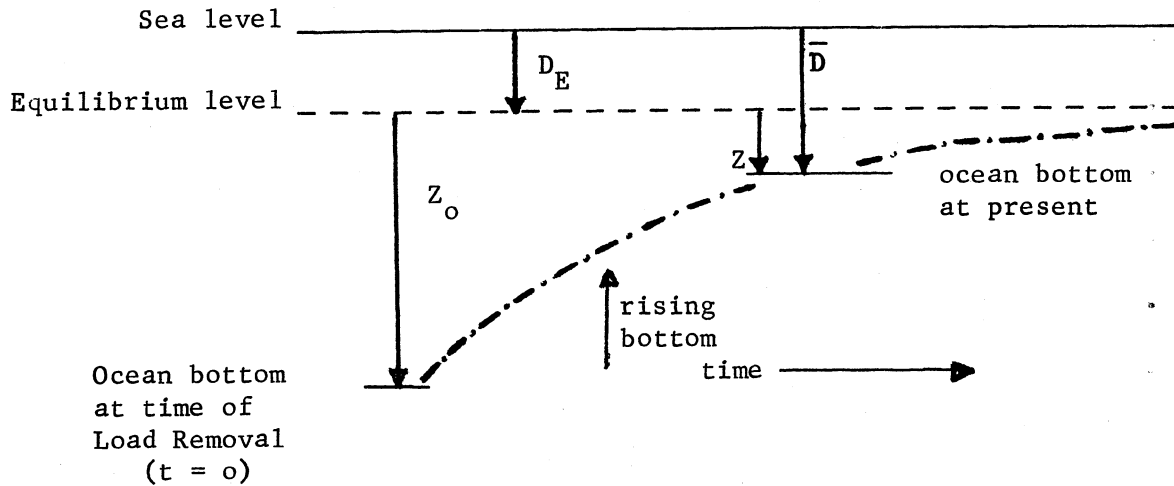
$$t = t'_r \ln \left(\frac{Z_0}{Z} \right) \quad (17)$$

where

$$t'_r = \frac{1}{k'} \quad \begin{aligned} & \text{(the relaxation time or} \\ & \text{time necessary for the} \\ & \text{depression } Z \text{ to diminish} \\ & \text{to } e^{-1} \text{ of its original} \\ & \text{value } Z_0 \end{aligned} \quad (18)$$

Fig. 25

Crustal Rise Diagram



The purpose of this study is to attempt to determine the length of time (t) since the assumed ice load was removed from the Ross Ice Shelf area. Therefore, to solve equation 17 for t , it is necessary either to measure indirectly or to estimate the values of Z , Z_0 and t_r' . An approximate Z can be determined from the mean free air anomaly (Δg) over the area by the equation:

$$Z = \frac{-\Delta g}{2\pi\gamma (\rho_m - \rho_w)} \quad (19)$$

Z_0 can be calculated from an estimated net ice load ($\rho_i N$), which represents the additional load on the crust. It is assumed here that the depth to the equilibrium level (D_E) was the same before the ice loading as it is now. Thus if the total thickness of the ice load were T the net ice load thickness is:

$$N = T - \left(\frac{\rho_w}{\rho_i} \right) D_E \quad (20)$$

where

$$\rho_i = .91 \text{ gm/cm}^3 \text{ (the mean ice density)}$$

Now,

$$Z_0 = \left(\frac{\rho_i}{\rho_m} \right) N \quad (21)$$

and from Fig. 25:

$$D_E = \bar{D} - Z \quad (22)$$

Therefore, Z_o in terms of T , \bar{D} , and Z becomes:

$$Z_o = \left(\frac{\rho_i}{\rho_m} \right) T - \left(\frac{\rho_w}{\rho_m} \right) (\bar{D} - Z) \quad (23)$$

Finally, t'_r can be determined, using equations 10, 16 and 18, by the expression:

$$t'_r = \left(\frac{1}{L} \times 9075 \right) \text{ yrs.} \quad (L \text{ in megameters}) \quad (24)$$

We now have equations for computing Z_o , Z , t'_r and thus t in terms of Δg , D , L and T . The mean free air anomalies (Δg) and mean depths (D), discussed at the beginning of the section, were determined from direct measurements. Since the values varied, depending on the method used for determining the mean, we shall adopt three pairs of values for Δg and D . These pairs are -15 mgal and 700 m, -12 mgal and 650 m, and -10 mgal and 600 m.

The task is now that of estimating the dimensions of the loaded area (and thus L) and the mean total ice thickness of the ice load (T). According to Hollin (1962), assuming a lowering of sea level by 150 m, the ice cap edge would have advanced about 550 km over the eastern half of the Ross Ice Shelf during the Wurm. This would have brought the grounded ice front to about 80°S latitude. Since the gravity data indicate low free air anomalies north of this latitude of the same order of magnitude as those south of it, the grounded ice front probably extended farther north than 80°S. In our calculations we shall assume two different loaded areas: (1) the area presently occupied by the Ross Ice Shelf, and (2) the area coincident with the continental shelf over the Ross Sea and extending to the -1000 m contour line (see the National Geographic Society Map of Antarctica 1962). These areas are referred to as Area A and B respectively. Area A has an area of about 525,000 km² and is approximated by a 650 x 850 km rectangle in our study. Equation (11) yields a value for L of 0.516 megameters. From equation (24) t'_r equals 17,600 years. Area B has an area of 986,000 km² and is approximated by a rectangle 800 km by 1300 km. For this area L equals 0.68 megameters, and t'_r equals 13,350 years. (For ease in calculation, the dimensions for Areas A and B were rounded off, giving a total area about 5% greater than that measured on the map. This decreases t'_r by less than 1.5% and does not effect the conclusions drawn from this study.) For Fennoscandia Vening Meinesz used a rectangle 2300 km x 1400 km, which gives 1.2 megameters, and 5,280 years for L and t'_r respectively.

To estimate the mean total ice load thickness (T) over Areas A and B, Hollin's equilibrium profile was integrated for each area over the average distance (perpendicular to the ice front), from the supposed ice fronts to the inland edge of the region. Using average distances of 600 km and 750 km, average ice thicknesses (T) of 2350 m and 2550 m were determined for Areas A and B respectively.

Having obtained values for $\bar{\Delta}g$, \bar{D} , L and T it is now possible to compute the values for Z , Z_0 and t (equations 19, 23 and 17). These values are listed in Table 14. Three values were used for $\bar{\Delta}g$ and \bar{D} and two for L in order to indicate how much t varies with the limits of these parameters. In order to see how t varies with the total ice load thickness (T), a second set of calculations was made using data from Table 14 and changing T by ± 500 m. The corresponding values of t are shown in Table 15.

Before drawing any conclusions from Tables 14 and 15 two corrections, which have been neglected for purposes of simplicity, should be discussed. First, in order that the data be treated according to the method used by Vening Meinesz, a correction for the elastic reaction of the upper layers of the earth must be applied. Elastic reaction is the quickest reaction to loading or unloading of the crust and takes place prior to the onset of viscous flow (upward) at the time of unloading, and after the substratum has begun flowing into the region beneath the unloaded area (downward). The elastic reaction correction used for Fennoscandia is given by a formulae determined from studies of a low pressure area moving across a continent, thereby producing upwarp. The formulae, derived by Darwin (Heiskanen and Vening Meinesz, 1958a) is:

$$H = \frac{gr\rho h}{2\pi\mu} \quad (25)$$

where

H = elastic reaction

$g = 980 \text{ cm sec}^{-2}$ (acceleration of gravity)

r = radius of the assumed load

ρ = density of the load

h = height of the load in the center

μ = rigidity of the upper layers of the earth

By setting r equal to $0.9 L$ and μ equal to $4 \times 10^{11} \text{ dynes cm}^{-2}$, as Vening Meinesz had done for Fennoscandia, the elastic correction for Z_0 and Z was computed. In the correction for Z_0 , ρh was represented by the net load removed (total ice load minus the remaining water load). In the correction for Z , ρh (the net load added) equalled the difference between the amount of mantle material that had flowed into the region and the amount of water that had flowed out since the time of load removal. As a result of this correction both Z_0 and Z are diminished. The values of $Z_{0,e}$ and Z_{e} (elastically corrected) were then used in formulae 17 to compute the values for t . The new values for t were 5% to 15% (average 10%) greater than the values shown in Tables 14 and 15.

TABLE 14

Comparison of Uplift in Fennoscandia
with the Assumed Uplift in the Ross Ice Shelf Area

Fennoscandia (1400 km x 2300 km)

Δg mgal	\bar{D} meters	L megameters	T meters	Z meters	Z_o meters	tr yrs	t yrs
-20		1.2	2,320	80	556	5,180	10,000

Ross Shelf Area A (650 km x 850 km)

Δg mgal	\bar{D} meters	L megameters	T meters	Z meters	Z_o meters	tr yrs	t yrs
-15	700	0.516	2,350	160.0	473.0	17,600	19,100
-12	650	0.516	2,350	128.0	479.0	17,600	23,200
-10	600	0.516	2,350	106.5	487.5	17,600	26,800

Ross Shelf Area B (800 km x 1300 km)

Δg mgal	\bar{D} meters	L megameters	T meters	Z meters	Z_o meters	tr yrs	t yrs
-15	700	0.680	2,550	160.0	539.0	13,350	16,200
-12	650	0.680	2,550	128.0	545.0	13,350	19,300
-10	600	0.680	2,550	106.5	553.5	13,350	22,000

TABLE 15

Computed Time (t) Since Load Removal Corresponding to
Variations in the Estimated Mean Total Ice Thickness (T)

For a Mean Free Air Anomaly of -15 mgal

	Mean Total Ice Thickness (T)	Time Since Load Removal (t)		Mean Total Ice Thickness (T)	Time Since Load Removal (t)
<u>Area A</u>	T (2350m)	19,100 yrs.	<u>Area B</u>	T (2550m)	16,200 yrs.
	T +500m	23,900 yrs.		T +500m	19,300 yrs.
	T -500m	13,500 yrs.		T -500m	12,200 yrs.

For a Mean Free Air Anomaly of -12 mgal

	Mean Total Ice Thickness (T)	Time Since Load Removal (t)		Mean Total Ice Thickness (T)	Time Since Load Removal (t)
<u>Area A</u>	T (2350m)	23,200 yrs.	<u>Area B</u>	T (2550m)	19,300 yrs.
	T +500m	28,000 yrs.		T +500m	22,400 yrs.
	T -500m	17,700 yrs.		T -500m	15,400 yrs.

For a Mean Free Air Anomaly of -10 mgal

	Mean Total Ice Thickness (T)	Time Since Load Removal (t)		Mean Total Ice Thickness (T)	Time Since Load Removal (t)
<u>Area A</u>	T (2350m)	26,800 yrs.	<u>Area B</u>	T (2550m)	22,000 yrs.
	T +500m	31,400 yrs.		T +500m	25,000 yrs.
	T -500m	21,400 yrs.		T -500m	18,100 yrs.

The second correction was applied to the calculated value of η . After attaining complete isostatic equilibrium, the lowest elevations in Fennoscandia, presently in the Baltic Sea and the Gulf of Bothnia, will still be below sea level (assuming 80 m of rise, Heiskanen and Vening Meinesz, 1958a). Furthermore, if we assume that Fennoscandia has risen by some 400 m since the ice load was removed (Heiskanen and Vening Meinesz, 1958a), the old shore line at the beginning of readjustment can be approximated by the 400 m elevation contour. Referring to a map of Norden (Somme, 1960), it is seen that the area below the 400 m elevation contour constitutes more than 2/3 of the area used by Vening Meinesz. A large portion of Fennoscandia probably remained below sea level during much of the readjustment period and therefore a correction should be made in the determination of viscosity (η) for the overlying water load.

The average value of η (determined with and without a water load) is $.85 \times 10^{22}$ poises and is considered the corrected value of η . Because t is proportional to η (see equation 10, 16, 17, and 18), the corrected values of t in Tables 14 and 15 are reduced by 15%. However, the two corrections (elastic reaction and water load) nearly cancel each other; therefore the values of t in Tables 14 and 15 are considered to be corrected values. It is concluded from these tables that if the negative isostatic anomaly over the Ross Ice Shelf area resulted from former ice loading, the ice load disappeared somewhere between 12,000 and 31,000 years before the present (B.P.).

Let us now take a slightly different viewpoint. The thick sedimentary column at Little America Station might indicate that sedimentation has been an important factor throughout the isostatic readjustment period. The large scatter of densities on the Δg vs. Δh plot tends to confirm that low density sediments are present over the major portion of the shelf. Furthermore, the relatively low Bouguer anomalies over the central area of the Ross Ice Shelf indicate that thick sedimentary sections are to be found there. If these sediments were transported into the area by the shelf ice, then we might expect a thinning of sediment toward the front of the shelf. Such sedimentary thinning is generally confirmed by the higher Bouguer anomalies found in the northwestern area of the shelf (Fig. 16). Regardless of the mechanics involved in deposition, the rate at which equilibrium is established would be accelerated if any sedimentation occurred after the ice load had been removed.

In the above calculations it was assumed that the ice load rested on the present ocean bottom surface. Let us now suppose that the ancient glacial bed surface is buried by sediment (Fig. 26). To include the effect of sedimentation, assuming a constant rate of sedimentation (R) of 2.03 gm/cm^3 material, we now introduce the following equation of motion:

$$\left(\frac{2\pi \eta}{L t} \right) \dot{z}_s + (\rho_m - \rho_w) g z_s - (\rho_s - \rho_w) g R t = 0 \quad (26)$$

where

$$\rho_s = 2.03 \text{ gm/cm}^3 \quad (\text{density of the sedimentary material})$$

whose solution is

$$z_s = z_{o,s} e^{-k't} + \frac{Rt}{(\rho_m - \rho_w)} + \frac{Rt_r'}{(\rho_m - \rho_w)} (e^{-k't} - 1) \quad (27)$$

To calculate z_s on the basis of the measured mean free air anomaly, we must compute the mean free air anomaly in the absence of sediment. This calculation is equivalent to applying a Bouguer correction for the sediments of thickness (Rt). The attraction of the additional sediment is:

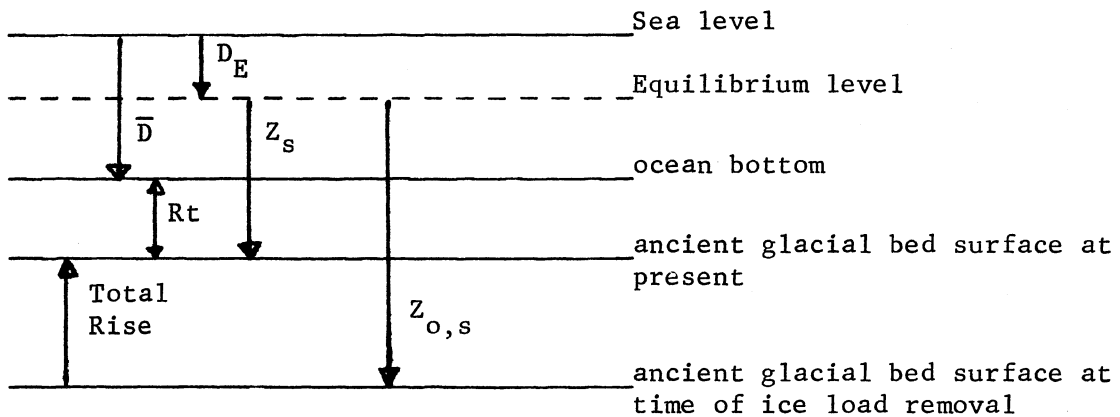
$$\Delta g = 2\pi\gamma (\rho_s - \rho_w) Rt \quad (28)$$

Hence, the present depression of the ancient glacial bed surface below equilibrium level is (see equation 19):

$$z_s = \frac{-(\bar{\Delta g} - \Delta g_s)}{2\pi\gamma (\rho_m - \rho_w)} = z + \left(\frac{\rho_s - \rho_w}{\rho_m - \rho_w} \right) Rt \quad (29)$$

Fig. 26

Crustal Rise Diagram Assuming
Sedimentation Contemporary with Adjustment



The maximum depression at $t = 0$ then becomes:

$$z_{o,s} = \left(\frac{\rho_i}{\rho_m} \right) T - \left(\frac{\rho_w}{\rho_m} \right) (\bar{D} + R_t - z_s) \quad (30)$$

Using equation 9 and substituting equations 29 and 30 into equation 27 we solve for R_t

$$R_t = \frac{(\rho_m - \rho_w) (z_o e^{-k't} - z)}{\left(\frac{\rho_w}{\rho_m} \right) (\rho_m - \rho_s) e^{-k't} + \left(\frac{1 - e^{-k't}}{k't} \right)} \quad (31)$$

We are now in a position to evaluate the relative importance of sedimentation on the shelf. Using equation 31 and assuming that both Fennoscandia and the Ross Shelf began their adjustment at the same moment (setting $t = 10,000$ years), we can calculate the amount of sediment deposited since the ice load was removed. An upper limit of 3000 m and a lower limit of 2000 m was assumed for the total ice load thickness (T) in both areas; the same sets of Δg and \bar{D} were used as in Table 14. The computed values of sediment, deposited since 10,000 years B.P. are shown in Table 16.

In compiling Table 16 sediments of thickness R_t were assumed to be deposited at a constant rate. In order to estimate any error that may be introduced by a nonconstant rate of sedimentation, we will consider the two extreme conditions: (1) all the sediment deposited immediately after ice removal, and (2) all the sediment deposited recently.

For condition one the solution is:

$$z_s = \left[z_{o,s} - \left(\frac{\rho_s - \rho_w}{\rho_m} \right) S \right] e^{-k't} + \left(\frac{\rho_s - \rho_w}{\rho_m} \right) S \quad (32)$$

where S is the sedimentary thickness. By replacing R_t with S in the equations for z_s and $z_{o,s}$ (Equations 29 and 30) and substituting these, into equation 32, the value of S can be determined. Using the underlined values in Table 16 (second line of Area B), the value of S is 515 m.

For condition two the solution is:

$$z_s = z_{o,s} e^{-k't} \quad (33)$$

Using the same procedure and assumed values, the solution for S is 358 m. The value for S in Table 16 is 477 m.

TABLE 16

Calculated Values of Sedimentary Deposition (Rt) since Ice Load Removal

Ross Shelf Area A

t (assumed) yrs.	$\frac{tr}{t}$	$e^{-k't}$	T (assumed) meters	$\bar{\Delta g}$ mgal	\bar{D} meters	Z meters	Rt (computed) meters
10,000	1.76	0.5665	3000	-15	700	160	494
10,000	1.76	0.5665	3000	-12	650	128	573
10,000	1.76	0.5665	3000	-10	600	106	635
10,000	1.76	0.5665	2000	-15	700	160	134
10,000	1.76	0.5665	2000	-12	650	128	215
10,000	1.76	0.5665	2000	-10	600	106	277

Ross Shelf Area B

t (assumed) yrs.	$\frac{tr}{t}$	$e^{-k't}$	T (assumed) meters	$\bar{\Delta g}$ mgal	\bar{D} meters	Z meters	Rt (computed) meters
10,000	1.335	0.473	3000	-15	700	160	390
<u>10,000</u>	<u>1.335</u>	<u>0.473</u>	<u>3000</u>	<u>-12</u>	<u>650</u>	<u>128</u>	<u>477</u>
10,000	1.335	0.473	3000	-10	600	106	545
10,000	1.335	0.473	2000	-15	700	160	59
10,000	1.335	0.473	2000	-12	650	128	145
10,000	1.335	0.473	2000	-10	600	106	211

As the sedimentation rate was probably greater at the beginning during ice retreat, condition one is the most likely deviation from a constant sedimentation rate. The difference in thickness calculated for condition one and for the assumption of a constant rate of sedimentation is small (i.e., 38 m); hence, the assumption of a constant sedimentation rate provides a good approximation.

The maximum sedimentary thickness corresponding to a maximum value of T is about 600 m (Table 16). If the ice load had been removed more recently than 10,000 years B. P., the calculated sedimentary thickness would be greater. An upper limit of 875 m can be determined by letting t approach zero on the right hand side of equation 31. This procedure is identical to equating the gravitational attraction of the ice load to that of the ocean and sedimentary column, taking into account the 12 mgal deficit. If, however, the ice load had been removed much earlier than 10,000 years B. P., the calculated sedimentary thickness would be less. For example, if the values of Δg , D , L and T , which gave 31,400 years for t in Table 15, are used in equation 31 and t is set at 31,400 years on the right side, then Rt becomes zero. Thus the value of Rt in equation 31 varies from 0 m to 875 m as t varies from 31,400 years to zero years. The continental shelf has probably not had an ice load for 8000 years or more, and therefore the maximum amount of sediment deposited since unloading is estimated to be 600 m. We conclude that the previous glacial bed must lie within 600 m of the present ocean bottom.

In the above calculations, which led to the values of t and Rt in Tables 14, 15 and 16, the assumption was made that the viscosity of the substratum in the Ross Sea area and Fennoscandia is the same. If this is true, the value for viscosity is of minor importance. In determining the time of load removal in the Ross Ice Shelf area, we are then dependent only upon the correctness of the value 10,000 years which Vening Meinesz used to represent the postglacial period of Fennoscandia and the assumption that t'_r is inversely proportional to L .

Recent evidence (Crittenden, 1963) has indicated, however, that the substratum may not react identically from area to area. We must therefore consider the effects, on t and Rt , of a relatively higher or lower viscosity beneath the Ross Sea area. Note that t'_r , and thus t , is proportional to η . Therefore, if the viscosity is lower beneath the Ross Sea, as Crittenden has calculated for the region beneath Lake Bonneville, the values of t in Tables 14 and 15 are reduced. Since $k't$ is proportional to t/η , a decrease in η is equivalent to an increase in assumed t in equation 31; the values of Rt in Table 16 are also reduced. The use of Crittenden's value of 10^{21} poises would reduce all values of t by a factor of 10. Such a reduction seems unlikely, since it requires that the continental shelf be loaded with ice within the last 3100 years. Therefore, the "effective viscosity" of the substratum in the Ross Sea area is probably close to that determined for Fennoscandia.

Crittenden entertained three different relationships between the relaxation time t_r and the value of L . These are (1) $t_r \approx \frac{1}{L^2}$ (2) $t_r \approx \frac{L}{H^3}$

(where H is the thickness of the flow layer) and (3) t_r independent of L . Let us determine the effect of these models on t and Rt . We have already used model one to determine the values in Tables 14, 15, and 16, and must now consider the other two models. Since L used for the Ross Shelf area is approximately $\frac{1}{2}$ the value of L used for Fennoscandia, if model two is adopted with H held constant, all values of t'_r and t should be reduced to approximately 1/8 of their values in Tables 14 and 15. When t'_r is reduced in equation 31, the values of Rt in Table 16 will also be reduced because $k't = t/t'_r$ (equivalent to increasing the assumed t in equation 31). If the thickness of the flow layer is reduced to $\frac{1}{2}$ of its value in Fennoscandia, the values of t and Rt are unaltered. For model three t'_r and t will be $\frac{1}{2}$ their value in Tables 14 and 15, and Rt will be less in Table 16. In all cases the value of t in Tables 14 and 15 and the values of Rt in Table 16 represent upper limits. The only situation that could make these values larger would be a higher "effective viscosity" beneath the Ross Sea area (note that if the load were not removed over a period of time small compared to the relaxation time, the same condition probably existed in Fennoscandia and the effect is thus averaged out in the empirical determination of η). Crittenden's determination of 10^{21} poises in the Lake Bonneville area is taken to mean that viscosities in the upper mantle may be lower than 10^{22} poises but since no values of η , determined in areas outside Fennoscandia, are higher, this figure is considered to be near the upper limit. Therefore, values of t and Rt (Tables 14, 15, and 16) are believed to be upper limits.

Since the mean Bouguer anomaly of +33 mgal on the Ross Ice Shelf corresponds to a mean thickness of 1350 m of low velocity material, based on the section at LAS, the ice load must have rested on at least 750-1350 m of low velocity material, present before the last ice advance. If the entire low velocity section is morainal, glacial processes prior to the last glaciation must have been responsible for depositing the additional material.

From the results of this comparative study it would appear that there is good general agreement between the uplift in Fennoscandia and the suggested uplift of the Ross Sea continental shelf area. The more advanced state of compensation of the Ross Sea area (-12 mgal), as compared with Fennoscandia (-20 mgal), is probably due to additional morainal deposition which occurred during and after glacial retreat. Sedimentation probably occurred in both areas during glacial retreat. The fact that the shelf area has remained below sea level since the ice removal may have been an important factor in advancing its state of compensation, by allowing the deposition to continue long after the retreat of the glacier.

It should be noted that the mean free air anomaly, determined from data taken only on the Ross Ice Shelf, was used to represent the isostatic anomaly over the center of the two supposed ice loaded areas. Although the approximation for the Ross Shelf Area A should be good, revision for Ross Shelf Area B may be necessary when data become available for the Ross Sea.

Conclusions

If the negative mean free air gravity anomaly over the Ross Ice Shelf results from former ice loading, the uplift in Fennoscandia is due to former ice loading, then the general agreement in the state of isostatic equilibrium between Fennoscandia and the Ross Sea continental shelf would indicate that the Wurm or Wisconsin glaciation was contemporaneous in both hemispheres. Vening Meinesz assumed 10,000 years as the length of the post glacial period in Fennoscandia. This figure is generally consistent with Milankovitch's glacial maximum of 25,000 years B.P. for the third phase of the Wurm (W3), corresponding to post glacial times of 20,000 years for Post Buhl in Switzerland, 13,000-14,000 years in Sweden, 20,000-25,000 years in the Niagara and Toronto regions, and 10,000 years for Lake Agassiz's final stage (Charlesworth, 1957). Post-Wisconsin in the Great Lakes has been determined at 11,500 years from carbon 14 dating of a drift sheet (Flint, 1957). Broecker and Farrand (1963) give radioactive dates of ~11,000 years (from H. Tauber) and 11,850 years for Europe and North America respectively; these are approximate post glacial periods. Since all calculated values of post glacial time on the Ross Shelf are under 31,000 years, the glaciation must have been associated with the third phase of the Würm and not the second (72,000 years B.P.; Milankovitch's value, Charlesworth, 1957).

The maximum amount of sediment deposited since glacial unloading is estimated to be 600 m. If, on the one hand, we assume that there has been no sedimentary contribution to the shelf since the time of iceload removal, then with reasonable variations of the mean free air anomaly, mean depth, estimated loaded area, and estimated ice load, the calculated times of ice removal lie between 12,000 and 31,000 years B.P. (Tables 14 and 15). On the other hand since the ocean bottom under the Ross Ice Shelf is composed mainly of a mixture of coarse and fine glacial till (Crary, 1961b), there must have been some sediment deposited after the ice retreated. Depending on the amount of sediment deposited, the time of ice removal is reduced from 31,000 years B.P. for zero sedimentary thickness to 10,000 B.P. for up to 600 m of sediment. It is doubtful that sedimentary thicknesses greater than 600 m were deposited since the last glacial retreat.

SUMMARY

(1) Ocean tides are detectable by gravimetric methods over the majority of the Ross Ice Shelf, including the far southern portions (Fig. 2). During the first and last quarter moon phases the ocean tides are difficult to detect but during full moon and new moon phases the amplitudes are large enough to distinguish the tidal components.

(2) Probable densities are assigned to the three layered velocity section measured at Little America Station (LAS) by Crary (1961) on the basis of velocity vs. density curves of Nafe and Drake (Talwani et al., 1959) and Woollard (1959), and on the basis of correlation between free air anomalies and ocean depths.

The density of the top 2.4 km/sec ocean bottom layer in the Ross Ice Shelf area is probably about 2.0 gm/cm^3 , based on gravity measurements used to determine the density of material making up Berkner Island in the Filchner Ice Shelf area (Behrendt, 1962a). The ocean bottom material in both areas is thought to have the same origin (mostly morainal).

The density of the middle 4.24 km/sec layer is considered to be about 2.6 to 2.7 gm/cm^3 , determined from velocity vs. density curves and from gravity and depth measurements in the northwest portion of the ice shelf (Area #1, see Fig. 1).

The density of the bottom 6.38 km/sec layer is determined to be 2.9 to 3.0 gm/cm^3 , also based on velocity vs. density curves and from gravity and depth measurements in the northwest sector of the ice shelf (Area #2, see Fig. 1). The density determination in Area #2 (3.0 gm/cm^3) may however reflect the density of diabase sills, frequently found in the area to the west. The 6.38 km/sec layer is tentatively associated with gabbro.

The mean density associated with the rise in ocean bottom at the eastern edge of the ice shelf (Mile 200 on the Byrd Trail), based on changes in gravity and bottom elevation, is between 2.4 and 2.8 gm/cm^3 . This may indicate an increase in the thickness of the middle layer which is 645 m thick at LAS.

(3) Thick sections of low density material are probably associated with the relatively low Bouguer anomalies in the center of the ice shelf area, generally lying east of the +30 mgal contour (Fig. 16). This material appears to thin in the northwest through southwest sector as evidenced by an increase in the Bouguer anomalies and depths in these directions. The leveling influence of the ocean on the low density surface materials seems to be reflected in the relatively smooth bottom over the central portion of the ice shelf area, compared with the rough bottom of the northwest portion. Thinning of the low density layer may also be inferred from the fact that in the northwest area of the ice shelf near McMurdo Sound, where local topography is greater, the correlation between free air anomalies and ocean bottom is best. Although the low density layer may be very thin or absent in Area #2 east of the Skelton Glacier, it is probably present to some degree (i.e. 300 m or more) in Area #1 farther to the east.

The thinning of the low density layer in the northwest through southwest sectors of the Ross Ice Shelf may suggest that the source of this material is Marie Byrd Land and that material is brought into the area by the ice shelf.

In the northeastern portion of the ice shelf, the low density layer is known, from seismic studies, to thin over Roosevelt Island. The layer is also known to thin from LAS to Mile 20 on the Byrd Trail and may be missing at Mile 40 and farther to the southeast.

(4) Over the majority of the ice shelf area there is probably much local variation in thickness of the low density layer as evidenced by a large scatter in points on the Δg vs. Δh graph (Fig. 23). The major density contrast below ocean bottom is thought to be that between the top and middle layer (~ 0.6 to 0.7 gm/cm^3) therefore the major cause of local changes in gravity, aside from ocean bottom topography, is probably a thinning and thickening of the low density top layer. If this is true then the surface underlying the low density layer has more local topography than the present ocean bottom. Topographic highs of this ancient surface would be found in the vicinity of stations 10.0, 29.0, 31.0, and 35.0 (RIST). The variation in thickness of the low density layer probably results from the influence of the ocean upon ice rafted sediments deposited on an ancient topographic surface.

(5) The gravity and magnetic data suggest a general increase in thickness of the middle layer in Area #1 (approximately 160 km east of the Skelton Glacier). The top surface of the middle layer is probably higher in Area #1 than at LAS, as indicated by the higher Bouguer anomalies in Area #1 (the shallowest water depths in Area #1 being comparable to those at LAS). Because the local topography is substantial in Area #1, the indicated density of 2.7 gm/cm^3 also suggest that this layer lies closer to the ocean bottom here than it does at LAS. The broad magnetic "low" in this same area may suggest a downwarping of the 6.38 km/sec layer which would indicate a downward thickening of the middle layer, in addition to the upward thickening indicated by the gravity data.

(6) The large Bouguer anomalies in Area #2 are probably due to a rise of the high density 6.38 km/sec layer or to the presence of diabase sills, known to be extensive to the west. The difference in Bouguer anomalies between LAS and Area #2 (approximately 100 km east of the Skelton Glacier) can be accounted for by a 650 m rise of the high density layer or an equivalent thickness of diabase sills. The good correlation between gravity and ocean bottom in this area of considerable local relief also indicates that a high density material lies fairly close to the ocean bottom.

(7) In general, over the majority of the ice shelf area, there is poor correlation between gravity and magnetic anomalies. Since in nearly all cases both data were recorded at the same stations, this observation implies that the major density and susceptibility contrasts lie at different depths. The major density contrast appears to be that between the top and middle layers; therefore the major susceptibility contrast must lie deeper. Because the shallowest magnetic depth determination places the source at a level corresponding to the top of the

6.38 km/sec layer at LAS, in an area where the Bouguer anomaly and depth are similar, the upper "magnetic horizon" is considered to lie somewhere within this layer. The upper two layers are thus considered to have negligible susceptibility. A lower limit to the susceptibility of the 6.38 km/sec layer is determined to be 0.001 cgs, perhaps as little as 1/5 the actual susceptibility.

(8) The similarity of "smooth" low amplitude magnetic profiles in both the central ice shelf area and the Ross Sea area to the north suggests that the two areas, both considered part of the Continental Shelf, are geologically similar. The "smooth" nature of the profiles probably indicates the absence of igneous rocks near the ocean bottom.

(9) The deepest sources of magnetic anomalies in the Ross Ice Shelf area appear to lie at depths no greater than 8 km to 13 km. The vertical magnetic anomaly map (Fig. 18) suggests that these "deep" features are confined to the peripheral areas of the ice shelf.

(10) The gravity and magnetic anomalies on and around Northern Roosevelt Island can be explained by granitic intrusions in the area. The low Bouguer anomaly on the island could result from the replacement of higher density country rock by lower density intrusives. The very low Bouguer anomaly at the northwestern edge of the island may be due to a thick section of low density sediment, in addition to the intrusion. The high magnetic anomalies situated along the northwest edge of the island may therefore be an edge effect of the boundary between the two rock types. Finally, the broad magnetic low, centered at the northeast end of the island and including parts of the island, may reflect the lower susceptibility of the intrusives.

(11) Former ice loading of the Ross Sea continental shelf is postulated as the cause of the negative mean free air anomaly (-12 mgal) over the Ross Ice Shelf and the calculated time of glacial unloading, using the method of Vening Meinesz, ranges between 12,000 and 31,000 years B.P. The general agreement in the state of equilibrium between Fennoscandia and the Ross Sea continental shelf would indicate that the Würm or Wisconsin glaciation was contemporaneous in both hemispheres. If substantial sedimentation has occurred since ice unloading the calculated post glacial period may be even less than 12,000 years. The maximum thickness of sediment deposited since glacial unloading is estimated to be 600 m.

The general geological picture as depicted from the above conclusions is consistent with the presence of Beacon sediments beneath the ice shelf. The thickening of the intermediate layer in Area #1 and presence of diabase sills in Area #2 might imply a general increase in thickness of the Beacon Group in a westward direction toward the mountains. It must be realized, however, that the gravity and magnetic data alone cannot prove the existence of the Beacon Group. A schematic cross section across the front of the ice shelf is included to illustrate the general geological interpretation in the Ross Ice Shelf area (see Fig. 27).

SCHEMATIC SECTION LAS TO SKELTON GLACIER

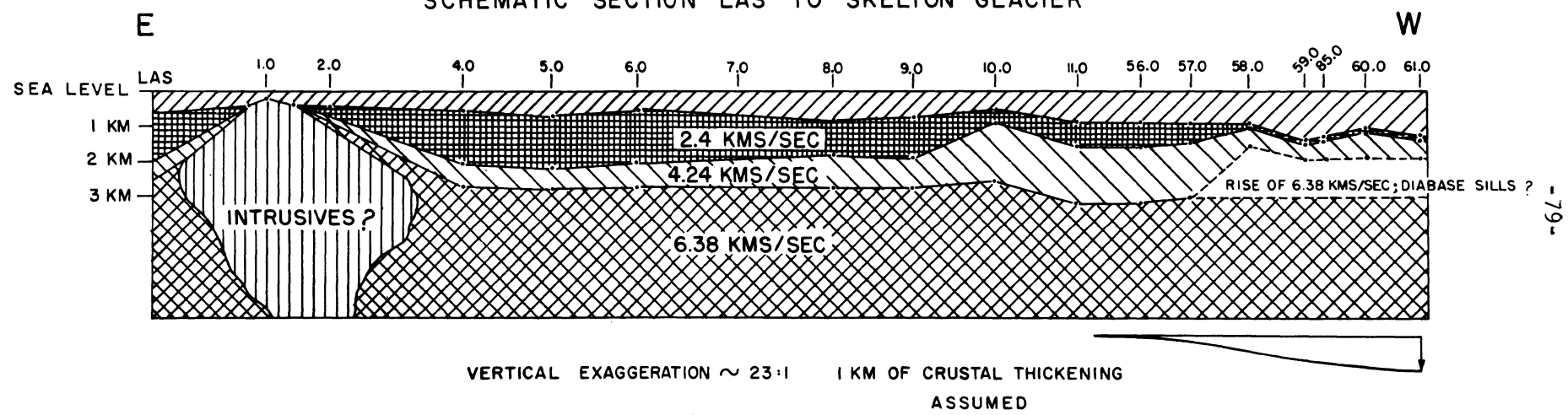


Figure 27

ACKNOWLEDGEMENTS

The author is particularly indebted to members of the Ross Ice Shelf Traverse: A. P. Crary, W. W. Boyd, Jr., W. J. Cromie, E. S. Robinson, S. DenHartog, F. Layman, and P. Schoeck. T. Hatherton provided for gravity ties between Scott Base and the RIST and J. Sparkman facilitated ties between McMurdo Sound and the RIST. Special credit is due to the personnel of the U.S. Navy Air Development Six Squadron, who furnished resupply flights for the traverse operations.

Gravity and magnetic data on the remaining traverses were obtained and reduced by the following: Operation High Jump airborne magnetic flight, J. R. Balsley: LAS-BS, C. R. Bentley and N. A. Ostenso; LAS-BT, L. D. McGinnis and J. Gniewels; VLT (58-59), L. D. McGinnis and S. DenHartog; DDT, E. S. Robinson.

Special appreciation is due C. R. Bentley for his helpful suggestions during the reduction of data and the preparation of the manuscript. Helpful advice was also obtained from A. P. Crary, N. A. Ostenso, E. C. Thiel, E. S. Robinson, J. C. Behrendt, S. DenHartog, L. D. McGinnis and M. B. Giovinetto.

REFERENCES

- Adams, R. D., D. A. Christoffel, Total Magnetic Field Surveys between New Zealand and the Ross Sea, *J. Geophys. Research*, 67, 2, 1962.
- Behrendt, John C., Geophysical and Glaciological Studies in the Filchner Ice Shelf Area of Antarctica, *J. Geophys. Research*, 67, 1, 1962a.
- Behrendt, J. C., R. J. Wold, T. S. Laudon, Gravity Base Station in Antarctica, *Geophys. J. Roy. Astro. Soc.*, 6, 3, 1962b.
- Bentley, C. R., A. P. Cray, N. A. Ostenso and E. C. Thiel, Structure of West Antarctica, *Science*, 131, 3394, 1960.
- Bentley, C. R., and N. A. Ostenso, Glacial and Subglacial Topography of West Antarctica, *J. of Glac.*, 3, 29, 1961.
- Birch, Francis, J. F. Schairer, and H. Cecil Spicer, Handbook of Physical Constants, *Geol. Soc. Am., Spec. Papers*, 36, Published by the Society, Jan. 31, 1942; Reprinted 1961.
- Broecker, Wallace S., and William R. Farrand, Radioactive Age of the Two Creeks Forrest Bed, Wisconsin, *Geol. Soc. Am.*, 74, 6, 795-801, June, 1963.
- Bull, C. and E. Irving, The Paleomagnetism of Some Hypabyssal Intrusive Rocks from South Victoria Land, Antarctica, *Geophys. J. Roy. Astron. Soc.*, 3, 2, 1960.
- Bull, C., E. Irving, I. Willis, Further Paleomagnetic Results from South Victoria Land, Antarctic, *Geophys. J. Roy. Astron. Soc.*, 6, 3, 1962a.
- Bull, C., B. C. McKelvey, and P. N. Webb, Quaternary Glaciation in Southern Victoria Land, Antarctica, *J. of Glac.*, 4, 31, 1962b.
- Charlesworth, J. K., The Quaternary Area with Special Reference to its Glaciation, two volumes, London, Edward Arnold (publishers) LTD, 1957.
- Coast and Geodetic Survey, Magnetograms and Hourly Values, Little America, Antarctica 1957-58, MHV-LA 58, Washington: 1960.
- Crarry, A. P. and F. G. Van Der Hoeven, Sub-Ice Topography of Antarctica Long. 160°W to 130°E, Symposium on Antarctic Glaciology, Pub. No. 55, International Association of Scientific Hydrology, Gentbrugge (Belgium), 1961a.
- Crarry, A. P., Marine-Sediment Thickness in the Eastern Ross Sea Area, Antarctica, *Geol. Soc. of Am. Bull.*, 72, 1961b.
- Crarry, A. P., E. S. Robinson, H. F. Bennett, W. W. Boyd, Glaciological Studies of the Ross Ice Shelf, Antarctica, 1957-60, IGY Glaciol. Rept. 6, *Am. Geog. Soc.*, 1962.

Crittenden, Max D. Jr., Effective Viscosity of the Earth Derived from Iso-static Loading of Pleistocene Lake Bonneville, J. Geophys. Research, 68, 19, 1963.

Davies, William E., Antarctic Stratigraphy and Structure, Antarctica in the International Geophysical Year, Geophysical Monograph No. 1, A.G.U. of the Nat. Acad. Sci., Nat. Res. Coun., Pub. 462, 1956.

Demenitskaia, R. M., Main Features of the Structure of the Earth's Crust in the Antarctic, Bull. Sov. Ant. Exped., 23, 1960.

Dobrin, Milton B., Introduction to Geophysical Prospecting, McGraw-Hill Book Co. Inc., 1952.

Farrand, William R., Postglacial Uplift in North America, Am. J. Sci., 260, 1962.

Flint, Richard Foster, Glacial and Pleistocene Geology, John Wiley and Sons, Inc. New York, Copyright 1957 (second printing 1961).

Gunn, B. M., and Guyon Warren, Geology of Victoria Land between the Mawson and Mulock Glaciers, Antarctica, New Zealand Geological Survey, Bull. N. S. 71, New Zealand Dept. Sci. Indus. Res., 1962.

Hamilton, Warren, and Philip T. Hayes, Geology of Taylor Glacier-Taylor Dry Valley Region, South Victoria Land, Antarctica, Geological Survey Research, 1960, Short Papers in the Geological Sciences Reprinted from Geol. Surv. Profes. Paper 400-B.

Harrington, H. J., Nomenclature of Rock Units in the Ross Sea Region, Antarctica, Nature, 182, 4631, 1958.

Hatherton, I., New Zealand I.G.Y. Antarctic Expeditions, Scott Base and Hallett Station, Bull. 140, New Zealand Dept. Sci. Indus. Res., 1961.

Heiland, C. A., Geophysical Exploration, Prentice-Hall, Inc., N. Y., 1940.

Heirtzler, J. R., G. Peter, M. Talwani, and E. G. Zurfluch Magnetic Anomalies Caused by Two-Dimensional Structure: Their Computation by Digital Computers and Their Interpretations, Tech. Rept. 6, CU-6-62 Nonr-Geology, Lamont Geol. Observ., 1962.

Heiskanen, W. A. and F. A. Vening Meinesz, The Earth and Its Gravity Field, McGraw-Hill Book Co., 1958a.

Heiskanen, W. A. and Uotila, U. A., Some Recent Studies on Gravity Formulas, Contributions in Geophysics, Pergamon Press, 1958b.

Hollin, J. T., On the Glacial History of Antarctica, J. Glac., 4, 32, 1962.

Jakosky, J. J., Exploration Geophysics, Trija Publishing Co., Newport Beach, Calif., 1950.

Klimov, L. B. and D. S. Solovyev, Correlation of Geologic Formations of the Shore of Ross Sea and Oates Coast, Infor. Bull. Sov. Ant. Exped., 16, 1960.

Lyuslikh, E. N., Isostacy and Isostatic Hypotheses, Sov. Res. Geophys., In English translation, 2, Trans. (TRUDY) Geophys. Inst. Acad. Sci. USSR, 38, (165), 1957. Copyright by A.G.U., 1960.

McKelvey, B. C. and P. N. Webb, Geological Investigations South Victoria Land, Antarctica, Part II - Geology of Upper Taylor Glacier Region, New Zealand J. Geol. Geophys., 2, 1959.

McGinnis, Lyle D., Magnetic Profile Ross Ice Shelf: Skelton Glacier: Victoria Land Plateau, Unpublished report, Univ. Wis. Geophys. Polar Res. Ctr., Madison, 1959.

Meyer, Ardo X., McMurdo to Pole Traverse, December 1960 - February 1961, Coast and Geodetic Survey, Washington 25, D. C., 1961.

Ostenso, N. A., Byrd Station Traverses, Group I, IGY Antarctic Oversnow Traverse Program, 1957-58, IGY Glaciol. Rept. Ser. 1, Preliminary Reports of the Antarctic and Northern Hemisphere Glaciological Programs, Am. Geog. Soc., 1958.

Passel, Charles F., Sedimentary Rocks of the Southern Edsel Ford Ranges, Marie Byrd Land, Antarctica, Proc. Am. Phil. Soc., 89, 1, 1945.

Peters, L. J., The Direct Approach to Magnetic Interpretation and Its Practical Applications, Geophys., 14, 1949.

Péwé, Troy L., Age of Moraines in Victoria Land, Antarctica, J. Glac., 4, 31, 1962.

Priestly, Raymond E. and T. W. Edgeworth David, Geological notes of the British Antarctic Expedition, 1907-09. Congress Géologique International, 11, II, 1910.

Robinson, Edwin S., Results of Geophysical Studies on the McMurdo to South Pole Traverse, Univ. Wis. Geophys. Polar Res. Ctr., Res. Rept. Ser. 62-6, 1962.

Robinson, Edwin S., Geophysical Investigations in McMurdo Sound, Antarctica, J. Geophys. Res., 68, 1, 1963.

Somme, Axel (Editor), A geography of Norden, Denmark-Finland-Iceland-Norway-Sweden, J. W. Cappelens Farlag-Oslo, 1960.

Stetson, H. C. and J. E. Upson, Bottom deposits of the Ross Sea, J. Sed. Petrol., 7, 1937.

Stuart, A. W. and A. J. Heine, Glaciological Work of the 1959-60 U. S. Victoria Land Traverse, J. Glac., 3, 30, 1961.

Talwani, Manik, George H. Sutton, and J. Lamar Worzel, A crustal Section across the Puerto Rico Trench, *J. Geophys. Res.*, 64, 10, 1959.

Thiel, E., Gravity Base Stations, Antarctica, *IGY Glaciol. Rept. Ser. 2*, Am. Geog. Soc., 1959.

Thiel, Edward, A. P. Crary, Richard A. Haubrich, and John C. Behrendt, Gravimetric Determination of Ocean Tide, Weddell and Ross Seas, Antarctica, *J. Geophys. Res.*, 65, 2, 1960.

Thiel, Edward and Ned A. Ostenso, The Contact of the Ross Ice Shelf with the Continental Ice Sheet, Antarctica, *J. Glac.*, 3, 29, 1961a.

Thiel, Edward, and Ned A. Ostenso, Seismic Studies on Antarctic Ice Shelves, *Geophys.*, 26, 6, 1961b.

Thomas, Charles W., Late Pleistocene and Recent limits of the Ross Ice Shelf, *J. Geophys. Res.*, 65, 1960.

Tsuboi, Chuji, Thickness of the Isostatic Earth's Crust in Various Parts of the United States of America, *Geophys. Notes*, 3, 5, 1950. Geological Institute, Tokyo Univ., Tokyo.

U. S. Navy Hydrographic Office, Report on Operation Deep Freeze I, TR-33, Washington, D. C. 1956.

Ushakov, S. A. and G. E. Lazarev, On the Isostatic Reflection of the Earth's Crust in the Antarctic under the Weight of the Ice Load, *Repts. Acad. Sci. USSR*, 129, 4, 1959.

Vacquier, V., and J. Affleck, A Computation of the Average Depth to the Bottom of the Earth's Magnetic Crust Based on a Statistical Study of Local Magnetic Anomalies, *Am. Geophys. Union, Tr.*, 1941.

Vacquier, V., N. C. Steenland, R. G. Henderson, and I. Zietz, Interpretation of Aeromagnetic Maps, *Geol. Soc. Am. Memoir 47*, 1951, Reprinted 1954, 1958.

Voronov, P. S., Attempt to Reconstruct the Ice Sheet of Antarctica at the Time of Maximum Glaciation on the Earth, *Infor. Bull. Sov. Ant. Exped.*, 23, 1960.

Wade, Alton F., The Geology of the Rockefeller Mountains, King Edward VII Land, Antarctica, *Proc. Am. Phil. Soc.*, 89, 1, 1945.

Warner, Lawrence A., Structure and Petrography of the Southern Edsel Ford Ranges, Antarctica, *Proceedings of the Am. Phil. Soc.*, 89, 1, 1945.

Webb, P. N. and B. C. McKelvey, Geological Investigations in South Victoria Land, Antarctica, Part I- Geology of Victoria Dry Valley, New Zealand *J. Geol. Geophys.*, 2, 1959.

Woppard, G. P., Crustal Structure from Gravity and Seismic Measurements, *J. Geophys. Res.*, 64, 10, 1959.

APPENDIX

DATA SUMMARY

TABLE I
LITTLE AMERICA STATION TO BYRD STATION TRAVERSE
January-February 1957 (LAS-BS)

<u>Station</u>	<u>Latitude</u> S	<u>Longitude</u> W	<u>Elev.</u> meters	<u>Observed Gravity</u> mgls	<u>Free Air Anomaly</u> mgls	<u>Bottom Elev.*</u> meters	<u>Boug Anom.*</u> mgls
LAS	78°11.9'	162°16.0'	44	982983.1	- 7.3	-607 S*	+34.5*
LAS	78°12.0'	162°15.0'	46	980.7	- 9.2	-607	
M1 6	78°16.2'	161°59.0'	43	971.9	-21.4	-768	
M1 9	78°17.6'	161°49.0'	48	970.3	-22.4	-765	
M1 14	78°21.0'	161°36.0'	54	969.5	-23.3	-749	
M1 20	78°24.8'	161°20.0'	58	978.3	-15.6	-597 S*	+25.4*
M1 25	78°28.1'	161°06.0'	59	985.8	- 9.7	-551	
M1 30	78°31.4'	160°51.0'	61	989.5	- 7.4	-555	
M1 35	78°34.7'	160°37.0'	61	989.2	- 9.6	-624	
M1 40	78°38.0'	160°22.0'	63	986.6	-13.5	-715 S*	+35.6*
M1 45	78°41.3'	160°08.0'	63	989.5	-12.6	-706	
M1 50	78°44.6'	159°54.0'	65	996.4	- 6.9	-669	
M1 55	78°47.9'	159°40.0'	64	983001.2	- 4.3	-655	
M1 60	78°51.3'	159°25.7'	67	002.7	- 3.8	-672 S*	+42.3*
M1 65	78°54.1'	159°09.0'	69	003.1	-4.4	-690	
M1 70	78°56.8'	158°43.0'	68	005.8	- 3.6	-686	
M1 75	78°58.6'	158°26.0'	70	008.2	- 1.6	-665	
M1 80	78°02.3'	158°19.5'	71	008.2	- 3.4	-699 S*	+44.6*
M1 85	78°05.2'	157°01.0'	71	012.4	- 0.8	-632	
M1 90	78°08.1'	157°43.0'	72	007.6	- 6.9	-691	
M1 95	78°10.9'	157°25.0'	73	004.7	-11.1	-722	
M1 100	79°13.8'	157°06.5'	69	005.5	-13.1	-720 S*	+36.3*
M1 105	79°16.2'	156°47.9'	69	007.1	-12.9	-673	
M1 110	79°18.5'	156°29.2'	67	003.9	-17.9	-703	
M1 115	79°20.8'	156°10.6'	65	003.1	-20.6	-698	
M1 120	78°23.1'	155°51.9'	65	982999.1	-25.8	-733 S*	+24.6*
M1 125	78°24.6'	155°31.6'	66	983002.6	-22.9	-754 S*	+28.9*
M1 130	78°26.0'	155°09.2'	66	000.2	-26.0	-794 S*	+28.5*
M1 135	78°27.5'	154°47.9'	67	982999.6	-27.1	-798	
M1 140	78°28.9'	154°26.5'	69	996.7	-30.2	-843 S*	+27.7*
M1 145	78°30.5'	154°03.9'	67	994.3	-34.1	-892	
M1 150	78°32.0'	153°41.2'	64	997.5	-32.6	-869	
M1 155	78°33.6'	153°18.6'	62	997.0	-34.6	-898	
M1 160	78°35.2'	152°56.0'	62	996.4	-36.1	-924 S*	+27.3*
M1 165	78°35.0'	152°32.4'	63	992.2	-39.9	-978	
M1 170	78°34.9'	152°08.7'	60	995.9	-37.0	-940	
M1 175	78°34.7'	151°45.1'	58	996.7	-36.7	-940	
M1 180	78°34.5'	151°21.5'	56	996.7	-37.2	-951	
M1 184	78°35.3'	151°02.5'	54	983012.2	-22.8	-745	
M1 187	78°31.2'	151°05.8'	51	006.8	-27.0	-807	
M1 191	78°27.7'	151°08.0'	67	013.8	-13.1	-609	
M1 195	78°26.8'	150°51.2'	175	982997.5	+ 4.4	-374	
M1 200	78°26.1'	150°25.9'	282	973.0	+13.3	-253 S	+21.5

*Bottom elevations from (LAS-BT) are used when same station had been occupied by (LAS-BS).

S = Seismically determined depths. All other depths determined from "free air anomaly depths" adjusted to seismic depths.

TABLE II
ROSS ICE SHELF TRAVERSE
October-February 1957-58 (RIST)

<u>Station</u> <u>(*)</u>	<u>Latitude</u>	<u>Longitude</u>	<u>Elev.</u> <u>meters</u>	<u>Observed</u> <u>mgls</u>	<u>Free Air</u> <u>Anomaly</u> <u>mgls</u>	<u>Bottom</u> <u>Elev.</u> <u>meters</u>	<u>Boug.</u> <u>Anom.</u> <u>mgls</u>	<u>Obs. Z</u> <u>Mar 58</u>	<u>Adj. Z</u> <u>Dec 60</u>	<u>Reg* Z</u> <u>corr-350</u>	<u>Anom. Z</u> <u>nearest 5</u> <u>gammas</u>	<u>Obs. H</u> <u>Mar 58</u>	<u>Reg* H</u> <u>Mar 58</u>	<u>Anom. H</u> <u>nearest 5</u> <u>gammas</u>	<u>Obs. F</u> <u>Mar 58</u> <u>(calc)</u>	<u>Reg* F</u> <u>Mar 58</u> <u>(calc)</u>	<u>Anom. F</u> <u>nearest 5</u> <u>gammas</u>	<u>Declination</u>
LAS	78°11.0'S	162°11'W	43	982982.4	- 7.8	-607 S +34.0	63,890	63,540	63,490	+ 50	--	--	--	--	--	--	102.7°E	
KF	78°12.0'	162°07'	45	981.0	- 9.3	-610	63,960	63,610	63,480	+130								
0.0 (0.0)	78°12.2'	162°07'	45	980.5	- 9.8	-602	63,970	63,620	63,480	+140								
0.2 (12.0)	78°19.5'	161°39'	52	968.1	-24.4	-719	63,730	63,380	63,430	- 50								
0.3 (17.5)	78°23.1'	161°25'	56	976.7	-16.7	-554	--	--	--	--								
0.4 (22.5)	78°26.8'	161°11'	57	982.1	-13.3	-456	63,605	63,255	63,325	- 70								
0.6	78°30.8'	162°22'	56	981.3	-16.7	-410	63,645	63,295	63,340	- 45								
0.8	78°33.3'	161°51'	56	955.3	-44.2	-800	63,765	63,415	63,365	+ 50								
0.10	78°37.8'	162°14'	57	953.8	-48.0	-801	63,640	63,290	63,380	- 90								
0.12	78°40.7'	162°24'	43	993.5	-14.3	-244	63,660	63,310	63,370	- 60								
0.13	78°42.3'	162°26'	43	995.4	-13.4	-204	63,615	63,265	63,365	-100								
0.14	78°45.3'	162°30'	93	994.0	- 1.1	- 13	--	--	--	--								
1.0	78°47.3'	163°00'	197	952.4	-11.7	-204 S - 3.6	63,650	63,300	63,390	+ 90								
1.1	78°47.6'	163°18'	114	966.3	-23.7	-257	63,720	63,370	63,420	- 50								
1.3	78°46.5'	163°53'	36	968.1	-45.3	-428	64,020	63,670	63,480	+190								
1.5	78°47.6'	164°21'	40	951.4	-61.5	-535	63,910	63,560	63,510	+ 50								
1.7	78°53.9'	164°35'	42	955.8	-60.0	-424	63,920	63,570	63,505	+ 65								
2.0	78°55.0'	164°50'	48	950.9	-63.6	-425 S - 34.4	63,855	63,505	63,515	- 10							109.4°E	
2.1	78°55.3'	164°50'	48	951.6	-63.1	-427	--	--	--	--								
2.2	78°56.0'	164°52'	48	952.7	-62.4	-425	--	--	--	--								
2.3	78°56.2'	164°52'	48	953.6	-61.7	-423	--	--	--	--								
2.4	78°56.9'	164°54'	48	955.3	-60.4	-413	63,990	63,640	63,520	+120								
2.5	78°57.2'	164°57'	48	955.8	-60.1	-417	--	--	--	--								
2.6	78°58.0'	165°02'	49	957.6	-58.3	-400	63,965	63,615	63,525	+ 90								
2.7	78°59.8'	165°14'	53	966.5	-49.3	-338	63,985	63,635	63,530	+105								
2.9	79°02.3'	165°31'	56	969.2	-47.0	-390	--	--	--	--								
2.11	79°05.6'	165°52'	57	960.9	-36.9	-339	64,015	63,665	63,550	+115								
2.13	79°10.0'	166°21'	58	993.5	-26.4	-321	63,925	63,575	63,565	+ 10								
3.0	79°11.8'	166°33'	58	983004.2	-16.7	-230	63,970	63,620	63,570	+ 50							111.9°E	
3.1	79°10.8'	166°54'	59	014.8	- 5.3	-115	63,975	63,625	63,605	+ 20								
3.3	79°10.0'	167°33'	61	982995.7	-23.3	-496	64,015	63,665	63,660	+ 5								
3.5	79°09.6'	168°17'	60	983002.3	-16.8	-534	64,090	63,740	63,715	+ 25								
4.0	79°09.2'	168°39'	59	006.5	-12.7	-539 S - 25.3	64,290	63,340	63,740	+200								
4.1	79°08.8'	168°56'	58	009.1	-10.1	-510	--	--	--	--								
4.2	79°08.3'	169°18'	55	013.5	- 6.4	-467	64,115	63,765	63,790	- 25							115.0°E	
4.3	79°07.8'	169°45'	56	--	--	--	--	--	--	--								
4.4	79°07.6'	170°06'	55	009.6	- 9.9	-524	64,125	63,775	63,855	- 80								
4.5	79°07.4'	170°28'	55	009.7	- 9.6	-574	--	--	--	--								
4.6	79°07.2'	170°56'	50	003.6	-17.1	-643	64,275	63,925	63,925	0								
5.0	79°07.0'	171°31'	49	082999.7	-21.3	-695 S +26.4	64,305	63,955	63,960	- 5							118.5°E	
5.1	79°05.7'	171°49'	53	998.4	-20.7	-700	64,260	63,910	63,990	- 80								
5.3	79°03.2'	172°36'	53	991.3	-26.3	-773	64,390	64,040	64,050	- 10								
5.5	79°01.1'	173°28'	50	998.5	-18.8	-655	64,520	64,170	64,115	+ 55								
6.0	78°59.7'	173°59'	51	983004.9	-11.3	-536 S +25.5	64,530	64,180	64,150	+ 30							119.8°E	
6.1	78°59.2'	174°29'	52	010.7	- 4.9	-466	64,460	64,110	64,180	- 70								
6.3	79°00.0'	175°17'	49	001.6	-15.4	-650	64,600	64,250	64,220	+ 30								
6.4	79°01.0'	175°43'	47	001.7	-16.4	-680	64,550	64,200	64,235	- 35								
6.5	79°00.6'	176°04'	48	005.7	-11.9	-624	64,600	64,250	64,260	- 10								
6.7	78°59.3'	176°47'	47	001.1	- 6.2	-555	64,605	64,255	64,310	- 55								

TABLE II con't.

ROSS ICE SHELF TRAVERSE
October-February 1957-58 (RIST)

Station	Latitude	Longitude	Elev. meters	Observed Gravity mgls	Free Air Anomaly mgla	Bottom Elev. meters	Boug. Anom. mgls	Obs. Z Mar 58 gamma	Adj. Z Dec 60 corr-350Y	Reg* Z Dec 60 gamma	Anom. Z nearest 5 gamma	Obs. H Mar 58 gamma	Reg* H Mar 58 gamma	Anom. H nearest 5 gamma	Obs. F Mar 58 (calc)	Reg* F Mar 58 (calc)	Anom. F nearest 5 gamma	Declination
7.0	78°58.6'S	177°06'W	46	983014.1	- 3.1	-530	64,635	64,285	64,330	- 45	--	--	--	--	--	--	124.5°E	
7.1	78°58.6'	177°29'	46	004.7	-12.5	-683	64,635	64,285	64,350	- 65	--	--	--	--	--	--		
7.2	78°58.5'	178°00'	44	982984.1	-33.6	-990	64,710	64,360	64,380	- 20	--	--	--	--	--	--		
7.3	78°59.2'	178°24'	46	990.0	-27.5	-863	64,870	64,520	64,395	+125	--	--	--	--	--	--		
7.5	79°00.5'	179°08'	48	987.3	-30.3	-1006	64,730	64,380	64,425	- 45	--	--	--	--	--	--		
7.7	79°02.8'	179°51'	51	998.1	-19.9	-925	64,755	64,405	64,445	- 40	--	--	--	--	--	--		
8.0	79°04.6'	179°41'E	51	983003.5	+15.5	-828 S	+41.3	64,840	64,490	64,455	+ 35	--	--	--	--	--	--	
8.1	79°03.9'	179°19'	51	006.9	-11.7	-872	64,815	64,465	64,475	- 10	--	--	--	--	--	--	131.9°E	
8.2	79°03.3'	179°02'	51	--	--	--	--	--	--	--	--	--	--	--	--	--		
8.3	79°02.7'	178°36'	52	016.8	- 0.8	-578	64,940	64,590	64,520	+ 70	--	--	--	--	--	--		
8.5	79°02.4'	177°44'	53	982997.7	-19.5	-817	64,945	64,595	64,550	+ 45	--	--	--	--	--	--		
9.0	79°02.6'	177°17'	53	983002.8	-14.5	-729 S	+35.5	64,950	64,600	64,565	+ 35	--	--	--	--	--	131.9°E	
9.1	79°01.2'	176°43'	53	015.3	- 1.1	-611	64,995	64,645	64,600	+ 45	--	--	--	--	--	--		
9.3	79°00.1'	175°51'	52	017.5	+ 1.3	-703	65,045	64,695	64,645	+ 50	--	--	--	--	--	--		
9.5	78°59.8'	175°11'	51	037.1	+20.8	-532	65,125	64,775	64,665	+110	--	--	--	--	--	--		
10.0	78°59.4'	174°50'	51	042.6	+26.5	-502 S	+61.0	65,095	64,745	64,680	+ 65	--	--	--	--	--	134.4°E	
10.1	78°57.6'	174°22'	52	039.4	+24.7	-485	65,150	64,800	64,705	+ 95	--	--	--	--	--	--		
10.3	78°55.0'	173°27'	53	026.2	+13.3	-572	65,110	64,760	64,760	0	--	--	--	--	--	--		
10.5	78°53.5'	172°44'	55	007.7	- 3.8	-725	65,100	64,750	64,800	- 50	--	--	--	--	--	--		
11.0	78°52.5'	172°22'	56	982993.2	-17.4	-871 S	+42.4	65,005	64,655	64,810	-155	--	--	--	--	--	139.7°E	
11.1	78°51.5'	172°03'	60	983.1	-25.7	-994	65,035	64,685	64,825	-140	--	--	--	--	--	--		
11.3	78°49.7'	171°30'	55	991.0	-18.3	-888	65,065	64,715	64,850	-135	--	--	--	--	--	--		
11.5	78°48.0'	170°56'	58	998.2	- 9.1	-756	65,210	64,860	64,880	- 20	--	--	--	--	--	--		
11.7	78°46.6'	170°28'	59	998.9	- 7.4	-732	65,120	64,770	64,900	-130	--	--	--	--	--	--		
12.0	78°46.1'	170°17'	59	983002.0	- 4.0	-680 S	+42.7	65,145	64,795	64,910	-115	--	--	--	--	--	142.3°E	
12.1	78°48.4'	170°17'	58	002.1	- 5.5	-707	65,120	64,770	64,885	-115	--	--	--	--	--	--		
12.3	78°56.5'	170°18'	60	008.3	- 3.3	-682	65,065	64,715	64,805	- 90	--	--	--	--	--	--		
12.5	79°05.0'	170°19'	61	003.0	-13.1	-823	64,975	64,625	64,730	-105	--	--	--	--	--	--		
12.7	79°11.9'	170°19'	62	005.8	-13.9	-842	64,850	64,500	64,665	-165	--	--	--	--	--	--		
13.0	79°15.1'	170°20'	62	003.1	-18.4	-905 S	+43.7	64,835	64,485	64,635	-150	--	--	--	--	--	144.7°E	
13.1	79°21.5'	170°21'	61	005.3	-20.1	-939	64,840	64,490	64,770	- 80	--	--	--	--	--	--		
13.3	79°39.5'	170°22'	59	028.0	- 7.7	-754	64,730	64,380	64,400	- 20	--	--	--	--	--	--		
13.4	79°48.1'	170°21'	59	038.7	- 1.6	-666	64,640	64,290	64,320	- 30	--	--	--	--	--	--		
14.0	79°54.6'	170°18'	60	048.9	+ 5.5	-562 S	+44.1	64,585	64,235	64,270	- 35	--	--	--	--	--	146.0°E	
14.1	80°02.1'	170°18'	61	055.1	+ 8.2	-502	64,675	64,325	64,190	+135	--	--	--	--	--	--		
14.3	80°16.5'	170°10'	57	052.5	- 3.0	-655	64,435	64,085	64,040	+ 45	--	--	--	--	--	--		
14.5	80°29.4'	170°03'	58	054.7	- 6.9	-654	64,270	63,920	63,915	+ 5	--	--	--	--	--	--		
15.0	80°37.0'	170°05'	57	062.0	- 3.6	-581 S	+36.2	64,270	63,920	63,835	+ 85	--	--	--	--	--	148.4°E	
15.1	80°43.7'	170°10'	57	061.2	- 7.7	-610	--	--	--	--	--	--	--	--	--	--		
15.3	80°57.1'	170°24'	56	069.1	- 6.4	-558	--	--	--	--	--	--	--	--	--	--		
15.6	81°07.4'	170°38'	56	059.5	-21.8	-670	--	--	--	--	--	--	--	--	--	--		
16.0	81°12.7'	170°45'	57	053.1	-29.4	-742 S	+21.6	63,805	63,455	63,460	- 5	--	--	--	--	--	149.1°E	
16.1	81°17.3'	170°51'	58	050.8	-33.4	-815	63,645	63,295	63,420	-125	--	--	--	--	--	--		
16.3	81°27.9'	170°05'	58	055.9	-33.1	-822	63,625	63,275	63,310	- 35	--	--	--	--	--	--		
16.5	81°39.3'	171°20'	58	069.9	-24.1	-703	63,570	63,220	63,180	+ 40	--	--	--	--	--	--		
16.7	81°47.5'	171°31'	58	073.4	-24.1	-718	63,470	63,120	63,095	+ 25	--	--	--	--	--	--		
17.0	81°51.4'	171°37'	59	076.0	-22.9	-695 S	+24.7	63,415	63,065	63,050	+ 15	--	--	--	--	--	150.6°E	
17.1	81°57.5'	171°55'	58	082.8	-18.9	-658	63,335	62,985	62,980	+ 5	--	--	--	--	--	--		
17.2	82°04.1'	172°15'	58	083.4	-21.1	-695 S	+26.6	63,225	62,875	62,910	- 35	--	--	--	--	--		
17.3	82°11.9'	172°38'	58	087.6	-20.1	-704	63,180	62,830	62,830	0	--	--	--	--	--	--		

TABLE II cont'd.
ROSS ICE SHELF TRAVERSE
October-February 1957-58 (RIST)

Station	Latitude	Longitude	Elev. meters	Observed Gravity mgls	Free Air Anomaly mgls	Bottom Elev. meters	Boug. Anom. mgls	Obs. Z Mar 58 gammas	Adj. Z Dec 60 corr-350r	Reg* Z Dec 60 gammas	Anom. Z nearest 5 gammas	Obs. H Mar 58 gammas	Reg* H Mar 58 gammas	Anom. H nearest 5 gammas	Obs. F Mar 58 (calc)	Reg* F Mar 58 (calc)	Anom. F nearest 5 gammas	Declination
18.0	82°19.3'S	173°00'E	60	983092.4	-17.5	-693 S	+30.0	63,080	62,730	62,745	-15	--	--	--	--	--	149.5°E	
18.1	82°27.4'	173°19'	62	902.4	-20.2	-848		63,025	62,675	62,640	+35	--	--	--	--	--	--	
18.2	82°33.7'	173°34'	64	108.1	-6.4	-721 S	+43.1	63,015	62,665	62,780	+85	11,550	11,520	+30	64,065	63,976	+90	--
18.3	82°40.6'	173°47'	65	105.5	-11.3	-686		62,890	62,540	62,505	+35	11,585	11,600	-15	63,948	63,916	+30	--
19.0	82°48.6'	174°03'	65	107.5	-12.3	-734 S	+38.1	62,730	62,380	62,420	-40	11,775	11,680	+95	63,826	63,847	-20	148.0°E
19.1	82°55.8'	174°23'	65	110.4	-12.1	-734		62,680	62,330	62,340	-10	11,845	11,760	+85	63,789	63,783	+5	--
19.2	83°03.7'	174°45'	66	112.6	-12.5	-728 S	+37.4	62,600	62,250	62,260	-10	11,915	11,845	+70	63,724	63,721	+5	--
19.3	83°11.5'	175°07'	67	116.2	-11.4	-726		62,530	62,180	62,165	+15	12,070	11,935	+135	63,684	63,644	+40	--
19.4	83°17.5'	175°04'	66	119.6	-10.4	-720		62,445	62,095	62,100	-5	--	--	--	--	--	--	
20.0	83°21.1'	174°54'	66	118.6	-13.0	-749 S	+38.4	62,345	61,995	62,055	-60	12,050	12,025	+25	63,499	63,553	-55	149.3°E
20.1	83°26.4'	174°22'	66	117.2	-15.9	-794		62,370	62,020	62,015	+5	12,095	12,065	+30	63,532	63,521	+10	--
20.2	83°31.8'	175°33'	66	121.0	-10.5	-718		62,425	62,075	62,050	+25	12,145	12,050	+95	63,595	63,552	+45	--
20.4	83°31.6'	176°49'	65	121.6	-10.1	-701		62,375	62,025	62,035	-10	12,195	12,090	+105	63,556	63,550	+5	--
20.6	83°21.4'	178°02'	70	119.3	-10.9	-706		62,595	62,245	62,020	+225	12,080	12,125	-45	63,750	63,540	+210	--
21.0	83°21.3'	178°45'	73	117.1	-12.1	-712 S	+36.7	62,590	62,240	62,010	+230	12,205	12,145	+60	63,769	63,530	+240	142.8°E
21.1	83°25.2'	179°23'	75	118.4	-11.5	-684		62,615	62,265	61,955	+310	12,205	12,210	-5	63,793	63,490	+305	--
21.3	83°35.0'	179°03'W	83	110.7	-20.1	-759		62,340	61,990	61,820	+170	12,360	12,380	-20	63,554	63,390	+165	--
22.0	83°39.2'	178°22'	82	111.4	-21.1	-738 S	+29.5	62,315	61,965	61,770	+195	12,465	12,430	+35	63,549	63,350	+200	140.6°E
22.1	83°46.1'	177°52'	82	112.3	-20.8	-759		62,315	61,965	61,740	+225	12,540	12,470	+70	63,564	63,330	+235	--
22.2A	83°43.0'	177°22'	87	--	--			62,130	61,780	61,710	+70	12,470	12,500	-30	63,369	63,310	+60	--
22.3	83°45.3'	176°47'	89	115.7	-16.6	-739		62,040	61,690	61,665	+25	12,405	12,550	-145	63,268	63,270	0	--
22.4	83°48.2'	176°02'	93	119.6	-12.4	-699		--	--	--	--	--	--	--	--	--	--	
22.5	83°50.8'	175°22'	93	120.2	-12.6	-724		62,190	61,840	61,585	+255	12,370	12,635	-265	63,408	63,210	+200	--
23.0	83°53.2'	174°45'	96	119.2	-13.5	-748 S	+37.8	62,345	61,995	61,555	+440	12,425	12,670	-245	63,571	63,190	+380	--
23.1	83°56.6'	174°02'	95	114.2	-19.9	-832		62,325	61,975	61,490	+485	12,680	12,735	-55	63,602	63,140	+465	--
23.2	83°59.0'	173°32'	96	115.6	-18.9	-797		--	--	--	--	--	--	--	--	--	--	
23.3	84°01.7'	172°58'	97	124.5	-10.6	-677		61,945	61,595	61,410	+185	12,705	12,825	-120	63,234	63,080	+155	--
23.5	84°07.6'	171°43'	99	117.7	-18.7	-735		62,045	61,695	61,325	+370	12,750	12,915	-165	63,341	63,010	+330	--
23.5A	84°07.3'	171°43'	94	117.4	-20.2	-735		--	--	--	--	--	--	--	--	--	--	
24.0	84°10.3'	171°09'	98	119.8	-17.7	-698 S	+30.2	62,060	61,710	61,280	+430	12,900	12,960	-60	63,390	62,980	+410	133.7°E
24.1	84°13.0'	170°34'	100	122.9	-14.7	-668		62,185	61,835	61,235	+600	13,070	13,000	+70	63,544	62,940	+605	--
24.3	84°18.6'	169°21'	100	124.6	-14.8	-693		61,980	61,630	61,145	+485	13,285	13,090	+195	63,388	62,870	+520	--
24.5	84°24.2'	168°14'	103	122.2	-17.9	-782		61,605	61,255	61,065	+190	13,445	13,175	+270	63,055	62,810	+245	--
25.0	84°27.0'	167°39'	103	122.5	-18.4	-782 S	+35.3	61,460	61,110	61,025	+85	13,405	13,220	+185	62,905	62,780	+125	130.5°E
25.1	84°31.6'	168°06'	111	104.8	-34.9	-902 S	+27.0	61,495	61,145	60,990	+155	13,320	13,240	+80	62,921	62,750	+170	--
25.2	84°24.4'	167°30'	105	128.1	-11.4	-649		61,725	61,375	61,045	+330	13,420	13,200	+220	63,167	62,800	+365	--
25.3	84°16.7'	167°21'	105	122.4	-14.9	-619		--	--	--	--	--	--	--	--	--	--	
25.4	84°10.7'	167°14'	106	115.1	-20.0	-635		61,935	61,585	61,165	+420	13,235	13,110	+125	63,333	62,900	+435	--
25.6	83°59.2'	167°00'	101	108.7	-24.4	-577		62,290	61,940	61,260	+680	12,995	13,025	-30	63,631	62,970	+660	--
26.0	83°53.3'	166°53'	99	099.7	-32.1	-638 S	+11.7	62,200	61,850	61,315	+535	12,965	12,985	-20	63,537	63,020	+520	127.5°E
26.1	83°49.0'	166°50'	97	116.2	-14.8	-439		62,025	61,675	61,360	+315	12,725	12,950	-225	63,317	63,050	+265	--
26.2	83°45.7'	167°06'	97	113.7	-16.3	-434		--	--	--	--	--	--	--	--	--	--	
26.4	83°40.3'	167°32'	95	109.6	-19.3	-497		62,120	61,770	61,460	+310	12,675	12,850	-175	63,400	63,130	+270	--
26.5	83°35.6'	167°55'	93	102.3	-25.6	-606 S	+16.0	61,940	61,590	61,510	+80	--	--	--	--	--	--	
26.6	83°34.7'	167°57'	92	095.1	-32.8	-678		--	--	--	--	--	--	--	--	--	--	
27.0	83°32.0'	168°02'	87	097.2	-31.3	-572 S	+ 8.0	61,665	61,315	61,560	-245	12,585	12,755	-170	62,936	63,210	-275	127.3°E
27.1	83°32.1'	168°00'	87	097.9	-30.6	-574		--	--	--	--	--	--	--	--	--	--	
27.4	83°46.1'	167°02'	99	113.2	-16.3	-428		--	--	--	--	--	--	--	--	--	--	
27.5	83°48.7'	166°32'	101	117.0	-12.7	-415		62,155	61,805	61,350	+455	12,675	12,965	-290	63,434	63,050	+385	--
27.6	83°48.5'	165°48'	101	111.4	-18.3	-529		61,870	61,520	61,310	+210	13,070	13,000	+70	63,235	63,020	+215	--
27.8	83°47.9'	164°06'	104	104.2	-24.4	-741		62,055	61,705	61,260	+445	13,205	13,075	+130	63,444	62,980	+465	--

TABLE II con't.

ROSS ICE SHELF TRAVERSE
October-February 1957-58 (RIST)

Station	Latitude	Longitude	Elev. meters	Observed Gravity mg/s	Free Air Anomaly mg/s	Bottom Elev. meters	Boug. Anom. mg/s	Obs. Z Mar 58 gammas	Adj. Z Dec 60 corr 350° gammas	Reg* Z Dec 60 gammas	Anom. Z nearest 5 gammas	Obs. H Mar 58 gammas	Reg* H Mar 58 gammas	Anom. H nearest 5 gammas	Obs. F Mar 58 (calc)	Reg* F Mar 58 (calc)	Anom. F nearest 5 gammas	Declination
28.0	83°47.5'S	164°14'W	105	983114.1	-14.0	-661 S	+31.3	61,940	61,590	61,230	+360	13,380	13,100	+280	63,369	62,960	+410	123.1°E
28.1	83°45.7'	163°16'	100	112.1	-17.0	-704	--	--	--	--	--	--	--	--	--	--	--	--
28.5	83°42.7'	163°12'	109	105.8	-19.5	-746	--	--	--	--	--	--	--	--	--	--	--	--
28.6	83°42.2'	163°11'	111	106.1	-18.4	-731	--	--	--	--	--	--	--	--	--	--	--	--
28.10	83°39.6'	163°12'	108	108.4	-16.1	-707	--	--	--	--	--	--	--	--	--	--	--	--
28.12	83°37.6'	163°12'	107	108.9	-15.3	-700	62,080	61,730	61,315	+415	13,135	13,045	+ 90	63,454	63,030	+425	--	
28.13	83°36.8'	163°13'	103	109.9	-15.3	-702	--	--	--	--	--	--	--	--	--	--	--	--
28.16	83°32.6'	163°15'	97	119.4	- 6.2	-579	62,100	61,750	61,365	+385	--	--	--	--	--	--	--	--
28.18	83°26.1'	163°21'	86	115.9	-10.9	-652	62,035	61,685	61,420	+265	12,870	12,960	- 90	63,356	63,110	+245	--	
28.19	83°22.7'	163°24'	83	118.1	- 8.4	-622	62,065	61,715	61,455	+260	12,850	12,935	- 85	63,381	63,140	+240	--	
28.20	83°16.7'	163°27'	80	121.4	- 4.0	-571	61,940	61,590	61,510	+ 80	12,805	12,885	- 80	63,250	63,190	+ 60	--	
29.0	83°10.6'	163°31'	77	127.3	+ 3.1	-486 S	+36.4	61,955	61,605	61,570	+ 35	12,840	12,835	+ 5	63,272	63,230	+ 40	122.2°E
29.1	83°04.8'	163°31'	76	134.1	+11.7	-309	62,055	61,705	61,625	+ 80	12,805	12,795	+ 10	63,362	63,280	+ 80	--	
29.2	83°01.0'	163°32'	75	131.4	+10.1	-302	--	--	--	--	--	--	--	--	--	--	--	--
29.3	82°55.5'	163°33'	72	121.3	+ 1.1	-391	62,080	61,730	61,700	+ 30	12,685	12,730	- 45	63,363	63,340	+ 25	--	
29.5	82°44.5'	163°34'	76	101.3	-13.5	-513	62,220	61,870	61,805	+ 65	12,635	12,645	- 10	63,490	63,430	+ 60	--	
30.0	82°38.0'	163°35'	78	091.2	-20.6	-595 S	+20.3	62,215	61,865	61,865	0	12,610	12,600	+ 10	63,480	63,480	0	120.3°E
30.1	82°34.0'	164°02'	77	090.7	-19.9	-585	62,185	61,835	61,910	- 75	12,550	12,555	- 5	63,439	63,515	- 75	--	
30.3	82°25.8'	164°57'	76	093.4	-14.2	-516	62,485	62,135	62,030	+105	12,450	12,445	+ 5	63,713	63,610	+105	--	
30.5	82°15.7'	166°05'	73	099.5	- 5.0	-412	62,500	62,150	62,180	- 30	12,330	12,300	+ 30	63,705	63,730	- 25	--	
31.0	82°11.4'	166°35'	72	087.8	-15.3	-583 S	+24.7	62,685	62,335	62,250	+ 85	12,265	12,230	+ 35	63,874	63,780	+ 95	122.7°E
31.1	82°03.1'	166°57'	72	088.6	-11.0	-482	62,675	62,325	62,340	- 15	12,190	12,155	+ 35	63,849	63,860	- 10	--	
31.3	81°48.0'	167°38'	65	086.8	- 8.7	-394	62,870	62,320	62,515	+ 5	12,010	12,000	+ 10	64,007	64,000	+ 5	--	
32.0	81°40.4'	167°59'	64	074.0	-18.6	-516 S	+16.8	62,945	62,595	62,595	0	11,900	11,920	- 20	64,060	64,060	0	122.4°E
32.1	81°33.6'	168°02'	63	076.1	-13.8	-453	62,840	62,490	62,650	-160	11,890	11,875	+ 15	63,955	64,110	-155	--	
32.3	81°16.8'	168°09'	59	065.2	-18.5	-543	63,500	63,150	62,790	+360	11,870	11,750	+120	64,600	64,220	+380	--	
33.0	81°10.1'	168°12'	56	075.8	- 5.8	-398 S	+21.5	63,170	62,820	62,840	- 20	11,860	11,700	+160	64,274	64,260	+ 15	121.1°E
33.1	81°01.4'	168°15'	57	066.0	-11.2	-473	63,165	62,815	62,915	-100	11,695	11,630	+ 65	64,239	64,325	- 85	--	
33.3	80°46.4'	168°19'	61	060.9	- 8.0	-462	63,610	63,260	63,035	+225	11,530	11,515	+ 15	64,647	64,420	+225	--	
34.0	80°40.4'	168°20'	63	059.8	- 5.6	-449 S	+25.2	63,490	63,140	63,090	+ 50	11,390	11,470	- 80	64,503	64,470	+ 35	119.1°E
34.1	80°30.0'	168°19'	66	058.1	- 1.3	-487	63,585	63,235	63,165	+ 70	11,425	11,395	+ 30	64,603	64,530	+ 75	--	
34.2	80°21.3'	168°18'	68	058.9	+ 4.4	-521	--	--	--	--	--	--	--	--	--	--	--	--
34.3	80°15.8'	168°17'	70	061.4	+10.2	-496	63,565	63,215	63,170	- 55	11,235	11,295	- 60	64,550	64,610	- 60	--	
35.0	80°10.4'	168°15'	69	059.2	+10.6	-559 S	+49.0	63,560	63,210	63,310	-100	11,320	11,260	+ 60	64,560	64,650	- 90	118.1°E
35.1	80°03.1'	168°19'	69	060.0	+15.1	-433	63,705	63,355	63,365	- 10	11,300	11,200	+100	64,699	64,690	+ 10	--	
35.3	79°47.0'	168°28'	66	062.0	+ 4.5	-461	63,845	63,495	63,490	+ 5	11,200	11,075	+125	64,820	64,790	+ 30	--	
36.0	79°39.8'	168°32'	64	029.0	- 4.8	-541 S	+32.3	63,830	63,480	63,540	- 60	11,030	11,025	+ 5	64,776	64,830	- 55	115.8°E
36.1	79°33.1'	168°34'	63	026.4	- 4.6	-535	63,865	63,515	63,590	- 75	11,040	10,980	+ 60	64,812	64,880	- 70	--	
36.3	79°18.7'	168°38'	63	013.7	- 9.4	-607	64,040	63,690	63,680	+ 10	10,930	10,875	+ 55	64,966	64,950	+ 15	--	
37.0	79°06.4'	168°40'	59	010.6	- 7.0	-569 S	+32.0	64,070	63,720	63,765	- 45	10,825	10,790	+ 35	64,978	65,020	- 40	114.3°E
37.A4	79°06.5'	168°40'	59	009.7	- 8.2	-588	64,085	63,735	63,750	- 15	--	--	--	--	--	--	--	
37.1	79°00.5'	168°42'	59	010.9	- 3.4	-497	64,220	63,870	63,795	+ 75	10,700	10,750	- 50	65,105	65,040	+ 65	--	
37.3	78°48.2'	168°46'	55	004.3	- 4.1	-463	64,285	63,935	63,875	+ 60	10,730	10,660	+ 70	65,174	65,100	+ 75	--	
38.0	78°42.7'	168°47'	54	982992.6	-13.0	-569 S	+26.0	64,240	63,890	63,910	- 20	10,705	10,620	+ 85	65,126	65,130	- 5	--
38.1	78°41.9'	168°17'	55	991.7	-13.2	-551	64,265	63,915	63,875	+ 40	10,750	10,665	+ 85	65,158	65,105	+ 55	--	
38.3	78°40.7'	167°19'	56	986.3	-17.6	-577	64,190	63,840	63,810	+ 30	10,905	10,750	+155	65,110	65,050	+ 60	--	

TABLE II con't.

ROSS ICE SHELF TRAVERSE
October-February 1957-58 (RIST)

Station	Latitude	Longitude	Elev. meters	Observed mgls	Free Air Anomaly mgls	Bottom Elev. meters	Boug. Anom. mgls	Obs. Z Mar '58 gammas	Adj. Z Dec 60 corr-350'	Reg* Z Dec 60 nearest 5 gammas	Anom. Z nearest 5 gammas	Obs. H Mar '58 gammas	Reg* H Mar '58 nearest 5 gammas	Anom. H nearest 5 gammas	Obs. F Mar '58 (calc)	Reg* F Mar '58 (calc)	Anom. F nearest 5 gammas	Declin- ation
39.0	78°39.5'S	166°40'W	55	982987.7	-15.7	-517 S	+19.8	64,105	63,755	63,760	- 5	11,035	10,815	+220	65,048	65,015	+ 35	--
39.1	78°39.1'	166°19'	55	989.2	-14.0	-373	--	--	--	--	--	--	--	--	--	--	--	--
39.3	78°37.8'	165°42'	54	980.5	-22.2	-298	--	--	--	--	--	--	--	--	--	--	--	--
39.4	78°37.2'	165°23'	50	966.2	-37.3	-414	--	--	--	--	--	--	--	--	--	--	--	--
39.5	78°36.5'	165°00'	47	954.2	-50.0	-441 S	-17.7	--	--	--	--	--	--	--	--	--	--	--
39.6	78°35.6'	164°39'	38	961.1	-45.4	-549	--	--	--	--	--	--	--	--	--	--	--	--
39.7	78°35.0'	164°24'	33	--	--	--	64,080	63,730	63,585	+145	--	--	--	--	--	--	--	
39.8	78°34.5'	164°11'	37	--	--	--	--	--	--	--	--	11,040	11,055	- 15	--	--	--	--
40.0	78°34.0'	163°57'	28	984.2	-24.3	-566 S	+14.6	64,090	63,740	63,550	+190	11,080	11,075	+ 5	65,041	64,850	+190	--
40.1	78°29.5'	163°47'	29	970.7	-34.8	-764	--	--	--	--	--	--	--	--	--	--	--	--
40.2	78°27.5'	163°43'	26	970.3	-35.1	-790	--	--	--	--	--	--	--	--	--	--	--	--
40.3	78°23.2'	163°33'	30	960.8	-40.8	-909	63,845	63,495	63,570	- 75	--	--	--	--	--	--	--	--
41.0	78°17.1'	163°19'	28	--	--	-615 S	--	63,850	63,500	63,565	- 65	11,010	11,065	- 55	64,793	64,865	- 70	--
41.1	78°14.4'	161°59'	47	--	--	--	63,830	63,480	63,460	+ 20	11,245	11,215	+ 30	64,813	64,788	+ 25	--	
LAS	78°11.0'	162°11'	43	982.4	- 8.4	-607 S	+33.4	63,890	63,540	63,490	+ 50	11,244	11,175	+ 70	64,870	64,810	+ 60	102.7°E

*Regional Value

(*) Mile marker on Byrd Trail.

S = Seismically determined depths. All other depths determined from "free air anomaly depths" adjusted to seismic depths.

TABLE III
LITTLE AMERICA STATION TO MILE 160 BYRD TRAIL (LAS-BT)

<u>Station</u>	<u>Latitude</u>	<u>Longitude</u>	<u>Elev.</u>	<u>Observed Gravity</u>	<u>Free Air Anomaly</u>	<u>Bottom Elev.</u>	<u>Boug. Anom.</u>	<u>Obs. Z Mar 58</u>	<u>Adj. Z Dec 60 corr-350r</u>	<u>Reg* Z Dec 60</u>	<u>Anom. Z nearest 5</u>	<u>Obs. H Mar 58</u>	<u>Reg* H Mar 58</u>	<u>Anom. H nearest 5</u>	<u>Obs. F Mar 58</u>	<u>Reg* F Mar 58</u>	<u>Anom. F nearest 5</u>
(*)	S	W	meters	mgls	mgls	meters	mgls	gammas	gamma	gammas	gammas	gammas	gammas	gammas	(calc)	(calc)	gammas
LAS (0)	78°11.0'	162°11'	42	982983.0	- 7.6	-607 S	+34.2	--	--	--	--	--	--	--			
41.1 (3.5)	78°13.5'	162°02'	47	974.8	-15.7	-688		63,830	63,480	63,465	+ 15						
49.3 (4.0)	78°13.8'	162°00'	47	969.7	-21.0	-762		63,840	63,490	63,460	+ 30						
41.2 (9.2)	78°17.0'	161°52'	48	968.5	-23.8	-765		63,760	63,410	63,425	- 15	11,407	11,350	+ 55	64,750	64,760	- 10
49.2 (9.8)	78°18.1'	161°40'	49	967.6	-25.0	-770		63,740	63,390	63,420	- 30						
49.1 (14.4)	78°20.5'	161°35'	53	967.0	-25.8	-754		63,640	63,290	63,390	-100						
41.3 (16.2)	78°22.0'	161°30'	54	970.5	-22.9	-597		63,670	63,320	63,375	- 55						
49.0 (20.0)	78°24.8'	161°20'	56	975.9	-18.6	-597 S	+22.4	63,590	63,240	63,350	-110	11,523	11,435	+ 90	64,610	64,702	- 90
41.4 (22.2)	78°26.6'	161°12'	56	981.2	-14.3	-557		--	--	--	--						
41.5 (26.6)	78°30.0'	161°00'	57	985.7	-11.5	-551		63,560	63,210	63,300	- 90						
48.6 (29.0)	78°31.0'	160°53'	58	989.1	- 8.4	-525		63,440	63,090	63,285	-195						
41.6 (33.5)	78°35.0'	160°40'	59	989.7	- 9.9	-580		63,380	63,030	63,250	-220						
48.5 (35.0)	78°35.2'	160°35'	59	990.1	- 9.6	-586		63,380	63,030	63,240	-210						
42.0 (40.0)	78°38.0'	160°22'	64	984.2	-15.6	-715 S	+33.6	63,380	63,030	63,205	-175	11,613	11,600	+ 15	64,419	64,589	-170
42.1 (45.2)	78°41.5'	160°05'	65	990.4	-11.1	-693		63,440	63,090	63,365	- 75						
48.3 (45.3)	78°41.6'	160°05'	65	990.6	-11.0	-691		63,380	63,030	63,165	-135						
48.2 (50.0)	78°45.6'	159°55'	67	997.3	- 6.0	-656		--	--	--	--						
42.2 (51.4)	78°46.0'	159°50'	67	999.5	- 4.0	-638		63,380	63,030	63,120	- 90						
48.1 (55.0)	78°48.9'	159°40'	68	983001.7	- 3.2	-659		63,340	62,990	63,095	-105						
48.0 (60.0)	78°51.3'	159°26'	71	003.2	- 2.1	-672 S	+44.1	63,300	62,950	63,060	-110	11,720	11,775	- 55	64,367	64,478	-110
47.7 (64.8)	78°44.5'	159°07'	72	005.4	- 1.4	-648		63,240	62,890	63,025	-135						
42.4 (67.1)	78°56.2'	158°55'	72	005.4	- 2.4	-671		63,300	62,950	63,010	- 60						
47.6 (69.8)	78°57.0'	158°50'	73	007.8	- 0.2	-648		--	--	--	--						
42.5 (74.6)	79°01.0'	158°25'	74	009.0	- 0.9	-671		63,360	63,010	62,960	+ 50						
47.5 (74.8)	79°00.0'	158°35'	74	008.8	- 0.5	-666		63,300	62,950	62,955	- 5						
43.0 (80.0)	79°02.3'	158°20'	76	008.4	- 1.6	-699 S	+46.4	63,210	62,860	62,920	- 60	11,892	11,945	- 55	64,306	64,371	- 65
47.3 (85.0)	79°05.6'	158°00'	77	012.9	+ 1.3	-631		--	--	--	--						
43.1 (86.0)	79°06.0'	157°56'	77	013.3	+ 1.5	-622		63,220	62,870	62,875	- 5	11,878	12,000	-120	64,310	64,337	- 25
47.2 (92.2)	79°10.4'	157°35'	78	006.9	- 7.0	-707		--	--	--	--						
43.2 (93.8)	79°10.6'	157°30'	79	007.2	- 6.5	-695		63,230	62,880	62,815	+ 65						
47.1 (95.0)	79°11.8'	157°22'	79	005.9	- 8.5	-718		63,220	62,870	62,805	+ 65						
47.0 (100.0)	79°13.5'	157°06'	76	005.7	-10.6	-720 S	+38.9	63,240	62,890	62,765	+125	12,019	12,140	-120	64,354	64,255	+100
46.7 (105.0)	79°16.3'	156°52'	79	007.9	- 9.0	-655		63,210	62,860	62,730	+130						
43.4 (107.4)	79°18.6'	156°40'	79	007.3	-10.9	-664		63,160	62,810	62,710	+100						
46.6 (110.0)	79°19.1'	156°37'	78	004.8	-14.0	-681		63,120	62,770	62,690	+ 80						
43.5 (112.6)	79°21.4'	156°25'	77	006.2	-14.1	-654		63,120	62,770	62,675	+ 95						
46.5 (115.0)	79°22.0'	156°15'	77	004.2	-16.5	-671		63,270	62,920	62,655	+265	11,932	12,255	-325	64,365	64,169	+195
44.0 (118.2)	79°23.2'	156°04'	77	982998.5	-22.8	-730 S	+27.3	63,480	63,130	62,635	+495	12,096	12,305	-210	64,609	64,159	+450
46.4 (120.0)	79°23.1'	155°52'	77	998.9	-22.4	-733 S	+28.0	--	--	--	--						
46.3 (125.0)	79°25.8'	155°30'	78	983002.5	-19.9	-754 S	+31.9	63,315	62,965	62,590	+375	12,292	12,370	- 80	64,484	64,127	+355
46.2 (130.0)	79°27.4'	155°10'	79	000.3	-22.7	-794 S	+31.9	63,200	62,850	62,555	+295	12,582	12,430	+150	64,409	64,104	+305
44.2 (131.0)	79°28.0'	155°00'	79	000.2	-23.1	-797		63,180	62,830	62,550	+280						
46.1 (135.0)	79°28.2'	154°50'	80	982999.4	-23.7	-796		62,970	62,620	62,520	+100						
46.0 (140.0)	79°28.9'	154°27'	81	996.6	-26.6	-843 S	+31.4	62,870	62,520	62,485	+ 35	12,567	12,515	+ 50	64,090	64,052	+ 40
44.4 (147.0)	79°31.5'	153°55'	76	995.2	-30.9	-887		62,870	62,520	62,435	+ 85						

TABLE III con't.
LITTLE AMERICA STATION TO MILE 160 BYRD TRAIL (LAS-BT)

<u>Station</u> (#)	<u>Latitude</u> S	<u>Longitude</u> W	<u>Elev.</u> meters	<u>Observed Gravity</u> mgls	<u>Free Air Anomaly</u> mgls	<u>Bottom Elev.</u> meters	<u>Boug.</u>	<u>Obs. Z Mar 58</u> gammas	<u>Adj. Z Dec 60 corr-350Y</u> gammas	<u>Reg* Z Dec 60</u> gammas	<u>Anom. Z nearest 5</u> gammas	<u>Obs. H Mar 58</u> gammas	<u>Reg* H Mar 58</u> gammas	<u>Anom. H nearest 5</u> gammas	<u>Obs. F Mar 58 (calc)</u>	<u>Reg* F Mar 58 (calc)</u>	<u>Anom. F nearest 5</u> gammas
44.5 (153.6)	79°32.0'	153°25'	73	982997.3	-30.0	-871		62,750	62,400	62,385	+ 15						
45.0 (160.0)	79°35.2'	152°02'	73	995.6	-33.5	-924 S	+29.9	62,670	62,320	62,340	- 20	12,674	12,700	- 25	63,922	63,946	- 25
44.6 (1.0 mi E of 44.0)	79°23.2'	156°10'	77	999.8	-21.5	-745		63,489	63,140	62,630	+510						
44.7 (2.0 mi E of 44.0)	79°23.2'	156°15'	77	983005.2	-16.1	-670		63,486	63,135	62,625	+510						
44.8 (3.0 mi E of 44.0)	79°23.2'	156°20'	77	003.6	-17.7	-699		63,422	63,070	62,620	+450						
44.9 (1.0 mi W of 44.0)	79°23.2'	156°00'	77	982999.5	-21.8	-749		63,436	63,085	62,635	+450						
44.10 (2.0 mi W of 44.0)	79°23.2'	155°55'	77	983001.1	-20.2	-730		63,378	63,030	62,640	+390						

*Regional Value

(*)Mile marker on Byrd Trail.

S = Seismically determined depths. All other depths determined from "free air anomaly depths" adjusted to seismic depths.

TABLE IV

TABLE IV con't.
VICTORIA LAND TRAVERSE 1958-1959 (VLT 58-59)

<u>Station</u>	<u>Latitude</u>	<u>Longitude</u>	<u>Elev.</u> meters	Observed mgls	Free Air mgls	Bottom meters	Boug. mgls	Obs. Z Nov 58	Adj. Z Dec 60 corr-240	Reg* Z Dec 60	Anom. Z nearest 5	Obs. H Mar 58	Reg* H Mar 58	Anom. H nearest 5	Obs. F Mar 58 (calc)	Reg* F Mar 58 (calc)	Anom. F nearest 5	Decli- nation
87.0	78°08.0'S	169°11'E	35	982991.7	+ 0.8	-920	S	+64.0										
88.0	78°04.5'	168°57'	31	987.1	- 2.9	-902	S	+59.1										
89.0	78°00.6'	168°40'	23	978.7	-11.3	-887	S	+49.7										
90.0	77°58.0'	168°21'	26	944.6	-42.9	-836	S	+14.5										
91.0	77°55.0'	168°06'	25	962.7	-23.3	-904	S	+38.9										
92.0	77°51.8'	167°50'	29	973.3	- 9.5	-774	S	+43.7										
93.0	77°52.7'	167°26'	25	947.4	-37.2	-925	S	+26.3										
93V	77°53.3'	167°15'	25	946.8	-38.1	--	--	--										
94.0	77°52.0'	167°16'	22	941.4	-43.6	-921	S	+19.7										
95.0	77°51.2'	167°06'	15	949.6	-37.1	-698	S	+10.9										
96.0	77°50.9'	167°01'	10	958.2	-29.9	-627	S	+13.2										
97.0	77°50.5'	166°56'	7	972.1	-16.6	-369	S	+ 8.8										
97A	77°51.0'	166°52'	6	974.0	-15.4	--	--	--										

*Regional Value

S = Seismically Determined Depths. All other depths determined from "free air anomaly depths" adjusted to seismic depths.

TABLE V
DISCOVERY DEEP TRAVERSE
March 1960 (DDT)

Station	Latitude S	Longitude E	Elevation meters	Observed Gravity mgls	Free Air Anomaly mgls	Bottom Elevation meters	Bouguer Anomaly mgls	Observed Z Mar 60* gammas	Adjusted Z Dec 60 corr +90°r	Regional Z Dec 60 gammas	Anomaly Z nearest 5 gammas	Smoothed Anomaly Z 3 station average gammas	Declination
1	77°52.3'	166°51.4'	4	982961.9	-30.1	-369 S ⁺		65,453	65,543	65,485	+ 60	--	
2	77°53.1'	167°01'	5	--	--	--		--	--	--	--	--	
3	77°53.9'	167°11'	10	976.8	-16.2	-921 S ⁺		65,372	65,462	65,462	+ 0	+145	
4	77°54.7'	167°21'	16	969.0	-24.6	-925 S ⁺		--	--	--	--	--	
5	77°55.6'	167°31.5'	19	996.4	+ 2.3	-518		65,716	65,806	65,438	+370	+130	
6	77°56.4'	167°42'	21	975.3	-19.2	-832		65,356	65,446	65,426	+ 20	+120	
7	77°57.2'	167°52'	21	972.5	-22.6	-884		65,273	65,363	65,414	- 30	+ 55	
8	77°58.0'	168°02'	25	975.1	-20.5	-856		65,482	65,572	65,403	+170	+ 25	
9	77°58.8'	168°13'	26	977.9	-18.2	-836 S ⁺		65,235	65,325	65,391	- 65	- 15	
10	77°59.6'	168°23'	26	--	--	--		--	--	--	--	--	
11	78°00.5'	168°34'	26	968.6	-28.5	-887 S ⁺		65,120	65,210	65,367	-155	- 95	
12	78°01.4'	168°44'	31	991.6	- 6.0	-740		65,200	65,290	65,355	- 55	- 80	
13	78°03.9'	169°01'	35	997.8	- 1.3	-902 S ⁺		65,232	65,322	65,344	- 20	- 35	
14	78°05.5'	169°10'	38	983001.7	- 1.5	-943		65,239	65,319	65,332	- 15	- 20	
15	78°07.1'	169°19'	42	005.6	+ 4.5	-920 S ⁺		65,198	65,288	65,320	- 30	-110	
16	78°08.7'	169°28'	45	006.2	+ 5.0	-874		64,926	65,016	65,296	-280	-100	
17	78°10.3'	169°36'	46	004.9	+ 1.9	-862		65,193	65,283	65,272	+ 10	-115	
18	78°11.8'	169°45'	50	000.4	- 3.6	-896		65,082	65,172	65,248	- 75	- 40	
19	78°13.4'	169°53'	49	982996.6	- 8.3	-924		65,072	65,162	65,224	- 60	- 30	
20	78°15.0'	170°02'	53	993.1	-11.2	-926		65,155	65,245	65,200	+ 45	- 70	
21	78°17.8'	170°01'	54	995.9	-11.7	-889		64,884	64,974	65,176	-200	-165	
22	78°20.6'	170°00'	56	998.2	-11.1	-836		64,726	64,816	65,152	-335	-245	
23	78°23.1'	170°01'	57	998.1	-12.6	-815 S ⁺		64,835	64,925	65,128	-205	-250	
24	78°25.1'	170°03'	58	994.8	-17.5	-878		64,809	64,899	65,104	-205	-260	
25	78°28.2'	170°04'	59	995.3	-18.4	-881		64,622	64,712	65,080	-370	-220	
26	78°30.7'	170°05'	59	983000.3	-14.9	-819		64,878	64,968	65,056	- 90	-195	
27	78°33.3'	170°07'	59	004.3	-12.5	-775		64,814	64,904	65,032	-130	- 75	
28	78°35.8'	170°08'	59	008.2	-10.1	-729		64,917	65,007	65,008	0	- 25	
29	78°38.3'	170°09'	60	009.6	-10.1	-719		64,953	65,043	64,984	+ 60	+ 15	
30	78°40.8'	170°10'	59	013.1	- 8.1	-679		64,856	64,946	64,960	- 15	- 60	
31	78°43.3'	170°12'	59	013.2	- 9.4	-688		64,621	64,711	64,938	-225	-120	
32	78°45.7'	170°13'	61	014.3	- 9.7	-680 S ⁺		64,700	64,790	64,915	-125	-170	
33	78°48.2'	170°15'	62	018.7	- 6.7	-647		64,643	64,733	64,893	-160	-140	
34	78°50.7'	170°17'	61	022.8	- 4.1	-619		64,646	64,736	64,870	-135	-150	
35	78°53.2'	170°18'	62	027.0	- 1.3	-588		64,600	64,690	64,848	-160	-150	
36	78°55.6'	170°20'	63	029.4	- 0.2	-580		64,583	64,673	64,825	-150	-140	
37	78°57.2'	170°09'	63	028.8	- 1.8	-612		64,609	64,699	64,811	-110	-135	
38	78°58.8'	169°58'	63	028.6	- 2.9	-637		64,570	64,660	64,798	-140	- 75	
39	79°00.3'	169°47'	63	029.1	- 3.2	-651		64,717	64,807	64,785	+ 20	- 40	
40	79°01.9'	169°36'	63	022.9	-10.4	-764		64,688	64,778	64,772	+ 5	+ 20	
41	79°03.3'	169°25'	62	013.3	-20.8	-925 S ⁺		64,706	64,794	64,759	+ 35	- 10	
42	79°04.8'	169°14'	61	014.3	-20.6	-934		64,580	64,670	64,746	- 75	- 55	
43	79°06.2'	169°03'	60	018.8	-16.9	-898		64,524	64,614	64,733	-120	- 65	
44	79°07.7'	168°52'	61	018.3	-17.8	-925		64,634	64,724	64,720	+ 5	- 55	
45	79°09.1'	168°41'	60	022.0	-15.3	-907		64,567	64,657	64,706	- 50	+ 40	

TABLE V con't.
DISCOVERY DEEP TRAVERSE
March 1960 (DDT)

Station	Latitude S	Longitude E	Elevation meters	Observed Gravity mgl s	Free Air Anomaly mgl s	Bottom Elevation meters	Bouguer Anomaly mgl s	Observed Z Mar 60*	Adjusted Z Dec 60 corr +90'	Regional Z Dec 60 gammas	Anomaly Z nearest 5 gammas	Smoothed Anomaly Z 3 station average gammas	Declination
46	79°10.5'	168°30'	61	983023.6	-14.5	-913		64,772	64,862	64,693	+170	+110	
47	79°12.0'	168°19'	62	024.7	-14.2	-922		64,804	64,894	64,680	+215	+135	147°E
48	79°13.3'	168°09'	62	025.1	-14.6	-945		64,591	64,681	64,668	+ 15	+135	
49	79°14.7'	167°59'	60	025.8	-14.6	-959		64,741	64,831	64,655	+175	+ 80	
50	79°16.0'	167°49'	62	027.5	-13.6	-963		64,608	64,698	64,643	+ 55	+ 90	
51	79°17.3'	167°39'	63	029.9	-11.9	-952		64,586	64,676	64,630	+ 45	+ 75	
52	79°18.7'	167°29'	65	032.4	-10.2	-944		64,651	64,741	64,618	+125	+ 60	
53	79°20.0'	167°19'	64	034.0	- 9.4	-950		64,527	64,617	64,605	+ 10	+145	144°E
54	79°22.0'	167°10'	65	035.8	- 8.6	-952		64,789	64,879	64,586	+295	+ 85	
55	79°24.0'	167°02'	65	037.1	- 8.4	-967		64,425	64,515	64,567	- 50	+170	
56	79°25.9'	166°53'	67	039.3	- 7.2	-964		64,717	64,807	64,548	+260	+125	
57	79°27.9'	166°45'	67	042.3	- 5.3	-953		64,601	64,691	64,529	+160	+210	
58	79°29.9'	166°36'	70	045.1	- 3.6	-943		64,631	64,721	64,510	+210	+180	
59	79°31.9'	166°27'	70	048.1	- 1.7	-932		64,570	64,660	64,491	+170	+210	
60	79°33.9'	166°19'	71	049.2	- 1.7	-946		64,639	64,729	64,472	+255	+190	
61	79°35.8'	166°10'	71	048.7	- 3.2	-986		64,510	64,600	64,453	+145	+225	
62	79°37.8'	166°02'	72	047.8	- 5.2	-1029		64,618	64,708	64,434	+275	+170	
63	79°39.8'	165°53'	72	043.5	-10.5	-1123 §	+66.8	64,413	64,503	64,415	+ 90	+145	148°E
64	79°41.4'	165°42'	74	041.9	-13.0	-1125		64,371	64,461	64,394	+ 65	+ 60	
65	79°43.1'	165°30'	77	037.2	-18.6	-1173		64,312	64,402	64,372	+ 30	+ 65	
66	79°44.7'	165°19'	80	033.8	-22.9	-1202		64,363	64,453	64,351	+100	+ 70	
67	79°46.3'	165°08'	82	028.9	-28.6	-1251		64,319	64,409	64,329	+ 80	+ 60	
68	79°48.0'	164°57'	80	024.1	-34.3	-1300		64,221	64,311	64,308	+ 5	+ 75	
69	79°49.6'	164°45'	80	021.2	-38.1	-1321		64,335	64,425	64,286	+140	+100	
70	79°51.2'	164°34'	78	018.0	-42.1	-1346		64,324	64,414	64,265	+150	+135	
71	79°52.8'	164°23'	78	017.4	-43.6	-1334		64,263	64,353	64,243	+110	+140	
72	79°54.5'	164°11'	77	016.2	-45.7	-1331		64,296	64,386	64,222	+165	+125	
73	79°56.1'	164°00'	78	014.3	-48.3	-1335 §	+43.5	64,204	64,294	64,200	+ 95	+130	153°E
74	79°57.9'	164°09'	76	016.7	-46.8	-1347		64,226	64,316	64,193	+125	+170	
75	79°59.8'	164°17'	76	024.3	-40.2	-1285		64,384	64,474	64,187	+285	+210	
76	80°01.6'	164°26'	79	036.0	-29.5	-1164		64,316	64,406	64,180	+225	+225	
77	80°03.5'	164°34'	73	046.8	-19.7	-1056		64,246	64,336	64,173	+165	+190	
78	80°05.3'	164°43'	68	055.5	-11.9	-977		64,261	64,351	64,167	+185	+210	
79	80°07.1'	164°51'	63	064.1	- 4.2	-895		64,345	64,435	64,160	+275	--	
80	80°09.0'	165°00'	56	068.8	- 0.4	-878		--	--	--	--	--	154°E
81	79°39.0'	166°45'	70 est.	051.8	- 1.8	-1025 §	+68.7	--	--	--	--	--	

*Reduced to 69,220' the assumed Scott Base value.

†Approximate reoccupation of VLT (58-59) Seismic Station.

§ = Seismically determined depths. All other depths determined from "free air anomaly depths" adjusted to seismic depths.

